FACTORS AFFECTING CRYSTALLIZATION, DISPERSION, AND AGGREGATION OF CALCIUM OXALATE MONOHYDRATE IN VARIOUS URINARY ENVIRONMENTS

By

KIMBERLY GAIL CHRISTMAS

A DISSERTATION PRESENTED TO THE GRADUATE SCHOOL
OF THE UNIVERSITY OF FLORIDA IN PARTIAL FULFILLMENT
OF THE REQUIREMENTS FOR THE DEGREE OF
DOCTOR OF PHILOSOPHY

UNIVERSITY OF FLORIDA

2001

Copyright 2001

by

Kimberly Gail Christmas

This work is dedicated to my caring and supportive mother,

Dorothy Christmas,

and

to my wonderful role model, my sister,

Nancy Christmas.

ACKNOWLEDGMENTS

I would like to thank all those who supported me and made this research project possible: to my advisor, Dr. Hassan El-Shall, for all of his help and guidance and his understanding during my recovery from my car accident, to Dr. James H. Adair for his support during the early years of my program, to my co-advisor, Dr. Laurie B. Gower, who helped me greatly since Dr. Adair's departure, and to my external committee member, Dr. Saeed R. Khan, for his help and guidance. I would also like to thank the other members of my committee, Drs. Christopher D. Batich and John J. Mecholsky Jr. from the Department of Materials Science and Engineering, and Drs. E. Dow Whitney and Brij M. Moudgil, who have kindly agreed to serve as alternate committee members for my defense. I would like to thank Drs. Joshua Adler and Yakov Rabinovich for their help with the AFM measurements and interpretation. I appreciate the help extended by Dr. Khan's group, specifically, Pat Glenton, Karen Byer, Sivagnanam ThamilSelvan, and Jeff Opalko, and by the ERC and CRIT staff.

I have learned so much from discussions with fellow graduate students in several different groups: the former Dr. Adair group, Dr. El-Shall group, Dr. Gower group, Dr. Moudgil group, and Dr. Goldberg group. I would like to acknowledge Pankaj Singh, Ahmad Hadba, Dr. Paul Demkowicz, Henrik Krarup, Dr. Drew Emery, Charley Malpass, and Dr. Chris Widenhouse for their discussions and help with my research. I would like to thank my ERC undergraduate students, Sohn Anazi, Nicole Grant, and Mallika Lavakumar, for their help with my research. A special thank you goes to Dr. Craig

Habeger for his invaluable mentoring on calcium oxalate. I thank my good friends, Bahar Basim, Dr. Kristie Leiser, and Elisabeth Richter-Belote, for their support, and especially David Christian who has been a pivotal person during the most difficult part of my graduate program. I thank my family, who is always a short phone call or drive away, for their understanding, unconditional love, and encouraging words.

Finally, special thanks go to the Engineering Research Center for Particle Science and Technology and the Industrial Partners of the ERC, General Electric Fellowship and NSF-MEDI Fellowship for financially supporting this research.

TABLE OF CONTENTS

page

ACKNOWLEDGMENTS iv

LIST OF TABLES ix

LIST OF FIGURES xi

ABSTRACT xiv

CHAPTERS

1 INTRODUCTION 1

- General Introduction 1
- Outline of Study 3

2 LITERATURE SURVEY 5

- Nephrolithiasis 5
  - Impact and Importance on Society 5
  - The Human Kidney 5
  - Urine Composition 8
    - Calcium 10
    - Oxalate 11
    - Citrate 11
    - Protein 12
- Kidney Stone Composition 12
  - The Crystalline Component 12
    - Phase stability of calcium oxalate 13
    - Solution and surface chemistry of calcium oxalate 13
  - The Matrix Component 14
    - Tamm-Horsfall protein (THP) 14
    - Mucin 17
- Crystallization 19
  - Supersaturation 20
  - Nucleation 21
  - Crystal Growth 23
  - Mixing Rate Effects on Crystallization 23
  - Crystal Aggregation and Dispersion 25

Particle-Particle Interactions 28
    Electrostatic Repulsion 28
    Steric Repulsion 32
    Attraction 34
    Interaction Energy 36
Adsorption 38
    Ions 38
    Small Molecules 38
    Macromolecules 39
Experimental Designs 39
    Plackett-Burman Design 40
    Central Composite Design 41
Characterization Techniques 42
    Atomic Force Microscopy 42
    Electrokinetic Measurements 43
    Protein Quantification 44
    Ion Chromatography 45

3 MATERIALS AND METHODS 47

Preliminary Studies 47
    Crystallization Study 47
        Saturated COM solution preparation 47
        COM particles without seeds using different mixing rates 47
        Characterization of grown COM crystals by two different mixing rates 52
        "Fine" COM particles with seeds 53
    Zeta Potential Measurements of COM in Presence of Different Solutions 57
        Sodium azide 57
        Bovine submaxillary glands mucin 57
        Addition of calcium to COM solutions 57
        Addition of oxalate to COM solutions 58
        Tris-HCl affect on COM particles 58
Detection of Bacteria in Artificial Urine 59
Aggregation and Dispersion Study 59
    Making Artificial Urine 60
    Screening Design (Plackett-Burman Design) 61
    Central Composite Design 65
    Verification of Central Composite Results 69
    Turbidity Tests 69
    Zeta Potential Determination 70
    Optical Microscopy Observations 71
    Particle Size Measurements 72
    Force Measurements via Atomic Force Microscopy 73
    Specific Surface Area Measurement using Brunauer, Emmett, and Teller (BET) Method 73
    Protein Adsorption 74
    Ions and Small Molecule Adsorption 76

Ion chromatograph analysis 77
Inductively coupled plasma 78

4 RESULTS AND DISCUSSION 79

Preliminary Studies 79
Crystallization Study 79
COM particles without seeds using different mixing rates 79
"Fine" COM particles with seeds 86
Zeta Potential Measurements of COM in Presence of Different Solutions 86
Sodium azide 86
Mucin 87
Addition of Oxalate to COM Solutions 88
Addition of Calcium to COM Solutions 90
Tris-HCl affect on COM particles 90
Detection of Bacteria in AUIS 91
Aggregation and Dispersion Study 92
Plackett-Burman Design 93
Central Composite Design 96
Zeta Potential Analysis 103
Particle Size Analysis 104
Force Measurements via Atomic Force Microscopy 105
Specific Surface Area Measurements using Brunauer, Emmett, and Teller Method 110
Protein Adsorption 110
Ions and Small Molecule Adsorption 119
Ion chromatograph analysis 120
Inductively coupled plasma analysis (ICP) 121
Theoretical Interaction Energy Curves 125

5 CONCLUSIONS AND FUTURE WORK 132

Conclusions 132
Future Work 136

APPENDIX ION CHROMATOGRAPH DATA 138

LIST OF REFERENCES 140

BIOGRAPHICAL SKETCH 152

LIST OF TABLES

Table Page

3.1. The total concentration of artificial urine displayed by the order of addition................61

3.2. Experimental Plackett-Burman Design for 15 Variables..63

3.3. Rotatable Central Composite Design with the 5 levels and 3 variables utilized in the experiments..67

3.4. Atomic force microscopy solutions utilized with COM. 74

3.5. The mucin standards prepared for the Modified Lowry Protein Assay. 77

4.1. Statistically determined values describing slowly mixed and rapidly mixed particle size distributions for the samples..85

4.2. Aggregation data for Plackett-Burman design. Absorbance Values used to calculate the aggregation coefficient of the Plackett-Burman design. 93

4.3. The Plackett-Burman calculated t values for different variables. The decisions to accept or reject the significance of variables on the bases of comparing t-value to critical value at 95% confidence level. 96

4.4. Aggregation data for central composite design..97

4.5. Ionic strength of each experimental runs from central composite design......................102

4.6. Aggregation coefficients from the verification study of central composite design. The aggregation coefficients extrapolated from the central composite data are also shown..103

4.7. Amount of protein adsorption and parking area of central composite design. 111

4.8. Central Composite Design with the concentrations of the variables and their corresponding aggregation coefficient...120

4.9. Calcium Concentration measured by ICP...122

A.1. Oxalate Concentration measured by Ion Chromatograph 139

A.2. Citrate Concentration measured by Ion Chromatograph..139

LIST OF FIGURES

Figure Page

2.1. The urinary system and section of the kidney are illustrated 7

2.2. A schematic representing a long-looped nephron which is not to scale. 8

2.3. The classical schematic representation of the overall free energy during nucleation 22

2.4. A schematic diagram of the electrical double layer. 30

2.5. The effect of ionic strength on the double layer 31

2.6. Possible conformations of adsorbed polymer on surfaces 33

2.7. A schematic of interaction energy as a function of separation distance 37

2.8. A schematic of atomic force microscopy. 43

3.1. Schematic representation of processing steps for the preparation of COM crystals without seeds using two different mixing rates. 50

3.2. Schematic of rapid mixing apparatus 51

3.3. Schematic representation of processing steps for the preparation of COM crystals with seeds. 56

3.4. A schematic of the procedure for making the Plackett-Burman design samples. 64

3.5. A schematic of 5 level, rotatable central composite design 66

3.6. A schematic representation of the preparation of the central composite design experimental runs and the analysis performed. 68

4.1. Scanning electron photomicrographs of COM particles. 81

4.2. A typical experimental COM X-ray diffraction pattern 82

4.3. Representative log normal of particle size distributions for slow mixing (sample HM25) and rapid mixing (sample RM17). 83

4.4. Representative photomicrograph of the fine COM particles used for the aggregation and dispersion studies. 87

4.5. The zeta potential compared to the weight percent of sodium azide in saturated COM solution ($8x10^{-6}$ M) with COM particles within 95% confidence interval. 88

4.6. The influence of oxalate on COM particle surface. Zeta potential as a function of oxalate concentration on COM particle surface in CO_2 free ultrapure water and 0.01 M Tris-HCl. within 95% confidence interval....89

4.7. The zeta potential of COM particles as a function of calcium concentration. The two solutions studied were CO_2 free ultrapure water and 0.01 M Tris-HCl solution within 95% confidence interval. 90

4.8. The zeta potential of COM particles as a function of Tris-HCl solution within 95% confidence interval....91

4.9. Dispersed sample versus an aggregated sample via optical microscopy. 95

4.10. Prediction Profiler of oxalate, citrate, and protein as a function of aggregation coefficient. 97

4.11. Interaction plots between citrate, protein and oxalate concentrations 99

4.12. Contour plots illustrating how the aggregation probability changes with respect to oxalate and protein concentration at constant citrate levels....101

4.13. Surface response aggregation of citrate versus oxalate at 5 ppm protein. 104

4.14. Particle size analysis data of central composite design samples....106

4.15. Interaction forces measured by atomic force microscopy versus separation distance between calcium oxalate monohydrate particle and silicon nitride tip in various solutions. 107

4.16. AFM force measurements under three solutions using a new COM sample....107

4.17. Interaction force between COM particle and artificial urine 109

4.18. Effect of citrate on the interaction forces between COM particles and SiN tip as a function of separation distance. 109

4.19. A contour plot illustrating how the amount of protein adsorbed on COM particle changes with respect to oxalate and protein concentrations at constant citrate concentrations of....112

4.20. Surface response for protein adsorption....113

4.21. Illustration of possible conformations of adsorbed protein to a crystal surface...........115

4.22. Protein Adsorption Isotherms 116

4.23. Schematic of possible citrate, calcium and protein adsorption. At high citrate concentration, there is less protein adsorption..........118

4.24. Prediction Profile of extracted calcium as a function of oxalate, citrate and protein concentration...........122

4.25. Surface response of extracted calcium as a function of oxalate and citrate concentrations 123

4.26. Surface response of extracted calcium as a function of oxalate and protein concentration at constant citrate concentration...........124

4.27. Theoretical DLVO trend for a sample in the central composite design..........128

4.28. Comparison of DLVO theory and steric on interaction energy. 129

4.29. Comparison of polymer layer thickness on steric energy 131

Abstract of Dissertation Presented to the Graduate School
of the University of Florida in Partial Fulfillment of the
Requirements for the Degree of Doctor of Philosophy

FACTORS AFFECTING CRYSTALLIZATION, DISPERSION, AND AGGREGATION OF CALCIUM OXALATE MONOHYDRATE IN VARIOUS URINARY ENVIRONMENTS

By

Kimberly Gail Christmas

August 2001

Chairman: Dr. Hassan El-Shall
Major Department: Materials Science and Engineering

The mechanisms for the formation of kidney stones are not well understood. One possible mechanism is the formation of aggregates in the nephron tubules of the kidneys. However, altering the urinary environment may be a method to help prevent the recurrence of the formation of kidney stones. The primary inorganic constituent found in kidney stones of North American patients is calcium oxalate monohydrate (COM). In this research, studies on the effect of mixing rate on COM precipitation showed that rapid mixing compared to slow mixing produced smaller particle sizes and a narrower particle size distribution due to the more uniform supersaturation level. The findings are consistent with the general contention that mixing directly influences nucleation rate while mixing rate has relatively little influence over rate of growth in precipitation processes.

Screening and central composite experimental designs are used to determine the effect of various factors on the aggregation and dispersion characteristics of previously grown calcium oxalate monohydrate (COM) crystals in artificial urinary environments of controlled variables. The variables examined are pH, calcium, oxalate, pyrophosphate, citrate, and protein concentrations in ultrapure water and artificial urine. Optical density measurements, zeta potential analysis, particle size analyzer, optical microscopy, AFM force measurements, protein adsorption, and ions and small molecule adsorption have been used to assess the state of aggregation and dispersion of the COM crystals and to elucidate the mechanisms involved in such a complex system. The data indicate that our model protein, mucin, acts as a dispersant. This is attributed to steric hindrance resulting from the adsorbed mucoprotein. Oxalate, however, promotes aggregation. Interesting interactions between protein and oxalate along with protein and citrate are observed. Such interactions (synergistic or antagonistic) are found to depend on the concentrations of these species. Surface responses for these interactions are presented and discussed in this dissertation. In summary, solution, surface, and interface chemistries interact in a complex manner in the physiological environment to either inhibit or promote aggregation. The data indicate the interactions between species play an important role in dispersion/aggregation of kidney stone constituents.

CHAPTER 1
INTRODUCTION

General Introduction

Kidney stone formation is a serious medical condition in industrialized nations and has a high recurrence rate (60-80%). Most kidney stones are comprised of an organic matrix with biomineral (1, 2). The organic matrix may contain lipids, cellular debris, and urinary proteins such as Tamm-Horsfall mucoprotein, osteopontin, albumin, and nephrocalcin. The biomineral may contain crystals like calcium phosphate and uric acid, but the majority of stones found in North American patients are mainly composed of calcium oxalate.

As in any biomineralization, the primary phenomenon underlying stone formation is formation of crystals. As long as the crystal(s) do not become larger than ~ 20 μm or greater, they are usually excreted from the body without any problems. It is when a crystal becomes larger than 20 μm (from retention, growth, and/or aggregation) that a kidney stone has a greater chance to be formed.

Due to the complex nature of the urinary environment, this process is under constant influence of a variety of urinary components. The urinary components include ions such as calcium and magnesium, small molecules such as citrate and oxalate, and macromolecules such as lipids and proteins. These factors interact with each other and with crystals, which can influence the various stages of crystallization and stone formation. Most investigators think the primary cause for the formation of kidney stones is by aggregation of crystals because kidney stones are usually found as aggregates.

Previous research on calcium oxalate has conflicting results as to the role of some urinary species. Citrate and urinary proteins are of particular interest in this study. For example, Kok et al. (3) showed that low citrate concentration contributes to crystal aggregation in stone-formers. They also showed that at higher citrate concentrations, aggregation was inhibited in urine (4). In contrast, Hess et al. (5) showed that citrate did not affect aggregation at various concentrations. Benkovic et al. showed that Tamm-Horsfall protein (THP) promotes aggregation (6). In a more recent work by Hess et al. (7), an increase in citrate (1.5-3.5 mM) caused an increase in inhibition of aggregation. In addition, THP with citrate enhanced the inhibitory effect of THP. In summary, there are conflicting conclusions about the role of various species such as citrate and protein in this complex system.

Most of these cited experiments were performed by changing one-variable-at-a-time instead of changing several variables at the same time to understand the whole system. While this typical research methodology nicely shows trends with a given variable, a combination of variables can sometimes lead to synergistic or antagonistic effects that will not be discerned in this methodology. An advantage of statistical experimental designs is that multiple variables at different levels can be evaluated with a limited number of experiments (8). As mentioned above, these designs can lead to estimation of main and interaction effects of the variables. Changing one-variable-at-a-time method could perhaps be a reason for the discrepancy in results in the mentioned investigations.

In summary, the mechanisms responsible for the formation of kidney stones are not well understood. There are several hypotheses for stone formation, but few studies have been designed to critically test them. However, altering the urinary environment may be a method to help prevent the recurrence of the formation of kidney stones. The goal of this research is to study the effect of primary factors on aggregation and dispersion of previously grown COM crystals in a urinary model system.

Outline of Study

In Chapter 1, a general introduction to kidney stone disease and the significance of aggregation is presented.

Chapter 2 discusses the human kidney, urine composition, and kidney stone composition. The mucoproteins, Tamm-Horsfall protein and mucin, are discussed and compared in detail. Previous research with relevancy to this work is discussed. In addition, the basics of crystallization, interparticle forces, adsorption, and characterization techniques are discussed.

Chapter 3 introduces the method employed for calcium oxalate monohydrate (COM) synthesis. The experimental procedure using screening and central composite experimental designs to determine the effect of various factors on the aggregation and dispersion characteristics of previously grown COM crystals in different urinary environments is presented. The techniques used to support the aggregation data, zeta potential determination, atomic force microscopy (AFM) force measurements, optical microscopy, particle size analysis, protein adsorption assay, and inductively coupled plasma, are discussed.

Chapter 4 contains the experimental results of the study as well as the statistical analysis of the results. A discussion of the results is given with relevancy to kidney stone formation.

Lastly, Chapter 5 highlights the main conclusions of the study and suggests future work.

CHAPTER 2
LITERATURE SURVEY

Nephrolithiasis

Impact and Importance on Society

Nephrolithiasis refers to crystal deposition inside the renal tubules. Biomineralization is an important phenomenon in both healthy individuals and those prone to certain pathological events including kidney stone disease, gout, and some forms of arthritis. Kidney stone disease has a significant effect on society. In 1996, the U.S. had 1,223 million doctor visits related to kidney stone disease (9). In hospitals, there were 251,000 people diagnosed with urinary stones (10). The cost of dealing with kidney stones was over $1.83 billion dollars in 1993 (11). Kidney stone disease affects as many as 15% of men and 7% of women in the U.S. (12). Of those people who form kidney stones, their chance of forming another stone such as calcium oxalate and calcium phosphate is 60-80% (13).

The Human Kidney

The primary functions of the kidneys are to process blood in order to regulate the balance of water and electrolyte in the body and to excrete metabolic waste products and foreign chemicals. This is achieved by altering the urinary excretion. The important inorganic ions that are regulated by the kidneys are water, sodium, potassium, chloride, calcium, magnesium, sulfate, phosphate, and hydrogen ion (14). The urinary waste created by a kidney is collected in the renal pelvis and then moves through the ureter to the bladder and is excreted by the urethra (Figure 2.1a).

The kidney is divided into two major regions; the inner section is called the medulla and the outer section is called the cortex (Figure 2.1b). The cortex section contains all the glomeruli. The medulla section contains parts of the nephron and collecting ducts. The medulla is divided into multiple cone-shaped masses of tissue called renal pyramids. The base of each pyramid originates at the border between the cortex and medulla and terminates in the papilla (projects into the space of the renal pelvis) (15).

Each kidney is comprised of approximately 1 million nephrons. A schematic of one nephron is displayed in Figure 2.2. A nephron contains a filtering component called the renal corpuscle and a tubule extending out from the renal corpuscle. The renal corpuscle consists of the glomerulus and Bowman's capsule, which are responsible for separating the protein-free filtrate from plasma (the first step in urine formation). Fluid filters from the glomerulus into the Bowman's capsule.

The nephron is made up of a single layer of epithelial cells on top of basement membrane. The basement membrane is comprised of mucopolysaccharides and glycoproteins and converts filtered fluid into urine. The structure and function of epithelial cells vary from segment to segment of the nephron. The order of fluid draining starts with Bowman's capsule leading to the proximal tubule to the descending thin limb of long nephron Henle's loop which ends at a hairpin loop into the ascending thin limb of Henle's loop. In long nephron loops, the epithelium thickens and is called thick ascending limb of Henle's loop. In short nephron loops, there is no thin ascending limb,

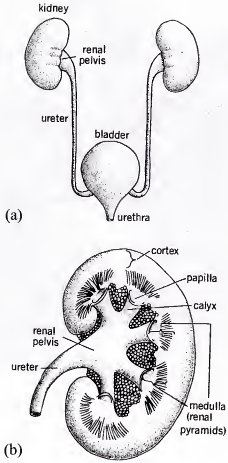

Figure 2.1. The urinary system and section of the kidney are illustrated. a) The urine formed in the kidneys is collected at the renal pelvis and flows through the ureter to the bladder and is eliminated by urethra. b) The section of kidney shows the outer section, cortex, and the inner section, medulla (Taken from Vander 1991 [14]).

but only thick ascending limb. The thick tubule (macula densa) passes between the arterioles supplying its renal corpuscle of origin. Then the fluid continues to drain into distal convoluted tubule followed by connecting tubule, which leads to the cortical collecting duct. There are approximately 10 cortical collecting ducts. The larger collecting duct runs downward into the medulla and becomes the medullary collecting duct. The collecting ducts merge to become larger ducts and empty into the renal pelvis through the papilla tips. In each kidney, there are about 250 large collecting ducts, which collect urine from about 4000 nephrons (15).

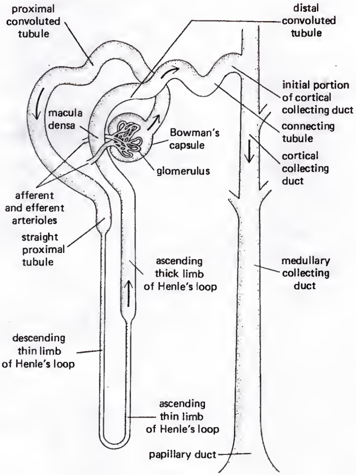
proximal convoluted tubule
distal convoluted tubule
initial portion of cortical collecting duct
macula densa
connecting tubule
Bowman's capsule
cortical collecting duct
glomerulus
afferent and efferent arterioles
straight proximal tubule
ascending thick limb of Henle's loop
medullary collecting duct
descending thin limb of Henle's loop
ascending thin limb of Henle's loop
papillary duct

Figure 2.2. A schematic representing a long-looped nephron which is not to scale (Taken from Vander 1991 [14]).

Urine Composition

Formation of urine begins with glomerular filtration of virtually protein-free plasma into Bowman's capsule. The final composition of urine at the renal pelvis is different from the glomerular filtrate. The filtered fluid is altered in the tubules either by tubular reabsorption of substances from the renal tubules into the blood or tubular secretion of substances from the blood into the renal tubules. The urinary excretion rate of a substance is equal to filtration rate minus reabsorption rate plus secretion rate (15). The glomerular filtration rate is about 180 L/day, meaning the entire plasma can be filtered 60 times each day. The filterability of solutes is determined by their size and electrical charge. The filterability of substances by glomerular capillaries decreases with increasing molecular weight. Negatively charged large molecules are filtered less easily than positively charged molecules of equal molecular size. Therefore, the glomerular capillaries do not filter much protein.

Most of the urinary proteins are synthesized along the tubular portion of the nephron by different cell populations. Tamm-Horsfall protein (THP) is synthesized by the epithelial cells located in the thick ascending limb of Henle. Bulk reabsorption of the glomerular filtrate takes place in the proximal tubule, followed by dilution in the loop of Henle. Then, in the distal nephron, osmotic concentration of the urine takes place through sodium and potassium excretion, and pH is regulated by adjustment of hydrogen and ammonium ions.

The final urine composition is a very complex solution of water, ions, inorganic salts, small molecules such as citrate and phosphate, macromolecules such as protein and lipids, and various other metabolites. The pH of urine ranges from 4.5–8.0, but generally urine is lower than neutral pH (15). Kidney stone formation is a result of how all of these components interact with each other with some components having more of an impact than others.

In relation to the mineral phase of a stone, there are four factors usually present in a kidney stone former are hypercalciuria (excess calcium), hyperoxaluria (excess oxalate), hypocitraturia (reduced citrate), and hyperuricosuria (excess uric acid) (16, 17). For this study, calcium, oxalate, citrate, and protein will be discussed in detail.

Calcium

Calcium is normally in concentrations of 8.9-10.1 dg/ml in the plasma. After filtration in the glomerulus, calcium is reduced to 55% of the calcium concentration found in the plasma and eventually to 0.5-2% (excreted urine) (18). Before filtration, the proximal tubule is a major site for reabsorption.

Hypercalciuria is defined as 0.1 mmol/Ca/kg/day (4mg/kg/24 hrs.) or greater of urine excretion (19). It has been demonstrated that calcium and oxalate excretion rates have a strong correlation. Recurrent stone-formers may have an abnormality of oxalate absorption in relation to calcium absorption (20). From experimental studies, calcium has been shown to affect oxalate concentration and crystalline forms. Calcium has been shown to bind to oxalate; therefore, the free oxalate concentration is reduced. Clinically, patients with normal calcium ranges tend to form calcium oxalate monohydrate phase over dihydrate (more common in hypercalciuric patients) (21).

Although hyperoxaluria is an important parameter for the formation of stones, calcium metabolism affects the oxalate kinetics. For example, in a low calcium diet of 34 healthy adults, the urinary oxalate excretion increased from 0.31 ± 0.08 mM per day to 0.45 ± 0.09 mM per day (22). Therefore, a low calcium diet caused an increase in oxalate excretion compared to a high calcium diet. Another study supports this data; there were 106 patients that showed daily urinary oxalate excretion is inversely proportional to calcium diet. This indicates that calcium present in the gut (stomach) binds to oxalate, therefore reducing the amount of oxalate for absorption (19).

Oxalate

Since the majority of urinary stones contain oxalate, then reducing the oxalate concentration would be beneficial to most stone-formers. Oxalate is obtained from a few sources. Oxalate is derived from endogenous metabolism (approximately 60%), end product of dietary ascorbate metabolism (25-30%), and dietary oxalate (10-15%) (17, 23-25). It is possible to lower the dietary oxalate to try to reduce the amount of oxalate in the kidneys. In an unconfirmed report, a dietary oxalate restriction helped 45% of the people (26). High amounts of oxalate can be obtained from foods such as nuts, chocolate, and dark-green leafy vegetables (27). It appears that reducing dietary oxalate may help some people, but not all. A study by Hatch showed that increased endogenous production of oxalate caused hyperoxaluria (28).

Citrate

Citrate concentration in plasma ranges from 0.05-0.3 mmoles/liter and exists as an alkaline citrate^{3-} ($C_6H_5O_7{}^{3-}$, molecular weight 189 g/mole) (29). In humans, citrate is freely filtered through the glomerulus and about 75% is re-absorbed in the proximal tubule (30).

As mentioned earlier, hypocitraturia is another major contributor to kidney stone disease. A major cause of hypocitraturia is acidosis in stone patients. This environment reduces urinary citrate by enhancing reabsorption of renal tubules and impairing uptake (31). Pak et al. demonstrated that treatment of hypocitraturia slowed down and even eliminated kidney stone formation (32, 33). Currently, potassium citrate supplementation is used to treat this condition by physicians (34). Potassium is used more frequently than sodium citrate because sodium can increase urinary calcium excretion.

In vitro studies have shown citrate to inhibit spontaneous precipitation of calcium oxalate (CaOx) within urinary concentration range; therefore, citrate is affecting nucleation (35). Citrate has also been shown to inhibit calcium oxalate growth as well as aggregation (36).

Protein

Animal protein diet in developed countries is a major dietary factor contributing to a relatively high stone rate. Protein contributes to several phenomena. The ingestion of protein increases renal acid excretion. Consequently, this increases renal reabsorption of potential base, such as citrate (16). Citrate is thought to help inhibit calcium stone formation. Another possible buffering source may be bone which releases calcium that, in turn, leads to the kidneys. Also, the acidic urinary environment inhibits renal calcium reabsorption (16). Several studies have shown that there is an increase of nephrolithiasis with an increase in protein intake (37, 38). A study involving potassium citrate taken orally by stone-formers resulted in an increase of citrate and THP excretion and less COM crystal agglomeration (39).

Kidney Stone Composition

A kidney stone is usually comprised of an organic matrix with biomineral (1, 2). A description of both components is presented.

The Crystalline Component

The crystalline component is usually a mixture of inorganic crystalline forms comprising up to 98% of the stone weight (40). The typical types of biominerals found are calcium oxalate monohydrate, calcium oxalate dihydrate, calcium phosphate (hydroxyapatite, carbonoapatite, brushite, octo-calcium phosphate, and whitlockite), uric acid, struvite, and cystine (36, 41, 42). The most prevalent biominerals formed are calcium oxalates.

Calcium oxalate monohydrate (COM) has been studied by several investigators with respect to its role in kidney stone formation. The results of these research efforts have led to a good understanding of its crystallography and physical chemistry in solution (43-54). Calcium oxalate is found in three forms: calcium oxalate monohydrate (COM), calcium oxalate dihydrate (COD), and calcium oxalate trihydrate (COT).

Phase stability of calcium oxalate

COM (whewellite; $CaC_2O_4{\bullet}H_2O$) is the most thermodynamically stable phase and the most prevalent form found in kidney stones is dumbbell-shaped and rounded. COD (weddellite; $CaC_2O_4{\bullet}2H_2O$) and COT ($CaC_2O_4{\bullet}3H_2O$) are metastable phases and require stabilizers for their existence and will eventually transform into COM (55). COT is rarely found in kidney stones or in the urine although it is often kinetically favored (36, 56). However, COT is thought to be a precursor for the formation of COM and COD; therefore, it has also been studied (55). COD is more probable to form in patients with hypercalciuria, which result in dipyramids (21, 57)

Solution and surface chemistry of calcium oxalate

Calcium oxalate monohydrate is sparingly soluble, equilibrates rapidly, does not form gels, has no hydroxlyated surface groups, and forms well-defined particles. Calcium oxalate (CaOx) has a low congruent solubility over the ranges from about pH 5 to pH 10 (58). At physiological temperature, COM has a concentration of $6.16\text{x}10^{-6}$ M in solution with a solubility product (k_{sp}) of $3.79\text{x}10^{-11}$ M (59). The stability constant of

$[CaC_2O_4^0](aq)$ at 37°C is 2,746; therefore, this complex species is moderately stable (59, 60). The surface charge on COM is controlled by the potential determining ions, Ca^{2+} and $C_2O_4^{2-}$, and follows a Nernst-Gouy-Stern surface charging model (58) with a pCa_{pzc} equal to 5.2.

The Matrix Component

The kidney stone matrix makes up to 2-3% of the total weight of the stone (61, 62). The matrix is comprised of proteins, lipids, carbohydrates, and cellular components (63). The matrix can be found in concentric layers or radial striations throughout the stone (64). The proteins commonly found in the urine are Tamm-Horsfall protein, osteopontin, uropontin, nephrocalcin, prothrombin fragment-1, inter-alpha inhibitor, and uronic acid rich protein. In this research, Tamm-Horsfall protein (THP) is of interest. However, since THP is expensive and not easily accessible, mucin is used instead. A discussion of the similarities between the two glycoproteins follows.

Tamm-Horsfall protein (THP)

Occurrence. Tamm-Horsfall protein (THP), also called uromucoid, was first discovered by Morner (65) and further characterized by Tamm and Horsfall as the urinary component capable of inhibiting viral hemagglutination (66). THP has been researched for more than 5 decades because of its biological significance and its involvement in kidney stones. The daily urinary excretion of THP ranges from 20-100 mg in adults (67). The average concentration is 50 mg/L. THP is the most abundant protein in urine and is a major constituent of urinary casts (68). THP is synthesized and located in the kidneys specifically in the thick ascending limb (TAL) of the loop of Henle (69).

THP is a member of the glycosyl phosphatidylinositol-linked membrane protein family, which are proteins associated with cell membranes (70). Most of the protein exists in the secreted form and is released into the tubular lumen. It has been found to exist on basolateral and luminal aspects of cell membranes and on the membranes of Golgi apparatus and endoplasmic reticulum (71, 72). THP has also been found in small amounts outside the kidney (71, 73, 74).

Biochemical Properties. THP is a glycoprotein of 80-90 kD. It can exist in a polymeric form of 70,000 kD discovered by Curtain (75). The polymeric form has been shown to break down to the monomeric form by addition of urea (75), 50% acetic acid (76), or 6 M guanidine hydrochoride and 0.05% sodium dodecyl sulfate (69).

The amino acid sequencing of THP (615 amino acids) did not exhibit any unusual amino acids (77). The amount of acidic residues such as aspartic and glutamic acids was higher than the other constituents. THP also contains 20% dicarboxylic amino acids and 30% carbohydrates including 14% neutral sugars, 10% hexosamines, and 6% N-acetylneuraminic acid (78, 79). It contains eight N-linked glycoslyation sites (80). THP has a low isoelectric point approximately pH 3.2 (78) mainly due to the presence of sialic acid residues (4%) and excess amount of five types of acidic residues on the glycoprotein (79). Therefore, the protein is highly negatively charged in urine.

THP tends to gel in the presence of various factors such as calcium and sodium ions (81), magnesium (81, 82), hydrogen ions (83, 84), albumin (85), and increase in concentration of THP itself (83). The self-aggregation of THP appears to be caused by cations binding to carboxyl groups. Gel formation is reduced in the presence of urea (75) and alkaline pH (81).

Function. Since THP is so abundant in human urine, it is assumed to have an important biological function. The self-aggregating feature of THP resulting in gel formation was widely studied. It was suggested that THP gel could be responsible for water impermeability of the thick ascending loop (TAL). Thus, THP may protect the tubular cells, similar to the effect of mucin on stomach lining (68). It may contribute to formation of urinary casts, since it aggregates with cast-forming human Bence-Jones protein (86).

Another possible function of THP is as a defense against infection. Orskov, Ferencz, and Orskov (87) showed E. coli with type I fimbriae were trapped by THP. In another study, bacteria coated with THP were less susceptible to phagocytosis compared to uncoated bacteria (88).

It has been shown that THP interacts with cells and molecules of the immune system. For example, THP interacts with cytokines such as tumor necrosis factor (89), and interleukins IL-2 (90) and recombinant IL-1 (91). In all cases, these cytokines bind to specific carbohydrate sequences found on THP. In conclusion, THP has the potential to be involved in several functions; however, the exact function(s) of THP are not confirmed.

THP and nephrolithiasis. While the role of THP is unclear, THP is found in the organic matrix of kidney stones. It may be merely a bystander or it may actively participate in stone formation. *In vitro* studies have shown conflicting results. THP has been shown to promote (92, 93), inhibit (94, 95), and have no effect (96) on stone formation. The action of THP may depend on the experimental environment (97). The accepted mechanism for inhibition of CaOx growth and aggregation by negatively charged macromolecules such as THP is by binding to the surface of preformed crystals (95, 98, 99). The binding most likely occurs with calcium ions (98). The macromolecule may induce a negative electrostatic surface charge and/or steric hindrance.

The binding of negatively charged macromolecules to crystal could result in a viscous binding, glue-like formation of macromolecules (95, 99, 100). The viscous binding counteracts repulsive electrostatic force (95, 99, 101); therefore, it can promote crystal aggregation (95). In a study by Hess et al. (101), there was a significant inverse correlation between THP viscosity and COM crystal aggregation inhibition. A preliminary study showed that inhibition of COM aggregation was related to concentrations of THP with citrate in whole urine (101). In contrast, a study with ultrafiltered urine did not exhibit citrate as an inhibitor (102). This shows citrate may need to interact with the macromolecules to inhibit aggregation.

Mucin

Mucin is used in this study instead of THP because it is less expensive and easily accessible. A description of mucin and a comparison to THP is discussed below.

Occurrence. Secreted mucins are found in mucus. The mucins are synthesized by the host. In humans, mucins are found in the colon, small intestines, trachea, stomach, respiratory tract, gall bladder, and salivary glands (103). Mucins can also be found in other organisms such as porcine and bovine mucins.

Biochemical properties. Mucin, a highly glycosylated glycoprotein, can range in molecular mass from 39 kD to 10,000 kD (103). Bovine submaxillary mucin (BSM), the mucin used in these studies, has molecular mass of 400 kD. Mucin consists of a central peptide core surrounded by oligossacharides that radiate out like the bristles of a bottle-brush (104). More than 50% of mucin is comprised of carbohydrates by weight. BSM has been reported to contain 56.7-70% carbohydrates mainly in the form of disaccharides consisting of sialic acid and N-acetylgalactosamine (105-108). The carbohydrates are organized as oligosaccharides that are O-linked to serine or threonine with 1-20 sugar residues per carbohydrate chain.

The protein backbone is rich in serine and threonine residues, which are clustered in the central part of the polypeptide. Most of the hydroxylated amino acids in this central region are O-glycosylated. Weiping et al. found potential N-glycosylation with some peptides (109). The glycosylated region is negatively charged due to sialic acid residues. In addition, mucins are also negatively charged due to sulfate residues on the oligosaccharides (110). This also attributes to the low isoelectric point that ranges from pH 3 to pH 5 (111). The non- (or poorly-) glycosylated regions of the peptide core are rich in aspartic and glutamic acid (104). The protein backbone is also comprised of proline, glycine, and alanine residues. The five amino acids residues (serine, threonine, proline, glycine, and alanine) comprise over 50% of amino acid residues. The prolines prevent α-helix formation which allows for the conformation of close packing of the carbohydrates (103). The epithelial mucins (secreted mucins) including bovine submaxillary mucins contain a cysteine-rich domain upstream of the carboxyl terminus in which the arrangement of cysteines is nearly identical to human von Willebrand factor (109, 112).

The protein backbone of bovine submaxillary mucin was hypothesized to be comprised of a number of repeating amino acid sequences by Pigman and co-workers (113). This hypothesis has been confirmed for all mucus glycoproteins (110).

Specifically in bovine submaxillary mucin, the repeated amino acid sequence is GTTVAPGSSNT (114).

Function. Secreted mucins have several functions in a body. Mucins give the elasticity, viscosity and gel forming properties to mucus. Mucins also act as a protective barrier between the organism and its environment by protecting the tissues from physical damage, toxins, microorganisms, and dehydration (103). Mucin is a competitor inhibitor to the adhesion of microorganisms to epithelial cells (115, 116).

Similarities to Tamm-Horsfall protein. THP and mucin have similar physicochemical properties. They are both highly glycosylated glycoproteins (more specifically, mucoproteins). They are both found on and synthesized by epithelial cell membranes. THP and mucin have similar amounts of bound sialic acid of 4% and 5%, respectively. This attributes to their low isoelectric point resulting as a highly negatively charged macromolecule. They are both capable of polymerizing and forming a gel.

There are some possible similarities with their biological functions. THP possibly has a protective effect on the tubular cells, similar to the effect of mucin on the stomach lining (68). Another possible function of THP is to act as an inhibitor of microorganisms to the adhesion to kidney cells (117), which is a property of mucin to different cells.

Crystallization

The primary phenomenon underlying biomineralization is the process of crystallization. For the formation of a kidney stone, a crystal must first be formed. Crystallization in the biological environment is not in a “pure” environment meaning there are usually other foreign species. The crystals formed are the result of interaction of various components of that system. This includes factors such as pH, urine constituents, quantity and size of particles, macromolecules, and alterations in cell surfaces of urinary epithelium. Proteins have been shown to be the most active macromolecules which act as controllers of crystallization (118). A crystal is formed by a nucleus that can grow into a crystal. Crystals can become larger in size by growth and stones can become larger by aggregation of crystals. Crystallization is also affected by supersaturation and mixing rate of the system.

Supersaturation

Supersaturation is the excess of free energy or thermodynamic driving force for the formation of crystals. This driving force is expressed as free energy (ΔG) by (119)

$$\Delta G = -RT\ln(Q/k_{sp}) \qquad [2.1]$$

where R is gas constant, T is temperature, Q is product of the initial activity of precipitating reactants and k_{sp} is product of activities at 25°C (99, 119).

The ion product at initial concentrations is given by,

$$Q = (Ca^{2+})_{t=0}\,(C_2O_4^{2-})_{t=0}$$

The activity (a_i) of a particular soluble c species, i, is related to concentration (c_i) through an activity coefficient ($f_{\pm z}$) given by (120)

$$a_i = f_{\pm z}\, c_i \qquad [2.2]$$

where ± z is the valence of the species. The ratio Q/k_{sp} is defined as the relative supersaturation (121). For a given salt when $Q/k_{sp} > 1$, then $\Delta G < 0$ and the solution is called supersaturated and has the potential to precipitate (99). Thus, through the common ion effect (i.e., by the addition of sodium oxalate, $Na_2C_2O_4$), if $(C_2O_4^{2-})_{eq}$ activity is high, Equation [2.3] dictates that $(Ca^{2+})_{eq}$ is low and vice-versa if $(Ca^{2+})_{eq}$ is high oxalate ion activity is suppressed.

The solubility product is defined by,

$$k_{sp} = (Ca^{2+})_{eq} (C_2O_4^{2-})_{eq} \qquad [2.3]$$

where "eq" indicates that the calcium and oxalate ion concentrations at equilibrium conditions. The solubility product is a thermodynamic constant that only changes with alterations in temperature or pressure. Thus, if citrate is added, then k_{sp} remains at a constant value but solubility of COM increases via the reaction:

$$CaC_2O_4 \bullet H_2O\,(s) + C_6H_5O_7^{3-} \rightleftarrows Ca^{2+}(aq) + C_2O_4^{2-}(aq) + CaC_6H_5O_7^{-} + CaC_2O_4^{0} \qquad [2.4]$$

The net effect of the above reaction is to shift the equilibrium toward the right hand side. Typically, free calcium will decrease because of the calcium that is sequestered in the soluble calcium complex ions, principally the $CaC_6H_5O_7^-$ species. As a consequence, oxalate activity increases and the solubility of the COM increases.

Nucleation

Nucleation is a beginning step in the formation of a crystal. During this step a crystal nuclei is formed only after overcoming the energy barrier for nucleation. Note, crystallization is dependent on saturation. The system must be supersaturated with respect to a particular mineral component. The energy barrier is dependent on Gibbs free energy of formation. From classical nucleation theory (thermodynamic theory) the free energy of formation (ΔG_f) for a spherical nucleus with radius r can be given by

$$\Delta G_f = 4\pi r^2 \gamma + 4/3\pi r^3 \Delta G_v \qquad [2.4]$$

where γ is interfacial energy per unit area of surface; ΔG_v is volume free energy. The effective combination of surface and volume terms is illustrated in Figure 2.3.

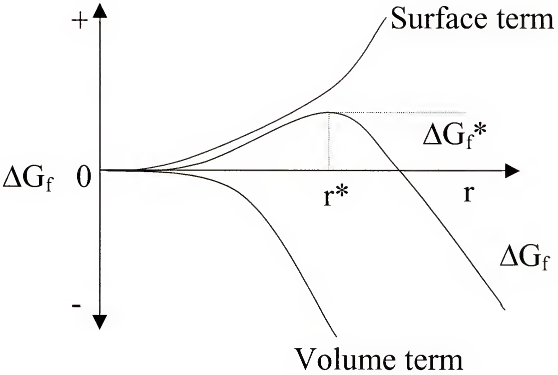

Figure 2.3. The classical schematic representation of the overall free energy during nucleation. The overall free energy change (middle curve) is a result of the two opposing energy terms. The maximum point on the middle curve represents the critical cluster size radius for nucleation to occur.

Nucleation can occur by two ways, homogeneous and heterogeneous nucleation. Homogeneous nucleation is the formation of nuclei due to supersaturation of the system alone without any foreign species. During homogeneous nucleation, an unstable cluster size is formed in the supersaturated solution (122). Depending on the solution concentration, the cluster continuously forms and dissolves until it reaches a critical radius. At critical radius, the cluster forms crystallites spontaneously where further growth is favored (123). It is unlikely that these conditions would exist in the urinary tract because there are many sites for heterogeneous nucleation. Therefore, nucleation is usually heterogeneous. Heterogeneous nucleation occurs on a foreign site such as other pre-existing crystals, macromolecules and cellular debris. For heterogeneous nucleation, lower supersaturation levels are sufficient to induce nucleation.

Crystal Growth

Crystal growth occurs by deposition of the solute on the nuclei. This can occur on the same type of nucleus (CaOx on CaOx) or on a different type of nucleus (e.g. CaOx on calcium phosphate nuclei). Therefore, stones are usually comprised of more than one type of crystal as previously mentioned. A coarsening of particles, called Ostwald ripening, can occur when varying particle sizes are present with some solubility. The smaller particles dissolve and the larger particles grow at the expense of the smaller ones. The driving force is the reduction of interfacial free energy; in essence, the lowering of the total excess surface energy of the system (123, 124). Crystal size and morphology can also be affected by ions, molecules and macromolecules in the same solution. The binding of these species on a crystal can promote or inhibit growth of specific faces of crystal. This will not be discussed in more detail because it is not a primary focus of this research.

Mixing Rate Effects on Crystallization

The action and rate of mixing affects the characteristics of the particles produced during precipitation (125-127). Rapid mixing promotes intimate contact between the reacting species under high shear conditions and thus results in more homogeneous and faster mixing than slow mixing (119, 122, 125-129). According to Nielsen (119), the mixing time controls the reaction when the half-life period or induction time is less than the mixing time. It has also been shown that unstirred solutions have a broader metastable zone than stirred solutions (128). Stirring of the solutions always leads to a narrower metastable zone (122). The metastable zone and supersaturation play a role in nucleation and growth of the particles, and thus affect the median size and breadth of the size distribution. If the supersaturation is less than the limit of the metastable zone then the clusters formed are predominately subcritical in size and the probability of nucleus formation is lower. The formation of a stable crystal nucleus can occur from a subcritical cluster either through growth or by the combination of two subcritical clusters. The probability of a stable nucleus forming decreases around the area of a cluster formation due to depletion of reactants. New material can enter this region through the actions of diffusion or stirring, followed by further nucleation (122). Ives et al. (129) concluded that for continuous flow systems to study growth via particle aggregation, a system with decreasing fluid velocity would produce coarser particles compared with particles grown in a uniform velocity.

In a study by Burns and Finlayson (43), slow mixing (mixing calcium chloride solution with potassium oxalate solution in an Erlenmeyer flask) was used to precipitate calcium oxalate at 38°C. At relative supersaturations less than 8.9, no precipitation was observed. At relative supersaturations between 10 and 50, large crystals (10 to 25 μm equivalent spherical diameter) were formed. The COM crystals were qualitatively uniform in both size and shape. When the relative supersaturation was further increased to between 80 and 140, the largest variation in both crystal size (10 to 120 μm) and shape of the precipitated COM occurred. Only at relative supersaturation levels greater than 140 were submicron crystals observed.

A study of calcium oxalate hydrate systems by Skrtic et al. (45) established that stirring conditions have a significant effect on the nature of the product. Calcium oxalate trihydrate (COT) was formed by a magnetic stirrer, whereas mixtures of COM and calcium oxalate dihydrate (COD) were formed by mechanical stirring. An unstirred solution produced a mixture of COM and COT. Skrtic et al. also qualitatively observed that higher temperatures (303 K and 310 K) caused a significant amount of dihydrate and trihydrate to transform to the thermodynamically stable phase of monohydrate within 1 hour (45). Füredi-Milhofer et al. (46) concluded that stirring precipitating solutions changes both the induction time and the composition of the precipitate. Stirred solutions tended to produce COT, while the unstirred solutions produced COM. Füredi-Milhofer et al. concluded that the formation of COT was related to kinetic features rather than to thermodynamic principles. In a study performed by Brown et al. (47), a significant correlation was observed between mechanical energy input and apparent interfacial energy. The induction time decreased with increasing shaker speed. In this study, the electrical sensing-zone technique similar to that employed by Robertson (130) was used to determine the effect of mixing rate of the reactants on size distribution of precipitated COM particles (131).

Crystal Aggregation and Dispersion

Aggregation is the process of crystals adhering together to form a larger mass. The aggregation of COM is recognized as an important part of kidney stone development (100, 132). Aggregation of crystals is thought to be one of the major mechanisms causing stone formation (133). The tubules of the kidney are large enough for small crystals, approximately 2 μm, produced daily (inner tubule diameter 14-100 μm) (134). These small crystals do not have enough time to become large enough crystals by growth alone to occlude because within the renal tract the flow is sufficiently fast to excrete small crystals. This is supported by the prediction of Finlayson and Reid (135) based upon the hydrodynamics in the nephron and measured rates of crystal growth for COM. Kok and Khan (134) indicated that freely flowing particles in the nephron could aggregate based on better estimates of diameters throughout the nephron. It has been shown that stone formers produce larger crystals and more aggregated crystals during crystalluria than non-stone formers (136-138). COM particles have also been shown to attach to epithelial wall of nephron in a rat model (135, 139). The attachment of aggregates to tubular cells can cause extensive damage and possibly lead to kidney dysfunction. In this research, we will be concentrating on the aggregation aspects of COM particles.

The actual mechanism(s) of aggregation in the kidney have not been critically studied. Aggregation can be controlled by several different forces including electrostatic repulsion or attraction, van der Waals forces, polymer bridging, and shear forces (36, 42, 99, 100, 140). Some other aggregation mechanisms, which encompass some of these forces, are heterocoagulation and secondary nucleation and growth (48). Heterocoagulation is aggregation of at least two different materials (48). Heterocoagulation occurs when two materials with different surface charge polarity are attracted by either electrostatic and or van der Waal attractive forces. A possible example is a positively charged COM particle coagulated with negatively charged hydroxyapatite. Secondary nucleation and growth is possible when a COM particle adheres to tubule walls of the kidneys. This allows for secondary nucleation to occur and/or subsequent growth due to aggregation of other crystals. The forces and aggregation mechanisms are discussed in a later section.

Disaggregation (dispersion) is favored by repulsion between the same charged crystals. On the other hand, shear force has a dual role. The shear force due to stirring of crystal suspensions or by solvent flow in tubules can cause disaggregation. While, shear forces can promote aggregation by increasing particle collisions (36).

Previous research on calcium oxalate has some conflicting results as to the role of some urinary species. Citrate and urinary proteins are of particular interest in this study. Most previous experiments were performed by changing one variable at a time instead of changing several variables at the same time to understand the whole picture. For example, low citrate concentration contributes to crystal aggregation in stone-formers (3). Kok et al. (1990) also showed that at higher citrate concentrations, aggregation was inhibited in normal and stone former urine (4). In contrast, Hess et al. (5) showed that citrate did not affect aggregation at various concentrations (10^{-6} to 10^{-3} M citrate) in a Tris-HCl buffer. However, it was shown that protein influenced aggregation depending on the pH concentration. For instance, at pH 7.2, Tamm-Horsfall protein (THP) and nephrocalcin (NC) inhibited aggregation. On the other hand, at pH 5.7, THP and NC promoted aggregation. At low THP concentration, crystal growth was not affected by THP (141). Benkovic et al. in their research, showed THP to promote aggregation (6). In a more recent work by Hess et al., an increase in citrate (1.5-3.5 mM) was found to cause an increase in inhibition of aggregation. In addition, THP with citrate enhanced the inhibitory effect of THP (7). In summary, there are conflicting statements about the role of various species such as citrate and protein in this complex system. To understand how particles could aggregate, the fundamentals of particle-particle interactions are discussed.

Particle-Particle Interactions

Particles in solution are constantly in motion. Small particles (<1 μm) are moving due to Brownian motion; whereas, larger particles (>5 μm) are moving due to gravity and convection currents. The constant movement of particles causes the particles to get closer to each other leading to possibility of interactions among these particles. Such interactions could result from several reasons as discussed later. Particle-particle interaction can lead to stabilization (dispersion) or aggregation. When repulsive forces dominate, the particles repel each other resulting in stabilization. If attractive forces dominate, the particles attract each other resulting in aggregation. The interaction forces such as electrostatic repulsion, steric repulsion, and van der Waals are discussed below. The determining factor for the behavior of particle-particle interactions depends on surface charge of the particles and solution in which the particles are suspended.

Electrostatic Repulsion

When a solid particle is immersed in a solution, surface charge may form due to surface adsorption of ions, surface ion imbalance, defect structures in the crystal lattice, or ionic exchange and dissociation of surface acids (142). The excess ions present on the surface of the solid and surrounding ionic species is illustrated by the Gouy-Chapman electrical double layer model (Figure 2.4). The double layer consists of an inner layer with oppositely charged ions to the surface, the Stern layer, and an outer layer called the Gouy-Chapman layer or diffuse layer. The charge density of the diffuse layer decreases rapidly with increasing distance from the solid surface.

The electrostatic potential for low potentials (25 mV or less) is given by the Debye-Hückel approximation (143).

$$\psi = \psi_o \exp(-\kappa x) \qquad [2.5]$$

where ψ is the potential as a function of distance into the solution, ψ_o is the surface potential, κ is the Debye-Hückel parameter (1/length) and x is the distance from solid surface. The thickness of the double layer is dependent on Debye-Hückel parameter.

$$\kappa = \left(\frac{e^2 \sum_i n_i^0 z_i^2}{\varepsilon k T} \right)^{1/2} \qquad [2.6]$$

where e is the charge of an electron, n_i is the number of ions of type i per unit volume in the bulk solution, z_i is the valence of ions of type i, ε is the dielectric permittivity of solvent, k is Boltzmann constant, and T is temperature (Kelvin). The thickness of the double layer, the Debye length, is $1/\kappa$. The Debye length is dependent on temperature and ionic strength. The ionic strength (I) is given by:

$$I = \frac{1}{2} \sum_i \left(c_i z_i^2 \right) \qquad [2.7]$$

where c_i is the solution concentration in molarity (moles per liter). As ionic strength is increased, the double layer is compressed due to the increased concentration of ions in solution. The increased concentration of ions near the charged particle surface causes the electrical surface charge to be neutralized by counterions in solution. A schematic showing the ionic cloud size change due to low and high ionic strength is illustrated in Figure 2.5.

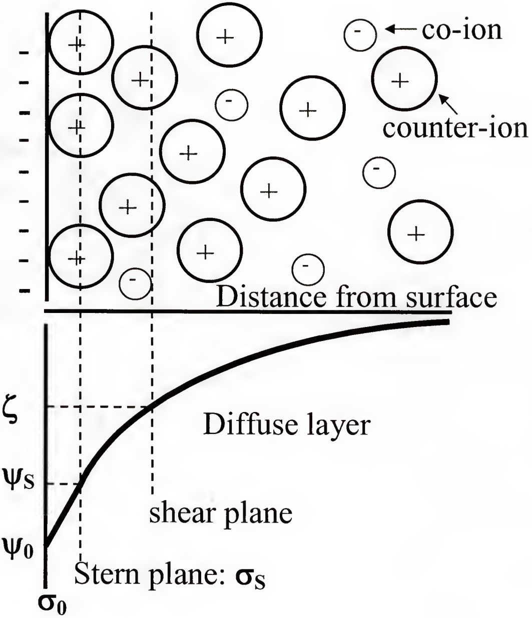

Figure 2.4. A schematic diagram of the electrical double layer.

As two particles of the same charge approach each other, the double layers will begin to overlap and the particles will repel each other due to electrostatic repulsion. If the double layer is compressed due to high ionic strength or low surface potential, then as the particles approach each other, van der Waals forces will take over and the particles will aggregate.

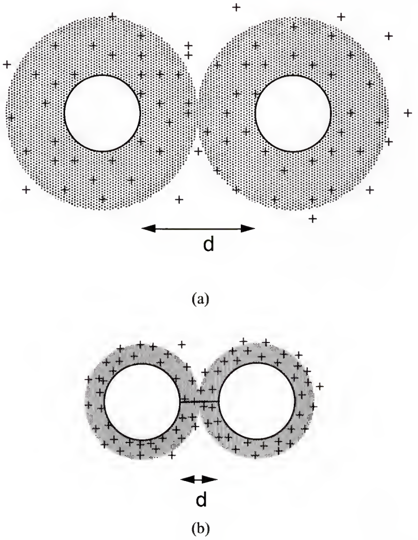

(a)

(b)

Figure 2.5. The effect of ionic strength on the double layer. a) At low ionic strength, the double layer separation is large b) At high ionic strength the double layer is compressed.

Steric Repulsion

Steric stabilization is stability imparted by polymer molecules (macromolecule composed of many monomer units) or protein molecules (copolymer of amino acids) adsorbed onto or attached to a particle. As two polymer/ protein coated particles approach each other a repulsion force is formed between the polymer/ proteins, and as a result, the coated particles repel each other. Steric stabilization is possible under certain conditions. If the polymer is in a good medium, then the polymer is not packed tightly against the surface. The polymer creates a barrier that cannot be easily compressed. As the polymer segments are forced together by approach of another surface, this restricts their interaction with the liquid (entropy decreases). Thus, an increase in free energy occurs due to a decrease in entropy and appears as a repulsive force as confirmed from Equation 2.8. The free energy of mixing (ΔG_{mix}) of adsorbed molecular chains is given by (144)

$$\Delta G_{mix} = \Delta H_{mix} - T\Delta S_{mix} \qquad [2.8]$$

where ΔH_{mix} is enthalpy of mixing and ΔS_{mix} is entropy of mixing. If ΔH_{mix} is positive and/or ΔS_{mix} is negative, then ΔG_{mix} is positive leading to repulsion. This is for a well-anchored soluble polymer that does not move out of the way of an approaching particle. Generally speaking, an uncharged polymer is not affected much by ionic strength like electrostatic repulsion. Note, at ionic strength > 10^{-2} M of 1:1 electrolyte, the electrical double layer is so small (3 nm) that the electrostatic repulsion may not overpower the van der Waals attraction (142).

Steric interactions are dependent on the quantity or coverage of adsorbed polymer layer on each surface, if the polymer is adsorbed from solution (reversible) or irreversibly grafted to the surface, and the quality of solvent (145). If the polymer is charged then the polymer can give electrosteric stabilization (electrostatic stabilization and steric stabilization).

Some possible conformations of adsorbed polymer are illustrated in Figure 2.6. The size of polymer can be described by the given equation

$$R_F = \alpha R_g \qquad [2.9]$$

where R_F is the Flory radius, α is the intramolecular expansion factor, and R_g is unperturbed radius of gyration. If coverage of polymer is neither too high nor too low, then bridging of polymer to more than one surface is favorable. Bridging can be formed between particles by a polymer (segment-surface attractive) attaching to another particle with unoccupied or exchanging binding sites.

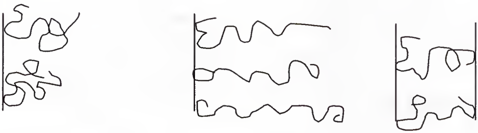

Mushroom shaped
$R_g = R_F$

Brush Border
$L >> R_F$

Bridging

Figure 2.6. Possible conformations of adsorbed polymer on surfaces. a) adsorption at low surface coverage with no overlap with another surface b) adsorption at high coverage c) bridging between two surfaces (Modified from Israelachvili)(145).

One theory of steric interactions is given by Alexander-de Gennes. At high coverage of adsorbed or grafted polymer chains, the polymer chains are forced so close together that they are forced to extend away from the surface (> Rg). For a brush in a theta-solvent, its thickness is given by (146)

$$L = \frac{nl^{5/3}}{s^{2/3}} = \Gamma^{1/2} R_F^{5/3} \qquad [2.10]$$

where L = thickness of brush, n = number of segments, l = effective segment length, s = mean distance between attachment points, Γ = number of monomers adsorbed per unit area. When two brush-bearing surfaces are closer than 2L from each other, the polymer concentration inside each barrier increases. This causes two forces to contribute to the interaction: 1) osmotic pressure and 2) elastic energy, which can be illustrated by Alexander-de Gennes theory (145, 147, 148)

$$P(D) \approx \frac{kT}{s^3\left[\left(\frac{2L}{D}\right)^{9/4} - \left(\frac{D}{2L}\right)^{3/4}\right]} \text{ for } D < 2L \qquad [2.11]$$

where k = Boltzmann constant, T = absolute temperature, D = distance between two interacting plates. The first term is osmotic repulsion between the coils, which favours their stretching and increases D. The second term is elastic energy of chains, which opposes stretching and decreases D.

Attraction

The tendency towards aggregation of particles can occur due to attractive energies, van der Waals and oppositely charged electrostatic potentials. The attractive van der Waals energies exist whether the particle is in solution or not. The van der Waals energies are comprised of intermolecular energies between ions, molecules, and electrons of the particles interacting across a dielectric medium (144). The van der Waals interactions are mostly due to Keesom, Debye, and London interactions (144, 145). The Keesom energies (orientation) are due to dipole-dipole interactions between particles.

The Debye interaction (induction) is dipole-induced dipole interaction where a permanent dipole in a particle induces electronic polarization in another interacting particle. Keesom and Debye only occur in the presence of a material with one or more dipoles. The London energies (dispersion) are more common because molecules do not need permanent dipoles. The London interaction occurs by the fluctuating electron distribution around one atom or molecule that creates a temporary dipole. This temporary dipole induces dipoles in a neighboring atom or molecule.

To model the van der Waals energies between two particles, there are two approaches, a microscopic approach (149, 150) and a macroscopic approach. The microscopic approach assumes an equation that sums the energies of all the atoms in one body with all the atoms in the other interacting body, and can be used to derive an expression for the energy of attraction. This can be carried out based on geometry such as plate-plate, sphere-plate, and sphere-sphere interaction. For example, for a sphere-sphere interaction (144):

$$W_{sph/sph} = \frac{AR}{12H} \qquad [2.12]$$

where W is the interaction energy, A is Hamaker constant (material constant in Joules), R is particle radius, and H is separation distance between the surfaces.

The macroscopic approach calculates the attraction between two materials based on differences in their dielectric spectra (151). Lifshitz and co-workers demonstrated that an understanding of the dielectric constant over as broad a frequency range as possible is required to reconcile all of the various possible intermolecular interactions between particles in order to calculate the most accurate Hamaker constant (145). An approximation of Hamaker constant, A_{131}, material 1 interacting with the same material through medium 3 can be calculated using the Tabor-Winterton approximation given by (152)

$$A_{131} = \frac{3kT}{4}\left(\frac{\varepsilon_1(0) - \varepsilon_3(0)}{\varepsilon_1(0) + \varepsilon_3(0)}\right)^2 + \frac{3h\omega_{UV}}{32\pi\sqrt{2}}\frac{\left(n_1^2 - n_3^2\right)^2}{\left(n_1^2 + n_3^2\right)^{3/2}} \qquad [2.13]$$

where k is Boltzmann's constant, T is temperature, $\varepsilon(0)$ is static dielectric constant, n is indices of refraction in visible range, h is Planck's constant, ω is characteristic absorption frequency in IR and UV regions.

The total van der Waals interaction energy between surfaces can be reduced by two phenomena, retardation (153-155) and screening (154).

Interaction Energy

The theoretical total interaction energy between two particles is the sum of van der Waals and electrostatic energies known as DLVO theory named after the founding scientists, Derjaguin-Landau-Verwey-Overbeek (156, 157). An interaction energy plot as a function of separation distance is illustrated in Figure 2.7 for two interacting particles across a medium. The repulsive and attractive energies are shown along with the total interaction energy curve (sum of the two energies). The electrolyte concentration and surface potential determines the interaction energy and behavior between two particles.

As two highly charged particles in dilute electrolyte with large double layer approach each other, the double layers begin to overlap and the particles repel each other due to electrostatics energies. This strong long-range repulsion peaks at the potential energy barrier to aggregation between 1-4 nm (145). If the surface potential is high, then the energy barrier will be high. In contrast, if the surface potential is low, then the energy barrier will be low.

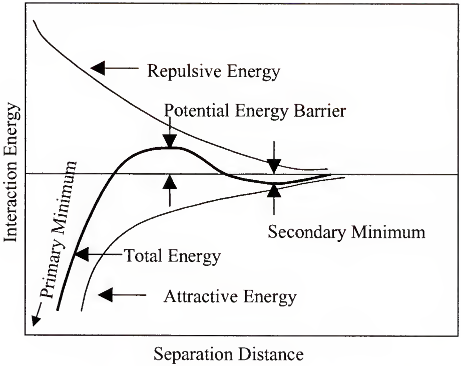

Figure 2.7. A schematic of interaction energy as a function of separation distance. The attractive, repulsive and total energy curves for two interacting materials are shown.

In more concentrated electrolyte solutions, a secondary minimum forms due to van der Waals attraction. A secondary minimum well arises usually beyond 3 nm before the energy barrier (145). When two interacting particles are in the secondary minimum, they form a weak aggregate that can be dispersed with the addition of energy.

If the surface potential of two approaching particles approaches zero (compressed double layer), then van der Waals attraction dominates. The two surfaces are attracted and results in the particles aggregating (interaction energy is located in the primary minimum of the potential energy well). When two particles are in the primary minimum energy well, the two materials are in contact and cannot be easily separated.

As ionic strength is increased, van der Waals attraction begins to dominate and instability may occur. This is comparable to the studied system, which has ionic strength ranging from 0.3–0.36 M. Under these conditions, DLVO assumes aggregation at all conditions. However, DLVO theory fails in describing this system because it does not take into account steric energy produced by proteins. In this study, the interaction energy includes van der Waals, electrostatics, and steric energies.

Adsorption

In previous sections, some of the ions, molecules, and macromolecules found in urine have been discussed. In order for most of these species to influence the formation or interaction of crystals, they must be adsorbed onto crystal surface. Some of the possible mechanisms for adsorption will be discussed for ions, small molecules, and macromolecules.

Ions

Some ions can act as inhibitors of crystal aggregation. They act either by complexing a promoter, by binding to the growth sites, or forming a complex with polyanions that blocks crystal growth sites (158). For example, magnesium is known as a chelator of oxalate ions. Magnesium forms a soluble complex with oxalate; thus, reducing CaOx supersaturation. This lowers the likelihood of CaOx crystal formation.

Small Molecules

Small molecules include mineral or organic acids and amino acids. Of particular interest are pyrophosphate and citrate. Pyrophosphate is mainly an inhibitor of calcium phosphate but has been shown to moderately inhibit the crystal nucleation of CaOx by increasing CaOx formation product (159). It has also exhibited crystal growth inhibition by attaching to the growth sites on crystals (160).

Citrate, a negatively charged species, is generally considered to competitively bind to calcium ions. This reduces CaOx supersaturation by reducing the amount of free calcium able to bind with oxalate; therefore, the amount of CaOx crystals formed is reduced. From some studies, citrate was shown to bind onto specific crystal faces and can modify the crystal shape and size (160-163). Low molecular weight species are not considered to be the primary urinary inhibitors (20-30% total inhibition) (164). Macromolecules appear to be the most efficient inhibitors based on *in vitro* experiments.

Macromolecules

The macromolecules role in inhibition is influenced by the concentration of the promoter of stone formation, ionic equilibrium of the medium, and possibly interactions with other urine species (101, 165). Proteins are known to adsorb onto many different substrates (166). The macromolecule of interest in this study is Tamm-Horsfall protein (THP). THP may adsorb onto the surface of CaOx crystal by binding to calcium (98). The adsorption of THP on CaOx crystals could form a steric barrier to other interacting crystals. A description of macromolecule adsorption was described in the Steric Repulsion section.

Experimental Designs

Typically, kidney stone research is performed using one-variable-at-a-time strategy to evaluate different factors. One-variable-at-a-time strategy does not give synergistic or antagonistic effects that can arise in a complex system. This technique is inefficient since the results do not span a region of confidence, and consequently, optimum results may not be obtained. Statistical experimental designs usually require fewer number of experiments, give main effects of several variables at same time, and the interaction effects between variables can be estimated. Most importantly, the optimum conditions can be more easily obtained. In addition, experimental designs may lead to the development of a mathematical model that can be obtained to predict factor effects within the design region. Another important advantage of statistical experimental designs is estimation of variance and its sources. Thus, information about statistical significance of the effects is obtained.

There are many different types of design of experiments (DOE) such as Taguchi, Plackett-Burman, factorial, central composite, Latin squares, Box-Behnken, etc. (167-169). When using DOE, one must first pick a design that best fits experimental needs. After experiments are conducted, main effects of factors are calculated from experimental values of the response variable. The main effects are tested for statistical significance and conclusions are drawn. The two experimental designs used in this research, Plackett-Burman and *rotatable* central composite, are discussed in the following paragraphs.

Plackett-Burman Design

The Plackett-Burman design is used as a screening design in the early stages of research to identify the most significant variables, especially when the number of variables is so large that excessive time and cost are required if studied by using one-variable-at-a-time strategy. Even other experimental designs that require a larger number of experimental runs may not be as useful at this stage. The Plackett-Burman design is based on $n = (N-1)$ where n is the number of variables and N is the number of experimental runs, which must be a multiple of four. For example, for 15 factors there would be 16 experimental runs. The selection of variables depends on the experimenter, but usually at least three variables are used as dummy variables. The dummy variables are used to calculate the variance of the experimental design.

A screening statistical design, called Plackett-Burman design, is utilized to determine which of the studied factors are statistically significant at a pre-determined confidence level. In this study, 16 experimental runs are used to study 15 factors.

Central Composite Design

Several different types of designs are useful when one is attempting to fit a response surface. A response surface is a way to plot a response variable as a function of two or more factors. Complete and fractional factorial experiments in completely randomized designs are extremely useful when one is exploring the factor space in order to identify the region where the optimum response is located.

When one has located the region of the optimum response, curvature can be pronounced. Three or higher level factorial experiments are often conducted in order to fit such response surfaces. Designs that give equal precision for fitted responses at points (factor-level combinations) that are at equal distances from the center of the factor space are termed as *rotatable* designs. Rotatability is a desirable property for response-surface models because prior to the collection of data and the fitting of the response surface, the orientation of the design with respect to the surface is unknown. Thus, exploration of the response surface is dependent on the orientation of the design. In particular, procedures such as the method of steepest ascent, which utilize the fitted response surface, can be jeopardized if some estimated responses are less precise than others.

One of the designs that make efficient use of the experimental units or test runs is the central composite design. In this study, a *rotatable* central composite design is used to determine the interaction effects of the three most significant factors and to give surface responses for the studied factors. The response surfaces are obtained from fitting the response variables to a second-order polynomial. In this design, the central points (0,0,0) were repeated several times to obtain the variance of the analysis.

Characterization Techniques

A few of the characterization techniques used in this research are discussed below, including atomic force microscopy, electrokinetic measurements, protein quantification, and ion chromatography.

Atomic Force Microscopy

The atomic force microscopy (AFM) is used to measure topography of a sample and interaction forces between a sample and an AFM tip (either tip or a particle attached to the tip) on an atomic level. A schematic of an AFM is illustrated in Figure 2.8. In brief, the AFM is operated by mounting a sample on top of the piezoelectric scanner. The AFM tip, also called cantilever, is above the sample. A laser reflects from the cantilever to a mirror onto a photodetector. As a sample is raised towards the tip, any interactions between the sample and tip cause the cantilever to bend up or down depending on whether the force is repulsive or attractive. Any movement of the cantilever is detected by a photodetector; therefore, the interaction force between a sample and tip are detected.

In this study, the AFM is used to measure the force between a silicon nitride (SiN) tip and a COM surface. The force measurements were performed using the SiN tip because the COM particles being used in this study were 10 μm x 20 μm; therefore, there is a greater chance for the tip to be on a particle. Also, the AFM technique measures at atomic levels and the COM particles being used were not atomically smooth. For the preliminary AFM study, just using the AFM tip interacting with a COM particle was the best choice to see if there are any repulsive forces in the presence of protein.

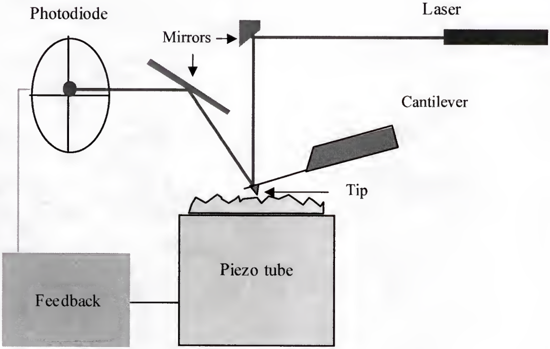

Figure 2.8. A schematic of atomic force microscopy.

Electrokinetic Measurements

Electrokinetic measurements are useful in determining zeta potential of particles (potential at the shear plane; illustrated in Figure 2.4). The electrokinetic technique that is discussed is electrophoresis.

In electrophoresis, an electrical field is applied to a suspension and the particles move in the field in the direction determined by the charge of the particle (towards the oppositely charged electrode). The particle velocity is measured under the applied electric field. The electrophoretic mobility, particle velocity per unit static electric field, can be determined from the particle velocity. The corresponding zeta potential, ζ, is calculated from electrophoretic mobility, μ_E, using Smoluchowski equation (143)

$$\zeta = \frac{\eta \mu_E}{D \varepsilon_0} \qquad [2.14]$$

where η is viscosity of solution, D is dielectric constant of solution, ε_0 is permittivity of free space. Several techniques can be used to determine electrophoretic mobility under an applied electric field, such as optical method, electrophoretic light scattering, and electroacoustics.

Protein Quantification

The Lowry protein assay is the most widely cited method for protein quantification. The modified Lowry protein assay developed by Pierce Chemical Co. (Rockford, IL) is discussed. The assay uses a modified cupric sulfate-tartrate reagent that replaces 2 of 3 reagents in the original Lowry method (Lowry alkaline copper-tartrate reagent) with 1 stable reagent. The modified Lowry assay contains two reagents, 2N Folin-Ciocalteu Reagent and Modified Lowry Protein Assay Reagent (cupric sulfate, potassium iodide, and sodium tartrate in an alkaline sodium carbonate buffer). The first step of the Lowry method is the reaction of the protein with reagent containing alkaline cupric sulfate in presence of tartrate (Equation 2.15). The second step involves the addition of dilute Folin-Ciocalteu phenol reagent to the product formed in the first step

(Equation 2.16). A water-soluble blue colored product is formed due to the reduction of Folin-Ciocalteu phenol reagent. The concentration of blue can be measured at 750 nm using an ultraviolet/visible spectroscopy and a calibration curve plotted.

Reaction 1: Protein (peptide bonds) + $Cu^{+2} \xrightarrow{OH^-}$ tetradentate-Cu^{+1} complex (1) [2.15]

Reaction 2: (1) + Folin phenol + Phosphomolybdic/phosphotungstic acid complex $\longrightarrow$ Blue colored complex read at 750 nm [2.16]

In this study, a modified Pierce Lowry Protein Assay was used to quantify the amount of protein adsorbed on COM particles.

Ion Chromatography

Ion chromatography is a high performance version of ion-exchange chromatography. There are two types of ion chromatographs, 1) suppressed-ion anion and cation chromatography and 2) single-column ion chromatography. The suppressed-ion anion and cation chromatography is the type of chromatography used in this study.

In the suppressed-ion anion chromatograph, a mixture of anions from a sample is separated by ion exchange with an eluent. The length of time that the anions remain on the column depends on the ionic strength and size of anion. The higher the ionic strength and/or larger the size of the anion, the longer the anion is retained. The ion exchange takes place with the eluent, which is 80 mM NaOH in this study. The eluent is then suppressed by being neutralized with a membrane ion suppressor in which cations are replaced with H^+ that turns the eluent into water. The membrane suppressor repels anions but allows cations to pass freely. Therefore, the electrical conductivity (method of detection) is negligible for the eluent and most samples will result in a detectable conductivity. The anion concentration is determined by performing a linear regression calibration. Generally, the higher the conductivity of anion means the higher the concentration.

The suppressed-ion cation chromatography is conducted in a similar manner as the previously described chromatograph. However, the membrane suppressor is replaced by an anion-exchange suppressor column loaded with OH^-.

A background of previous literature and an understanding of the kidneys, crystallization, interparticle forces and adsorption have been given. The materials and methods used in this study are described in the next chapter.

CHAPTER 3
MATERIALS AND METHODS

Preliminary Studies

Crystallization Study

Saturated COM solution preparation

A 1.0 M solution of calcium chloride dihydrate ($CaCl_2 \bullet 2H_2O$, A.C.S. Grade, 74%-78% assay, Fisher Scientific Inc., Fair Lawn, NJ) was prepared in deionized (DI, < 0.06 μS/cm specific conductivity) water. A 1.0 M solution of potassium oxalate monohydrate ($K_2C_2O_4 \bullet H_2O$, A.C.S. Grade, 100.8% assay, Fisher Scientific Inc., Fair Lawn, NJ) was prepared in a similar manner. The two solutions were mixed together and allowed to precipitate for 5 minutes. The precipitation occurred instantaneously. The suspension was centrifuged, supernatant decanted, and the solids washed with DI water until the measured conductivity of the supernatant reached a plateau (fairly constant value). The precipitate was dried overnight at 90°C. The obtained powder was examined by X-ray diffractometer and determined to be COM. The powder was placed into a wet 12,000 Da dialysis bag. Any residual air in the dialysis bag was removed. The dialysis bag was placed into DI water and allowed to dialyze for 24 hours before being used.

COM particles without seeds using different mixing rates

COM particles were grown by homogeneous nucleation at two different mixing rates, slow mixing and rapid mixing. A processing schematic for the preparation of COM crystals without seeds is shown in Figure 3.1. A 500 ml 10^{-3} M solution of calcium chloride dihydrate ($CaCl_2 \cdot 2H_2O$, A.C.S. Grade, 74%-78% assay, Fisher Scientific Inc., Fair Lawn, NJ) and a 500 ml 10^{-3} M solution of potassium oxalate monohydrate ($K_2C_2O_4 \cdot H_2O$, A.C.S. Grade, 100.8% assay, Fisher Scientific Inc., Fair Lawn, NJ) were prepared in deionized (DI, < 0.06 μS/cm specific conductivity) water. The calcium solution was prepared daily to minimize calcium carbonate formation by reaction with carbon dioxide in the air. The solutions were filtered through a 0.22 μm filter paper (AcetatePlus, supported, plain, 47 mm, Micron Separations Inc., Westboro, MA) and stored in Nalgene® bottles. Using the computer program, EQUIL (52), the relative supersaturation for the Ca^{2+}(aq) and $C_2O_4^{2-}$(aq) solutions combined was calculated to be 58, with an ionic strength of 3.8×10^{-3} M.

Slow mixing. In the slow mixing method, the two 500 ml solutions of calcium and oxalate were equilibrated to physiological temperature, 37°C, in an isothermal water bath (Thermopet NTT-120, Tokyo Rikakikai, Co., Ltd.). The $K_2C_2O_4$ solution was transferred to a HDPE container (Fisherbrand) and the $CaCl_2$ solution was added. The $K_2C_2O_4/CaCl_2$ solution mixture was shaken manually several times by moving the container up-and-down and kept in a water bath at 37°C for 22 hours to allow precipitation of COM particles.

Rapid mixing. Figure 3.2 illustrates the flow system of rapid mixing apparatus that was used to precipitate calcium oxalate monohydrate via nozzle mixing along with a schematic of the nozzle in cross-section. To conduct all precipitation runs at physiological temperature (37°C), the flow system was enclosed in an insulated box thermally regulated with four heating lamps operated by a temperature controller and an internal fan for forced convection heat transfer. The temperature of the system was maintained at 37 ± 1°C. The 35"x 35"x 16" temperature control box was composed of five plywood sides on a 1"x 1" frame board. The five sides were insulated with 3/4" insulation boards with a Plexiglass® viewing window on the front wall. Polypure tubing connected each of the polyvinylchloride (PVC) sample containers (one for $CaCl_2$ and one for $K_2C_2O_4$) to the polymer mixing nozzle, and polypure tubing connected the mixing nozzle to a collection vessel. The fluid flow dynamics in the rapid mixing nozzle was determined to be in the turbulent regime. The Reynolds numbers for the inlet and outlet of the nozzle were calculated to be 6130 and 3531, respectively. Both of these Reynolds number values are well above the minimum value of 2300 to be considered in the turbulent regime (170). Each PVC container was calibrated to a flow rate of approximately 115 ml/min using DI water. Between each run, the mixing system was flushed with DI water.

The $K_2C_2O_4$ and $CaCl_2$ solutions were heated to 37°C in the constant temperature bath. The heated 500 ml solutions were transferred to their respective PVC containers and the heat source (four 100 W light bulbs) and the fan were immediately turned on. The temperature of the mixing system was controlled by a J-type thermocouple connected to a temperature controller (Parr Instrument Company, Moline, IL). The rapid mixing apparatus was heated to an average temperature of 37°C and held constant for 30 minutes. The sample cylinders were pressurized to 0.21 MPa (30 psi) utilizing an external ultra-high purity argon gas tank (Figure 3.2). The shut-off valves were simultaneously opened and the precipitating solution emerging from the nozzle was collected in a 1.9 L HDPE container within 10 minutes. The precipitating solution was transferred to the isothermal bath at 37°C, where COM particles were aged for 22 hours.

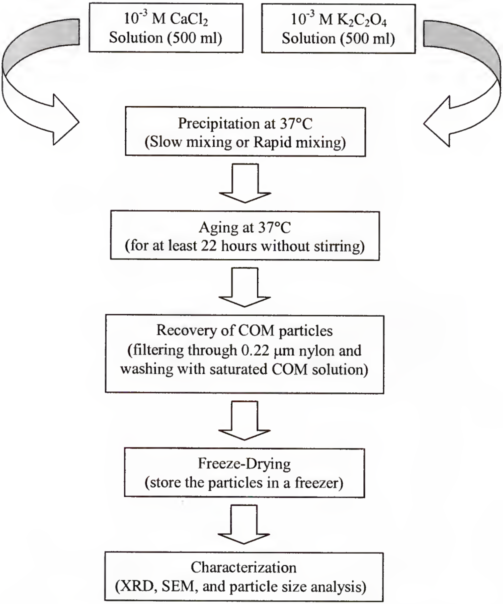
10^{-3} M $CaCl_2$ Solution (500 ml)
10^{-3} M $K_2C_2O_4$ Solution (500 ml)
Precipitation at 37°C (Slow mixing or Rapid mixing)
Aging at 37°C (for at least 22 hours without stirring)
Recovery of COM particles (filtering through 0.22 μm nylon and washing with saturated COM solution)
Freeze-Drying (store the particles in a freezer)
Characterization (XRD, SEM, and particle size analysis)

Figure 3.1. Schematic representation of processing steps for the preparation of COM crystals without seeds using two different mixing rates.

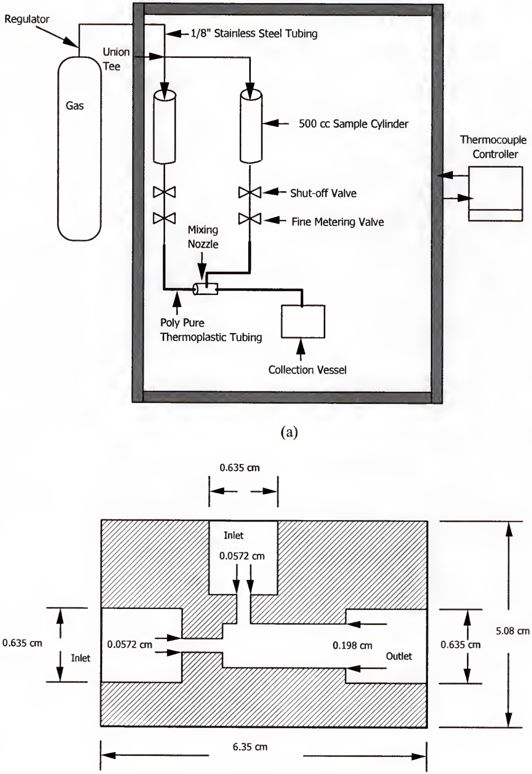

(a)

(b)

Figure 3.2. Schematic of rapid mixing apparatus (a) Flow system, (b) cross-sectional side view of the mixing nozzle.

After the precipitation time of COM crystals, the pH of the precipitated solution was measured (PHM64 Research, Radiometer, Copenhagen, Denmark) and the solution was filtered using 0.22 μm filter paper (AcetatePlus, supported, plain, 47 mm, Micron Separations Inc., Westboro, MA). The collected particles were washed with 200 ml of saturated COM solution to remove the spectator ions while minimizing dissolution of particles. The particles were then placed in a vial containing saturated COM solution, with the exception of samples RM16 and RM17. These two samples were freeze-dried for 5 hours (Labconco Freeze Dryer 4.5, Labconco Corp., Kansas City, MO.) then stored in a freezer. In previous crystallization, the collected precipitate was stirred with a paddle stirrer. It was discovered that the stirring caused more interpenetrating twins to be formed due to the shear force. Also, Photometric Dispersion Analyser (PDA) was used to measure the induction time, but the Tygon tubing that ran through the PDA acted as a nucleating site.

Characterization of grown COM crystals by two different mixing rates

X-ray diffraction (XRD) patterns of all precipitates formed by slow mixing and rapid mixing were obtained using an X-ray diffractometer. XRD samples were prepared by mixing a small amount of each sample with 1 drop of methanol on XRD slide. Each X-ray diffraction pattern was compared to the JCPDS reference patterns, 20-231 (calcium oxalate monohydrate).

The particle morphology of the COM particles from each batch was determined by scanning electron microscopy (SEM, JSM6400, 35CF, JEOL, Boston, MA). Each SEM sample was prepared by mounting a microscope coverslip on a SEM mount via carbon paint. A small amount of each sample was placed on a coverslip. Each SEM mount was sputter coated with gold-palladium in the presence of Argon gas. The SEM was operated at working distance of 15 mm and the voltage ranged from 10-15 kV depending on whether or not the particles were charged at the higher voltage.

Particle size and size distributions were measured using an electrical sensing zone technique (ELZONE 80XY, 48 μm aperture and 95 μm aperture, Particle Data Incorporated, Elhurst, IL). The particle sizing preparation involved lightly sonicating the COM particles in 5% NaCl/ saturated COM solution before measuring the sample in the ELZONE. An extrapolation technique was used to obtain a complete particle size distribution. Extrapolation was conducted using the computer program PeakFit© (version 4.0, Jandel Scientific, San Rafael, CA). The log-normal particle size probability distribution was used to fit the population distribution to perform an extrapolation to a nearly complete, log-normal probability distribution.

Strictly speaking, the mean ($\bar{z}$) and standard deviation (σ_z) for log-normal probability distributions should be reported in natural logarithm space. For the purpose of this dissertation, the natural logarithm space values of the log-normal probability distributions have been converted to real space (in micron units) and are therefore reported as exp ($\bar{z}$) and exp (σ_z) to provide a more relevant physical perspective for kidney stone disease. For example, a log-normal distribution mean of $\bar{z} = 2.5$ is reported as 12 μm, while a standard deviation of 0.4 is reported as $-\sigma_z = 8.2$ μm and $+\sigma_z = 18$ μm.

"Fine" COM particles with seeds

"00" COM seed particles preparation. A 1.0 M 50 ml solution of $CaCl_2{\bullet}2H_2O$ was prepared in deionized (DI, < 0.06 μS/cm specific conductivity) water. A 1.0 M 50 ml solution of $K_2C_2O_4{\bullet}H_2O$ was prepared in a similar manner. The solutions were filtered with 0.22 μm filter paper (MAGNA, nylon, supported plain, MSI, Westboro, MA). The two solutions were added to a polymer container and instantly precipitated. The powders were centrifuged and rinsed with saturated COM solution until the measured conductance stabilized. The seeds were freeze dried and stored in the freezer for future use.

Optimization of fine COM particles. The goal was to produce COM particles with the size of less than 1 μm with a prismatic shape and with few interpenetrating twins. To achieve this goal, several batches of COM particles were made. The order of addition of calcium, oxalate and seed solution was important. Also, the amount of seed solution added made an effect on the size and shape of the particles. The 2 v/o COM seed solution amount varied from 0.2 ml to 1 ml using isopropanol as a dispersant to 2 L total volume. The precipitating solutions were stirred overnight. Each sample was analyzed under SEM to observe the morphology and particle size. After many different combinations, the method for preparing fine COM particles was determined. It was also determined that by not continuously stirring the precipitating solution that the particles produced had less penetrating twins. This is probably due to a reduction in shear force.

Preparation of fine COM particles. A 10^{-3} M solution of potassium oxalate monohydrate ($K_2C_2O_4 \cdot H_2O$, A.C.S. Grade, 100.8% assay, Fisher Scientific Inc., Fair Lawn, NJ) was prepared in deionized (DI, < 0.06 μS/cm specific conductivity) water. A 10^{-3} M solution of calcium chloride dihydrate ($CaCl_2 \cdot 2H_2O$, A.C.S. Grade, 74%-78% assay, Fisher Scientific Inc., Fair Lawn, NJ) was prepared in a similar manner. The solutions were prepared daily. The solutions were vacuum filtered through a 0.22 μm filter paper (MAGNA-R, nylon, supported plain, 47 mm, MSI, Westboro, MA) so that any undissolved powder would be removed. Each solution was poured into its respective 4.9 L polymer container. Figure 3.3 displays a schematic of the processing steps for the seeded COM particles. During the filtering of the solutions, a 2 volume percent seed solution of 5.0 ml of isopropanol (2-Propanol) and approximately 0.1 g of “00” COM seeds were mixed in a small vial. The seed solution was sonicated for 5 minutes to well disperse the seeds. Once all of the solutions were prepared, then they were combined in the following order: 2.0 L of potassium solution, 1.6 ml of seed solution, shaken, 2.0 L of calcium solution and shaken. The precipitating solids were allowed to grow for 24 hours. After 24 hour period, the particles were vacuum filtered using a 0.45 μm filter paper (MAGNA-R, nylon, supported plain, MSI, Westboro, MA). The collected particles were washed with 200-300 ml COM saturated solution to remove any residual ions on the particles. Each batch of particles was freeze dried and stored in the freezer for future experiments.

XRD was used to verify the fine COM particles having a pure COM phase. SEM was used to determine the morphology and approximate particle size. Each SEM sample was prepared by placing a small amount of each sample with one drop of methanol on a coverslip mounted on SEM via carbon paint. The particles and methanol were mixed to create an evenly distributed sample. Each SEM mount was sputter coated with gold-palladium in the presence of Argon gas. Particle size was measured using laser light scattering technique (Coulter LS 230, Beckman Coulter Corp., Miami, FL).

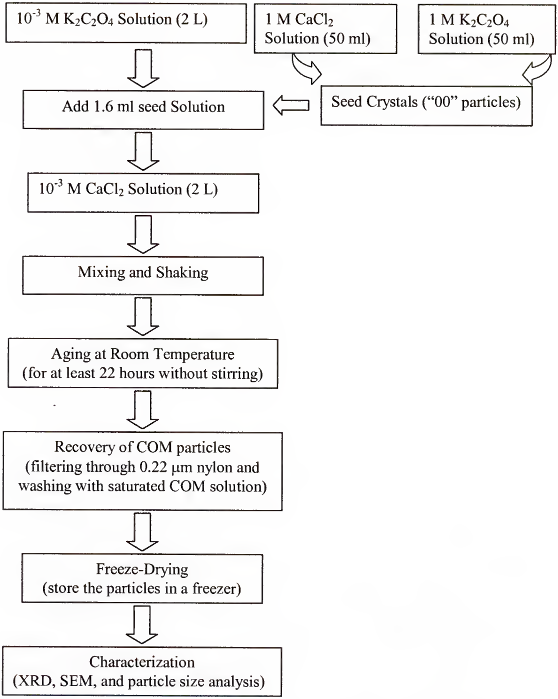
10^{-3} M $K_2C_2O_4$ Solution (2 L)
1 M $CaCl_2$ Solution (50 ml)
1 M $K_2C_2O_4$ Solution (50 ml)
Add 1.6 ml seed Solution
Seed Crystals ("00" particles)
10^{-3} M $CaCl_2$ Solution (2 L)
Mixing and Shaking
Aging at Room Temperature (for at least 22 hours without stirring)
Recovery of COM particles (filtering through 0.22 µm nylon and washing with saturated COM solution)
Freeze-Drying (store the particles in a freezer)
Characterization (XRD, SEM, and particle size analysis)

Figure 3.3. Schematic representation of processing steps for the preparation of COM crystals with seeds.

Zeta Potential Measurements of COM in Presence of Different Solutions

This study was performed to determine if sodium azide affects zeta potential of COM and the effect of calcium and oxalate on zeta potential of COM.

Sodium azide

The effect of sodium azide on COM particles was determined by zeta potential measurements. Sodium azide is commonly used as a bactericide to prevent the growth of bacteria and to destroy any bacteria in a solution. A 0.02 weight percent of sodium azide is commonly used in the presence of protein. Solutions ranging from 0 weight percent of sodium azide to 0.1 weight percent of sodium azide (NaN_3, Laboratory Grade, Fisher Scientific Inc., Fair Lawn, NJ) were produced with the addition of 0.35 g/L of fine COM particles previously produced. The solutions were equilibrated overnight and measured using ZetaPlus, Zeta Potential Analyzer (Brookhaven Instruments Corp., Holtsville, NY). A Palladium electrode was used to make the measurements.

Bovine submaxillary glands mucin

The zeta potential of mucin (mucin type I from Bovine Submaxillary glands, Sigma) was determined in ultrapure water, citrate buffer, and 0.05 M Tris (hydroxymethyl)-aminomethane Hydrochloride (Tris-HCl, Reagent Grade, Fisher Scientific Inc., Fair Lawn, NJ, pH = 8) using ZetaPlus, Zeta Potential Analyzer (Brookhaven Instruments Corp., Holtsville, NY). Tris solution is known to keep proteins well intact.

Addition of calcium to COM solutions

The zeta potential of COM particles in the presence of calcium was determined over a concentration range of 10^{-2}–10^{-5} M of calcium. The samples were prepared by using 15 ml of CO_2 free ultrapure water that was placed in a sterile 15 ml centrifuge tube.

The COM particles (0.25 g/L) were added to the water and the appropriate amount of calcium. The sample was incubated at 37°C being stirred for 2 hours. After the incubation period, the pH was measured and the zeta potential of the sample was measured using ZetaPlus, Zeta Potential Analyzer (Brookhaven Instruments Corp., Holtsville, NY). The zeta potential of various calcium concentrations with 0.01 M Tris-HCl solution in the presence of COM was also determined in a similar manner.

Addition of oxalate to COM solutions

The zeta potential of COM particles in the presence of oxalate was determined over a concentration range of 10^{-2}–10^{-5} M of oxalate. The samples were prepared in a similar way as described in the previous section. The COM particles (0.25 g/L) were added to the 15 ml CO_2 free ultrapure water and the appropriate amount of oxalate. The sample was incubated at 37°C being stirred for 2 hours. After the incubation period, the pH was measured and the zeta potential of the sample was measured using ZetaPlus, Zeta Potential Analyzer (Brookhaven Instruments Corp., Holtsville, NY). The zeta potential of various oxalate concentrations with 0.01 M Tris-HCl solution in the presence of COM was also determined in a similar manner.

Tris-HCl affect on COM particles

The zeta potential of the addition of Tris-HCl to ultrapure water was measured to determine if Tris-HCl adsorbs to the surface of COM particles. The amounts tested were 10^{-4}, $5x10^{-4}$, 10^{-3}, $5x10^{-3}$, and 10^{-2} of Tris-HCl. The COM particles (0.25 g/L) were added to 15 ml solution of the appropriate Tris-HCl concentration. The zeta potential was measured using ZetaPlus, Zeta Potential Analyzer.

Detection of Bacteria in Artificial Urine

Two bacteria tests, Bactericult and Dilution tests using Mueller-Hinton agar, were performed using the same samples to determine if bacteria will grow in the artificial urine (AUIS) without bactericide. Five samples were prepared which was ultrapure water at 37°C, ultrapure water with COM particles at 37°C, AUIS at 37°C, AUIS with COM particles at 37°C, AUIS with COM particles at room temperature. The samples were 40 ml and were equilibrated overnight at their respective temperatures. The next day mucin was added to each sample in concentration of 10 ppm and the samples were heated at 37°C for 2 ½ hours. After the heating time, the samples containing the particles were centrifuged.

The supernatant was placed in a Bactericult tube and immediately poured out. Each tube was incubated at 37°C. The Dilution tests using Mueller Hinton agar can detect small amounts of bacteria. The dilution of each sample was performed in the following manner: 1 ml of sample solution was put in 9 ml sterile water, 1/10 ml added to Mueller Hinton agar. Each sample had 400 μl of 1000 ppm mucin added (Final concentration of 10 ppm). A glass rod, soaked in 70% alcohol, was sterilized by a flame. Then the glass rod was used to spread the 1/10 ml sample solution around the agar. Each sample was diluted 1x, 2x, and 3x and placed on the Mueller Hinton agar in the same manner described previously. The agar plates were incubated at 37°C for 24 hours.

Aggregation and Dispersion Study

In this study, screening and central composite statistical experimental designs (described in Chapter 2) are used to determine the effect of various factors on the aggregation and dispersion characteristics of previously grown calcium oxalate monohydrate (COM) crystals in different urinary environments. The Plackett-Burman design was used to screen out which of the 8 factors being considered were the most statistically significant. In other words, it is a tool that helps determine which factors made the greatest impact on the aggregation or dispersion of COM particles in different urinary environments. A central composite design was used to determine if there were any interactions between the three most significant factors determined from the Plackett-Burman design.

Making Artificial Urine

The artificial urine ion solution (AUIS) was made in two parts, “5x” and “1x”. The “5x” AUIS was made of the constituents shown in Table 3.1 (171). Note, normally “5x” contains sodium citrate, but this is altered in the experiments. After the ingredients were added to ultrapure water, the powders were dissolved by stirring followed by vacuum filtering (0.22μm SFCA membrane, sterile). The “5x” AUIS was stored at 4°C for up to a week.

The second part of AUIS, “1x”, was made of the constituents shown in Table 3.1. Note, normally calcium chloride and sodium oxalate are added in “1x” AUIS, but these factors are changed in this experimental design. The pH was adjusted to 6.0 with 20 weight percent of sodium hydroxide at temperatures close to 37°C. The “1x” AUIS was filtered with 0.22 μm filter paper (Nylon, Osmonics Inc.) under vacuum.

Table 3.1. The total concentration of artificial urine displayed by the order of addition.

	Compound	Solution Concentration (M)
"5x" AUIS	NaCl	0.1055
	$NaH_2PO_4 \bullet 2H_2O$	0.0323
	$MgSO_4$	0.00385
	Na_2SO_4	0.01695
	KCl	0.0637
"1x" AUIS	NH_4Cl	0.0363
	NH_4OH	0.00062

Screening Design (Plackett-Burman Design)

The variables examined in the screening stage were calcium (10^{-4} M and 10^{-2} M), oxalate (10^{-4} M and 10^{-2} M), pyrophosphate (10^{-6} M and 10^{-4} M), citrate (10^{-4} M and 10^{-2} M), pH (5 and 8), protein concentration (0 ppm and 10 ppm), and order of addition of calcium (Day 1 and Day 2) in ultrapure water and artificial urine. The levels were chosen to encompass the extreme conditions found in urine. The Plackett-Burman design used for this study had 15 factors and 16 experimental runs (Table 3.2). For each experimental run, a sample and a control were made. The only difference between the two was the control did not have COM particles. Each sample was labeled the corresponding experimental run number, whereas, the control had the letter "C" after the run number. A schematic of the procedure followed in making the sample and control for Plackett-Burman design is represented in Figure 3.4. The sample was made by adding COM crystals (0.35 g/L) to the desired solution (ultrapure water or artificial urine) including oxalate and calcium (Day 1), and then the pH was altered using 0.001 M–1 M HCl and 0.001 M–1 M NaOH. Each sample was sonicated for 5 min. after the addition of the COM particles. The sample and control were equilibrated for over 12 hours shaking (Labquake Shaker, Barnstead/ Thermolyne) in an incubator at 37°C. The samples prepared with ultrapure water were prepared at a constant ionic strength of 0.15 M by the addition of sodium chloride. The pyrophosphate, citrate, calcium (Day 2), and protein (Mucin Type 1 from Bovine Submaxillary Glands, Sigma) were added after the equilibration time to make a total sample volume of 50 ml and shaken for 2 hours at 37°C. Again, the pH was adjusted before and after the addition of protein using diluted HCl or diluted NaOH. Protein was added after the pH was altered, so it would not have conformational changes due to pH. All of the concentrated solutions were filtered through 0.20 μm syringe filter (Sterile, SFCA membrane, 26 mm, Corning Incorporated, Corning, NY) before being added to the samples. All of the varying concentration additives (citrate, oxalate, calcium, pyrophosphate, and sodium chloride) were first made at a higher concentration in AUIS solution. A solution of 1500 ppm of mucin was made in ultrapure water. Turbidity measurements and zeta potential measurements were performed on all the experimental runs as described in sections later in this chapter. The data analysis performed is presented in Chapter 4.

Table 3.2. Experimental Plackett-Burman Design for 15 Variables

Run No.	Variable Levels														
	1	2	3	4	5	6	7	8	9	10	11	12	13	14	15
1	+	-	-	-	+	-	-	+	+	-	+	-	+	+	+
2	+	+	-	-	-	+	-	-	+	+	-	+	-	+	+
3	+	+	+	-	-	-	+	-	-	+	+	-	+	-	+
4	+	+	+	+	-	-	-	+	-	-	+	+	-	+	-
5	-	+	+	+	+	-	-	-	+	-	-	+	+	-	+
6	+	-	+	+	+	+	-	-	-	+	-	-	+	+	-
7	-	+	-	+	+	+	+	-	-	-	+	-	-	+	+
8	+	-	+	-	+	+	+	+	-	-	-	+	-	-	+
9	+	+	-	+	-	+	+	+	+	-	-	-	+	-	-
10	-	+	+	-	+	-	+	+	+	+	-	-	-	+	-
11	-	-	+	+	-	+	-	+	+	+	+	-	-	-	+
12	+	-	-	+	+	-	+	-	+	+	+	+	-	-	-
13	-	+	-	-	+	+	-	+	-	+	+	+	+	-	-
14	-	-	+	-	-	+	+	-	+	-	+	+	+	+	-
15	-	-	-	+	-	-	+	+	-	+	-	+	+	+	+
16	-	-	-	-	-	-	-	-	-	-	-	-	-	-	-

Plackett-Burman Variables Used in the Dispersion Study:

Variables	Low Level (-)	High Level (+)
1) pH	5	8
2) citrate	10^{-4}M	10^{-2}M
3) dummy ♣		
4) dummy		
5) pyrophosphate	10^{-6}M	10^{-4}M
6) calcium	10^{-4}M	$5X10^{-4}$M
7) oxalate	10^{-4}M	10^{-2}M
8) dummy		
9) protein concentration	0 ppm	0 ppm
10) dummy		
11) type of solution	Ultrapure Water	Artificial Urine
12) dummy		
13) dummy		
14) order of addition of calcium	Day 1	Day 2
15) dummy		

♣ dummy variables are used to calculate the variance of the experimental runs

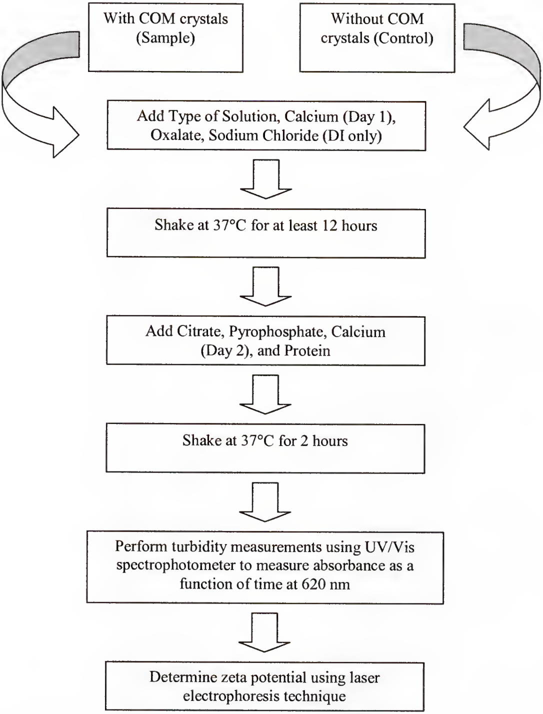
With COM crystals (Sample)
Without COM crystals (Control)
Add Type of Solution, Calcium (Day 1), Oxalate, Sodium Chloride (DI only)
Shake at 37°C for at least 12 hours
Add Citrate, Pyrophosphate, Calcium (Day 2), and Protein
Shake at 37°C for 2 hours
Perform turbidity measurements using UV/Vis spectrophotometer to measure absorbance as a function of time at 620 nm
Determine zeta potential using laser electrophoresis technique

Figure 3.4. A schematic of the procedure for making the Plackett-Burman design samples.

Central Composite Design

A central composite design was used to further investigate the three most significant factors (oxalate, citrate, and protein concentration) determined from the screening design. Five levels were used which encompass the extreme concentrations found in urine (Figure 3.5). The central composite experimental design having 17 experimental runs is illustrated in Table 3.3. For each run, a sample and a control were made; the only difference is the control did not have COM particles. Each sample had previously grown COM crystals (0.35 g/L) added to the artificial urine at pH = 6 and was sonicated for five minutes. The AUIS used had 10^{-4} M $CaCl_2$ added instead of 10^{-3} M $CaCl_2$, which is the concentration in the AUIS recipe. It was recognized in preliminary experiments that 10^{-3} M $CaCl_2$ could cause the precipitation of COM depending on the oxalate concentration. Therefore, calcium was suppressed at 10^{-4} M. Each run had the following constituents added in the following order: oxalate (8.5×10^{-5} M–1.37×10^{-2} M), citrate (8.5×10^{-5} M–1.37×10^{-2} M), diluted HCl (adjust pH = 6), and protein (1.6 ppm–18.4 ppm). The concentrated oxalate and citrate solutions were prepared in AUIS and were sonicated until they were completely dissolved followed by syringe filtration (Sterile, 0.20 μm SFCA membrane, 26 mm, Corning Incorporated, Corning, NY). After the additives were added, the sample and control were equilibrated and shaken for 2 hours at 37°C (Figure 3.6). The total volume of each sample was 50 ml. It was observed that the sodium citrate increased the pH greater than the equivalent amount of sodium oxalate. Turbidity measurements, zeta potential measurements, particle size analysis, optical microscopy observations, and protein adsorption studies were performed on all the experimental runs, which are described in detail in the next sections. The computer program, JMP® (SAS Institute, Inc.), was used to perform the statistical analysis for the central composite design. The data was analyzed by fitting the response variables to a second order polynomial model.

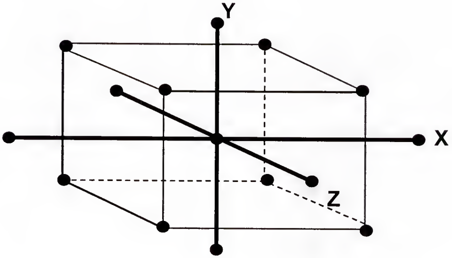

Figure 3.5. A schematic of 5 level, rotatable central composite design. The X, Y, and Z axes represent the 3 variables, oxalate, citrate, and protein. The circles represent each experimental run.

Table 3.3. Rotatable Central Composite Design with the 5 levels and 3 variables utilized in the experiments.

Run No.	Oxalate	Citrate	Protein
1	-1	-1	-1
2	-1	-1	+1
3	-1	+1	-1
4	-1	+1	+1
5	+1	-1	-1
6	+1	-1	+1
7	+1	+1	-1
8	+1	+1	+1
9	-1.68	0	0
10	+1.68	0	0
11	0	-1.68	0
12	0	+1.68	0
13	0	0	-1.68
14	0	0	+1.68
15	0	0	0
16	0	0	0
17	0	0	0

Levels

Variables	-1.68	-1	0	+1	+1.68
Oxalate (M)	$8.5x10^{-5}$	$1.0x10^{-4}$	$5.1x10^{-3}$	$1.0x10^{-2}$	$1.37x10^{-2}$
Citrate (M)	$8.5x10^{-5}$	$1.0x10^{-4}$	$5.1x10^{-3}$	$1.0x10^{-2}$	$1.37x10^{-2}$
Protein (ppm)	1.6	5.0	10.0	15.0	18.4

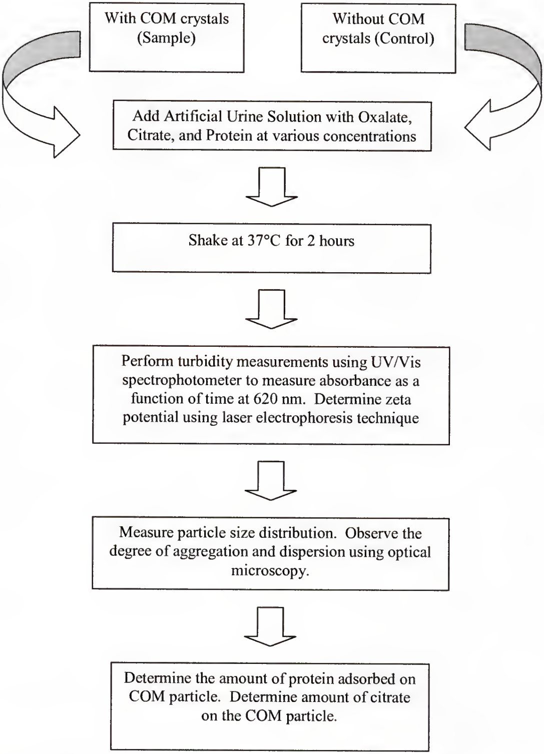
With COM crystals (Sample)
Without COM crystals (Control)
Add Artificial Urine Solution with Oxalate, Citrate, and Protein at various concentrations
Shake at 37°C for 2 hours
Perform turbidity measurements using UV/Vis spectrophotometer to measure absorbance as a function of time at 620 nm. Determine zeta potential using laser electrophoresis technique
Measure particle size distribution. Observe the degree of aggregation and dispersion using optical microscopy.
Determine the amount of protein adsorbed on COM particle. Determine amount of citrate on the COM particle.

Figure 3.6. A schematic representation of the preparation of the central composite design experimental runs and the analysis performed.

Verification of Central Composite Results

The central composite design utilizes a statistical model to determine the effect of various species in a system on a response variable (in this case, aggregation). To determine if the results obtained from the central composite were valid, the oxalate concentration was varied while keeping the other two variables, citrate and protein, constant. Specifically, the effect of varying oxalate concentrations on aggregation of previously grown COM particles was studied. Five samples were made where the oxalate concentration ($8.5\text{x}10^{-5}$–$1.37\text{x}10^{-2}$ M) was varied while the citrate ($3.21\text{x}10^{-3}$ M) and protein (5 ppm bovine submaxillary glands mucin) concentration were kept constant. The samples were prepared in a similar manner as the central composite design. The only difference was the citrate was added to "5x" AUIS instead of being added after the addition of oxalate. Turbidity tests and zeta potential measurements characterized the samples.

Turbidity Tests

Optical density measurements at 37°C over a fixed period of time were used to assess the state of aggregation or dispersion of the COM crystals under different chemical environments using an ultraviolet/visible spectrophotometer (UV-Vis spectrophotometer, Perkin/Elmer Lambda 3B). A wavelength of 620 nm was used to measure the amount of light that was being absorbed by the sample containing the COM particles for each run, the control was used as the background for the respective sample, unless the control had precipitate within it. In the precipitation case, deionized water would be used to run both the sample and the control, and then the results of the two would be subtracted to obtain the absorbance values of that Run. This applied only to the Plackett-Burman design. Otherwise, the background was subtracted from the absorbance of the sample.

The setup of the UV-Vis spectrophotometer entailed a heated water pump attached to the sample cell via rubber tubing, and the temperature of the sample cell was maintained at 37°C. A small magnetic stirrer that fits into the cuvette holder (cell) was used to stir the solution in the cuvette. For each run, 3ml of the control (being stirred) was placed in a cuvette, and 2ml of the sample (being stirred) was placed in another cuvette with a 7 x 2mm stir bar placed in the middle of the cuvette. The sample was stirred for 3 minutes to keep the particles suspended in order for each sample to have the same time zero. The turbidity measurements were recorded every 30 seconds for 13 minutes. To compare the optical density values to the degree of aggregation, an aggregation coefficient value was determined as discussed further in the Results section. The aggregation coefficient was determined as follows:

$$\text{Aggregation Coefficient} = \frac{(A_{T0} - A_{T10})}{10} * 1000 \qquad [3.1]$$

where A_{T0} is Absorbance at time = 0 min, A_{T10} is Absorbance at time =10 min, and 1000 is used as an arbitrary factor to convert AC into a whole number instead of fractions.

Zeta Potential Determination

The zeta potential of the same sample used in the turbidity test was determined using a laser electrophoresis technique (Lazer Zee Meter, Model 501, PenKem Inc.). The measurement was taken after the turbidity test was performed. The temperature of the solution was measured before and after the zeta potential was determined. The average of the two temperatures was used to calculate the zeta potential taking into account the temperature difference from room temperature (20°C). The formula used to convert the measured zeta potential to the actual zeta potential [ZP (T)] taking the temperature (T) into consideration is given by

$$ZP\ (T) = T*[1-0.02*(T-20)] \qquad [3.2]$$

For each run, the cell was thoroughly cleaned, and the voltage was set at 140 V. There were 10-12 measurements taken for each sample and the average zeta potential and standard deviation was calculated. Resuspension of the sample was sometimes necessary if the particles settled too quickly.

Optical Microscopy Observations

Since the aggregation coefficient value is arbitrarily estimated from the absorbance data, it was necessary to validate such values against other techniques such as optical microscopy and particle size analysis. To validate the aggregation coefficient (change in optical density over a fixed period of time), the samples were prepared in the same manner as described for the central composite design and were evaluated under an optical microscope. For the optical microscope analysis, a small aliquot of sample was taken 1) before the addition of the citrate, oxalate, and protein, 2) after the addition of the additives, and 3) after the 2 hour equilibration time. Two ml of each sample was filtered through 25 mm SS syringe with 0.22 μm filter paper (MAGNA-R, nylon, supported plain, MSI, Westboro, MA) into a petri dish (Falcon, crystal grade polystyrene, sterile, 35 x 10 mm). One drop of the unfiltered sample was added to the petri dish. Before an aliquot of sample was taken, the sample container was shaken to insure the COM particles were evenly distributed, so the aliquot taken was a true representation of the composition of the sample. The sample in the petri dish was observed within 10 minutes under the optical microscope (Olympus BX60, Olympus Optical Co., Ltd.) through 20x and 50x objective lenses, transmittance, and Bright Field mode. A digital camera (Spot, RT Slider Diagnostics Instruments Inc., Marietta, GA) was used to take representative pictures of each sample. The camera was calibrated using a Nikon stage micrometer and the approximate magnification to the camera was 200-500x.

Particle Size Measurements

The particle size of central composite design samples was measured to also validate the aggregation coefficient. The samples were prepared the same as described for the central composite design. The particle size of the samples was measured using laser light scattering technique (Coulter LS 230, Beckman Coulter Corp., Miami, FL). The sample for the particle size analyzer was obtained from a stirring solution of the sample in 60 ml Nalgene bottle using a disposable pipet. A small portion of the disposable pipet was cut to make sure that the opening of the pipet was large enough to insure the free-flow of particles.

Before adding the particles to the Coulter, the instrument was flushed with DI water three times to clean the system. The background solution used for the sample was saturated COM solution. The stirrer speed of the Coulter LS 230 was set at 80 and the run length was 90 seconds. If the obscurations were less than 0% and the PIDS were less than 2%, then the sample was added. The sample was loaded until the PIDS read between 52 and 55% then the particle size of the sample was measured. The particle size measurement was evaluated using com.rfd as the optical module.

Force Measurements via Atomic Force Microscopy

Atomic force microscopy (AFM) was used to determine the interaction forces versus separation distances between a COM crystal and the silicon nitride (SiN) tip in different solutions. The solutions used were ultrapure water, artificial urine without citrate and oxalate, artificial urine with protein and varying concentrations of citrate and oxalate at pH = 6. Table 3.4 gives a detailed list of the solution constituents. The sample preparation of COM particles on an AFM stud was challenging. Microscope slides were cut into squares, Shell epoxy glue was heated on the slide, and the glue was smoothed out using a razor blade. After the glue was cooled for about 4 min., COM particles were sprinkled on the glue. The excess COM particles were blown away with compressed Air. The AFM was operated by Drs. Yakov Rabinovich and Joshua Adler using the fluid cell and contact tip (thick, long tip, spring constant = 0.12) and by following the method of Ducker and Senden (172). The first set of sample fluids run (10 ppm protein samples) utilized only 1 COM stud. The last two sample fluids run (18 ppm protein samples) utilized 1 COM stud per solution because it was determined once protein adsorbed onto COM particles it was not reversible. Each time a new COM stud was used, the COM stud was analyzed using DI water followed by AUIS without protein, citrate, and oxalate, and then the sample fluid. The raw AFM data (deflection (V) versus distance traveled (nm)) was converted to force versus separation distance by AFM Analysis program (173).

Specific Surface Area Measurement using Brunauer, Emmett, and Teller (BET) Method

The specific surface area (m^2/g) of fine COM particles was determined using Autosorb 1, gas sorption system (Quantachrome Corp., Boynton Beach, FL). The analysis was performed using a five point BET (0.10, 0.15, 0.20, 0.25, 0.30) using Nitrogen gas and Krypton gas. The COM particles were outgased at 40°C for 24 hours before analysis.

Table 3.4. Atomic force microscopy solutions utilized with COM.

Solution type	Protein concentration (ppm)	Oxalate concentration (M)	Calcium concentration (M)
Ultrapure water	None	None	None
Artificial Urine (AUIS)	None	None	None
AUIS	10	0.0051	8.5×10^{-5}
AUIS	10	0.0051	0.0001
AUIS	10	0.0051	0.0051
AUIS	10	0.0051	0.01
AUIS	10	0.0051	0.0137
AUIS	10	0.0137	0.0137
AUIS	18	0.0051	8.5×10^{-5}
AUIS	18	0.0051	0.0137

Protein Adsorption

Several methods were used to try to determine the amount of protein adsorbing onto a known amount of COM particles. The first method involved taking a sample of the initial amount of mucin and comparing it to the amount of mucin that did not adsorb onto the particles (residual amount) using a Lowry Modified DC protein assay via UV/Vis spectrophotometer. The residual amount of mucin ended up having a larger concentration compared to the initial mucin concentration. One possible conclusion is that calcium or citrate could be complexing with mucin and causing precipitation of mucin in solution. This hypothesis was tested by adding 0.01 M calcium to a mucin solution and adding 0.01 M citrate to mucin solution. The calcium with mucin immediately coagulated and made the suspension cloudy. Therefore, this method could not be used. Another method that was attempted was using Total Organic Carbon (TOC) instrument. The TOC showed that in the measured solutions citrate had a larger amount of organic carbon than the amount of mucin being tested. Therefore, citrate was masking any mucin present in the samples.

The procedure that was developed and utilized was based on references (174-176). The method involved making the samples as described in the central composite design. After the 2 hour agitation at 37°C, each sample was vacuum filtered through 0.22 μm filter paper (AcetatePlus, supported, plain, 47 mm, Osmonics Inc.). The COM particles were collected from the filter paper. The collected particles were demineralized in 0.25 M EDTA at pH 8 with 0.02 weight percent of sodium azide for 2 days at 4°C. The demineralized sample was dialyzed in a 7,000 Da dialysis cassette (Slide-A-Lyzer, Pierce Chemical Co.) against 4 L of saline solution (0.9% NaCl) being stirred in a cold room (~ 4°C). The saline solution was made from 5 M NaCl solution previously filtered through 0.45 μm filter paper (AcetatePlus, supported, plain, 47 mm, Osmonics Inc.). The saline solution was used instead of just water to reduce the concentration gradient between 0.25 M EDTA and the dialyzing solution. From a previous study, dialyzing against water created such a large concentration gradient that the dialyzing water was entering the dialysis bag versus the EDTA being removed from the dialysis bag. The saline solution was changed twice a day for 2 days. It was verified that this was sufficient amount of time to remove the EDTA; therefore, the EDTA did not interfere with the Modified Lowry Protein Assay reagent (Pierce Chemical Co.). A 1 N Folin-Ciocalteu was made by diluting the 2 N Folin-Ciocalteu by 50% with DI water. A stock solution of 850 μl of 200 ppm mucin was prepared and used in making the standards. The diluent used was ultrapure water. The mucin standards made are shown in Table 3.5.

Duplicates were made for each standard and sample analyzed by the protein assay. For each sample, 200 μl of sample was added to 2, 10 x 75 mm test tubes. At 15 second intervals, 1 ml Modified Lowry reagent was added, vortexed, and incubated at room temperature for 10 minutes. At 15 second intervals, 100 μl of the diluted 1 N Folin-Ciocalteu reagent was added, vortexed and incubated at room temperature for 30 minutes. The samples were measured in polystyrene semi-cuvettes using an UV/Vis Spectrophotometer at 750 nm. The absorbance of each tube versus the blank was measured and recorded.

Ions and Small Molecule Adsorption

The amount of citrate, oxalate, and calcium remaining in solution was determined using Ion Chromatograph and Inductively Coupled Plasma (ICP). The samples used were the same samples used for the Protein Adsorption. Not mentioned in the protein adsorption section was that a control was made for each sample. The only difference was the control did not have COM crystals. After each sample and control were filtered through 0.22 µm AcetatePlus filter paper, the supernatant was collected and kept frozen in the freezer until analysis.

Table 3.5. The mucin standards prepared for the Modified Lowry Protein Assay. The number 2 signifies that the two standards made for the given concentration were made separately; whereas, for the lower concentrations the standards were made in the same test tube and then aliquot into two test tubes.

Volume of mucin to add	Volume of diluent to add	Final mucin concentration (ppm)
2 (200 µl) stock	0	200 ppm (A)
2 (100 µl) stock	2 (100 µl)	100 ppm (B)
2 (50 µl) stock	2 (150 µl)	50 ppm (C)
75 µl stock	525 µl	25 ppm (D)
100 µl (D)	400 µl	5 ppm (E)
2 (40 µl) (E)	2 (160 µl)	1 ppm (F)
0	2 (200 µl)	0 ppm, blank (G)

Ion chromatograph analysis

Citrate, oxalate, and calcium concentrations were measured using ion chromatograph (LC20 Ion Chromatograph, Dionex Corporation, Sunnyvale, CA). The background eluents used were 0.22 µm filtered 80 mM sodium hydroxide (50% w/w certified Fisher Scientific Inc., Fair Lawn, NJ) and 9 mM methane-sulfonic acid (Sigma, St. Louis, MO) for anion column and cation column, respectively. The flow rate was 1 ml/min. which was pressurized by Helium gas. The anion column was calibrated using linear regression with 0.125 mM, 0.25 mM, 0.5 mM, 1 mM, and 2 mM oxalate (sodium oxalate, 0.05 N, LabChem Inc., Pittsburgh, PA) and citrate (citric acid, 1 M, LabChem Inc., Pittsburgh, PA). The cation column was calibrated using linear regression with 0.0625 mM, 0.125 mM, 0.25 mM, 0.5 mM, and 1 mM calcium (100 mM calcium reference solution certified 1,000 ppm ± 1%, Fisher Scientific, Fair Lawn, NJ). The samples were diluted by 1:10 with 1 mM hydrochloric acid (HCl, Reagent A.C.S., Fisher Scientific, Fair Lawn, NJ). Each sample was analyzed in duplicates of 0.5 ml vials. If the species in the sample were not detectable within the calibration limits, then the sample was diluted by 10:1 with 1 mM HCl.

Inductively coupled plasma

The calcium was not clearly detected in most of the samples analyzed by the ion chromatograph; therefore, the calcium was analyzed by Inductively Coupled Plasma (ICP, Perkin Elmer Optima 3200RL Optical Emission Spectroscopy, Norwalk, CT). The instrument was calibrated using 0 ppm (ultrapure water), 1 ppm, and 10 ppm calcium (calcium reference solution certified 1000 ppm ± 1%, Fisher Scientific, Fair Lawn, NJ) and evaluated using non-linear regression. Some of the samples were diluted 1:2, 1:3, 1:4, 1:5, and 1:10 with ultrapure water depending on the approximate concentrations from the ion chromatograph data. For each sample, 5 readings were taken at the following wavelengths: 315.887 nm, 317.933 nm, 393.366 nm, and 396.847 nm.

In summary, a description of the experimental materials and methods was presented. The results and discussion of the data obtained from these experiments is discussed in Chapter 4.

CHAPTER 4
RESULTS AND DISCUSSION

Preliminary Studies

Several tests and techniques have been investigated in order to find the best conditions and materials for the dispersion/ aggregation study. The following paragraphs present details of such preliminary work.

Crystallization Study

The crystallization study was conducted to understand factors (rate of mixing) that affect COM crystallization and to produce COM particles for the aggregation and dispersion study. COM crystals were grown by homogenous and heterogeneous nucleation.

COM particles without seeds using different mixing rates

In human kidney stone disease, prismatic particles of COM are often observed while dendritic and polycrystalline aggregates are rarely encountered (2, 53, 177). As shown in Figure 4.1, the prismatic morphology, commonly observed for COM particles precipitated from 10^{-3} M $CaCl_2$ and 10^{-3} M $K_2C_2O_4$ solutions, is the dominant morphology in both the rapidly and slowly mixed samples. The dominant crystal lattice planes (010) and $(10\bar{1})$ of COM (49) are also shown in Figure 4.1. However, the micrographs in the figure show some slight differences between the slowly mixed and rapidly mixed particle morphologies. Figure 4.1(a) shows jackstones (interpenetrating twins) and well-defined prismatic particles with smooth surfaces for the particles produced in rapidly mixed solutions. In contrast, the particles produced in slowly mixed solutions display some flat, almost dendritic particles in addition to jackstones and prismatic particles as displayed in Figure 4.1(b). Notice that the bar scales on the SEM micrographs are different for rapidly and slowly mixed samples. The COM particles produced were phase pure calcium oxalate monohydrate verified by XRD. A typical XRD pattern is illustrated in Figure 4.2.

According to Sohnel and Garside (125), precipitate particle morphology depends on the supersaturation at which growth occurs. The local supersaturation for the rapidly mixed solutions at which nucleation and growth took place would be expected to be lower than the supersaturation in the slowly mixed solutions at which nucleation and growth took place. This could explain the slight difference in shape between the slowly mixed and rapidly mixed samples. Based on qualitative observations, the induction times were longer for rapidly mixed solutions than for the slowly mixed. The longer induction times are consistent with the premise that the more rapidly mixed solutions have a more uniform supersaturation level homogeneously distributed throughout the solution phase. In contrast, the slowly mixed solutions result in more widely distributed local supersaturation levels. The regions in the slowly mixed solutions where supersaturation is highest will result in more rapid nucleation and growth of particles resulting in shorter induction times.

The electrical sensing zone (ESZ) technique used to measure particle size distribution was originally used by Robertson and more recently by Ryall et.al on COM suspensions (54, 178, 179). The ESZ technique is based upon the change in voltage as a

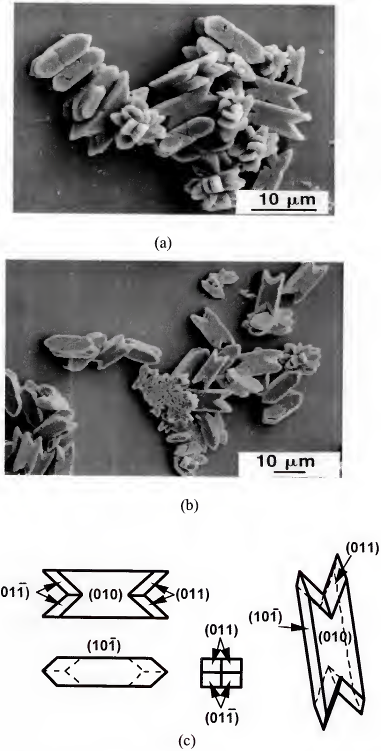

Figure 4.1. Scanning electron photomicrographs of COM particles. a) rapid mixed particles (sample RM17); b) slow mixed particles (sample HM25); c) Calcium oxalate monohydrate particles of this morphology have two dominant crystal faces, the (010) and (10$\bar{1}$) (Habeger 1995 [49]).

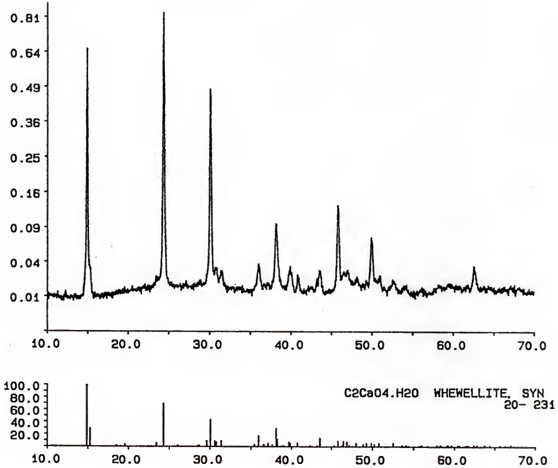

Figure 4.2. A typical experimental COM X-ray diffraction pattern at top and JCPDS file for whewellite, $CaC_2O_4{\bullet}H_2O$ on bottom.

particle suspended in an electrolyte passes through an aperture in a tube (131). The technique is theoretically limited to particle sizes from 2 to 45 percent of the aperture size, which in the current work was either 48 or 96 μm in diameter. In practice, the lower particle size limit is usually set slightly higher to minimize spurious particle counting due to electrical noise and/or contamination of very fine particles such as dust. The actual particle size distributions are usually truncated on either or both ends by the limitations imposed by theoretical limits of the technique.

The particle size distributions for the slowly mixed and rapidly mixed samples, examples of which are shown in Figure 4.3, indicate that monomodal and bimodal distributions are typical under these synthesis conditions for both rapidly and slowly mixed solutions. It should be noted that in both of the COM synthesis methods described here, the reactant solutions were not stirred after the initial mixing. In preliminary experiments it was also found that stirring the precipitating solution after mixing produced COM particles with a greater degree of twinning and large cluster formation, presumably due to secondary nucleation as described by Nancollas and others (54, 180, 181). The extent of twinning and the formation of jackstones were greatly reduced by not

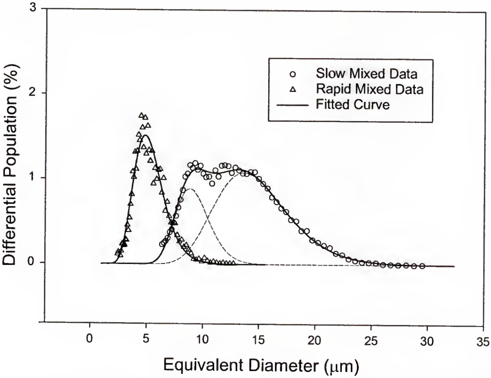

Figure 4.3. Representative log normal of particle size distributions for slow mixing (sample HM25) and rapid mixing (sample RM17). Correlation coefficient (R^2) is 0.98 and 0.96, respectively. See Table 4.1 for additional details.

stirring the precipitating solutions. Since COM has a monoclinic crystal structure with low symmetry, it has a tendency to form a variety of morphological forms due to the differences in surface energies for different habit planes. The jackstones are typically composed of the prismatic habits (010) and $(10\bar{1})$, but they appear to form from a common nucleation site (49). The growth in several different twin crystallographic directions appears to be promoted by a secondary nucleation mechanism. Comparisons between the SEM photomicrographs in Figure 4.1 and the particle size distributions in Figure 4.2 indicate that the jackstone morphologies probably make up the finer size fraction of particles from both the rapidly and slowly mixed solutions.

The log-normal probability distribution parameters, mean and standard deviation, are summarized in Table 4.1 for each of the five individual batches for particles from either the rapidly or slowly mixed samples. The percentage of each peak in any bimodal distributions is also shown. The arithmetic, normal mean of the mean particle sizes from each batch was also calculated and is indicated in the table. For those samples displaying a bimodal distribution only, the major peak was used to calculate the average arithmetic mean based upon the mean particle size in the individual distributions. In general, the major peak in each distribution correlates to the larger prismatic particles shown in Figure 4.1 while the finer fraction is associated with the multiple twinned, jackstone-type particles. Furthermore, comparison of the average value for the larger and more significant fraction of each distribution indicates that the particles formed from the slowly mixed solutions are significantly larger than particles from the rapidly mixed solutions.

Table 4.1. Statistically determined values describing slowly mixed and rapidly mixed particle size distributions for the samples.

	Sample Number	Percent of Distribution	Mean of the Distribution in Real Space (μm)	Log Normal Standard Deviation (μm)	Range of Log Normal Probability Distribution in Real Space (μm)	Correlation Coefficient
	HM24	100	12	0.40	8.1- 18	0.98
	HM25C*	63	14	0.24	11 - 17	0.98
	HM25F*	37	8.8	0.17	7.4 - 10	0.98
Slowly	HM26C	59	11	0.28	8.3 - 15	0.98
Mixed	HM26F	41	4.1	0.47	2.6 - 6.5	0.98
Samples	HM27	100	11	0.37	7.6 - 16	0.96
	HM28C	78	15	0.25	12 - 19	0.97
	HM28F	22	8.3	0.42	5.5 - 13	0.97
	Arithmetic Mean of HM Mean Value		13±2.6			
	RM16C	87	4.6	0.24	3.7 - 5.8	0.98
	RM16F	13	3.8	0.08	3.5 - 4.1	0.98
	RM17	100	4.8	0.27	3.7 - 6.2	0.96
Rapidly	RM18C	56	7.8	0.23	6.2 - 9.8	0.99
Mixed	RM18F	44	5.0	0.18	4.2 - 6.0	0.99
Samples	RM19C	62	5.5	0.27	4.2 - 7.2	0.98
	RM19F	38	3.0	0.27	2.3 - 3.9	0.98
	RM20	100	4.7	0.36	3.3 - 6.7	0.98
	Arithmetic Mean of RM Mean Value		5.5±1.9			

* C represents the coarser fraction of the distribution
F designates the finer fraction of the distribution

The arithmetic average size and 95% confidence interval for the five batches of slowly mixed particle size distributions is 13 ± 2.6 μm, based upon the log normal mean for each particle size distribution for each batch. In contrast, the average size for the mean sizes of each batch of particles produced in rapidly mixed solutions was significantly smaller with a mean size and 95% confidence interval equal to 5.5 ± 1.9 μm. This is consistent with the observations of Sohnel and Garside (125) that a narrow particle size distribution is obtained by rapid nucleation followed by an abrupt halt to allow for crystal growth to occur without agglomeration of particles. For the study of kidney stone disease, the more narrowly distributed, rapidly mixed samples are more desirable as a model system to minimize the effects of particle size distribution on studies related to aggregation and adhesion in physiological conditions.

“Fine” COM particles with seeds

The “fine” COM particles were used for the aggregation/dispersion study because the particle size of 1.1 μm equivalent spherical diameter is close to the size of crystals formed in normal urine. There are some interpenetrating twins (jackstones) with prismatic morphology illustrated in Figure 4.4. The COM particles produced were phase pure COM by XRD (Figure 4.2).

Zeta Potential Measurements of COM in Presence of Different Solutions

Sodium azide

Sodium azide (NaN_3) is normally used at 0.02 weight percent concentration to destroy and prevent growth of bacteria. Since protein was being used in the solutions of this study, NaN_3 was considered to be used as a bactericide. In other words, NaN_3 would

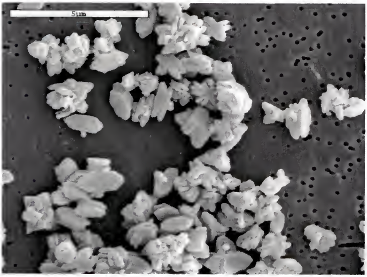

Figure 4.4. Representative photomicrograph of the fine COM particles used for the aggregation and dispersion studies.

prevent bacteria from degrading the protein. First, NaN_3 was studied to ensure that it did not effect the surface properties of COM. From the zeta potential data (Figure 4.5), it was determined that NaN_3 does affect the charge of COM particles as a function of concentration. The zeta potential becomes less negative as NaN_3 is increased and becomes positively charged at 0.03 weight percent. The effect at 0.02 weight percent is debatable. Due to the large standard deviation resulting in positive zeta potential, it was concluded that NaN_3 should not be used in the presence of COM particles for surface studies.

Mucin

The calculated average zeta potential values of 3000 ppm mucin measured in ultrapure water and 0.05 M Tris-HCl were –36 ± 5.6 mV and –17 ± 4.4 mV, respectively. This confirms that mucin, an acidic glycoprotein, is negatively charged. In addition, the intensity of the zeta potential charge is lower in the presence of 0.05 M Tris. This is attributed to an increase in ionic strength, which will reduce electrostatic forces between molecules. The 3000 ppm mucin in citrate buffer could not be measured accurately because the conductance was too high for the instrument. The measured data was very scattered. An interesting observation was that mucin dissolved more easily in the ultrapure water than in the citrate buffer. The effect of oxalate and calcium on COM particles is discussed below.

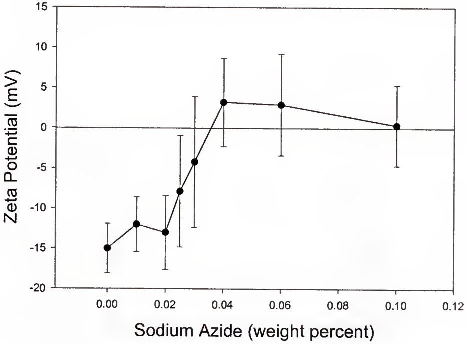

Figure 4.5. The zeta potential compared to the weight percent of sodium azide in saturated COM solution ($8x10^{-6}$ M) with COM particles within 95% confidence interval.

Addition of Oxalate to COM Solutions

The addition of oxalate to solutions containing COM particles creates a negatively charged surface on COM particles (Figure 4.6). It is clear that the negative potential increases as oxalate concentration increases. This is attributed to that fact that oxalate ions are potential determining ions for COM. Specifically, the addition of oxalate in the two solutions studied, CO_2 free ultrapure water and 0.01 M Tris-HCl, created a negatively charged COM surface since the zeta potential of COM particles without oxalate is close to zero (the obtained values are 1.2 ± 1.3 and 2.1 ± 4.1 for ultrapure water and 0.01 M Tris-HCl, respectively). These values are not shown in Figure 4.6 or Figure 4.7 since the data was plotted on a log scale (Log 0 = infinity).

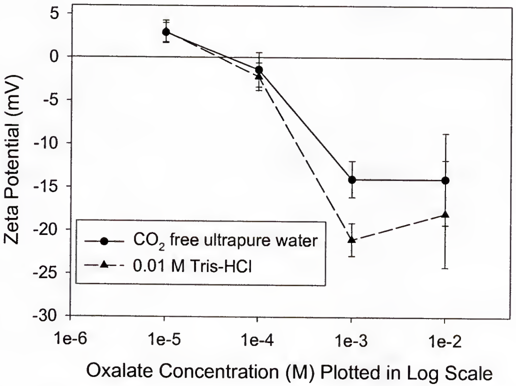

Figure 4.6. The influence of oxalate on COM particle surface. Zeta potential as a function of oxalate concentration on COM particle surface in CO_2 free ultrapure water and 0.01 M Tris-HCl. within 95% confidence interval.

Addition of Calcium to COM Solutions

The addition of calcium to COM particles in CO_2 free ultrapure water and 0.01 M Tris-HCl solution creates a positively charged surface on COM particles (Figure 4.7). The zeta potential values are similar for both solutions.

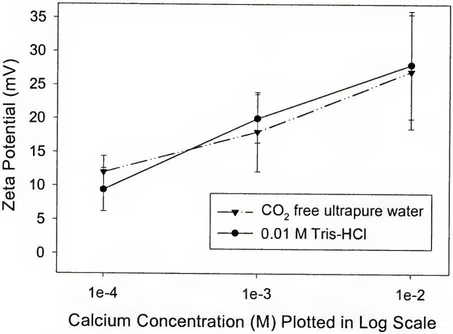

Figure 4.7. The zeta potential of COM particles as a function of calcium concentration. The two solutions studied were CO_2 free ultrapure water and 0.01 M Tris-HCl solution within 95% confidence interval.

Tris-HCl affect on COM particles

The effect of Tris-HCl on the zeta potential of COM particles is illustrated in Figure 4.8. The Tris-HCl does not seem to affect the zeta potential charge when taking into account the variation of zeta potential values. The zeta potential at 0 M Tris-HCl was determined to be 6.59 ± 2.25 mV.

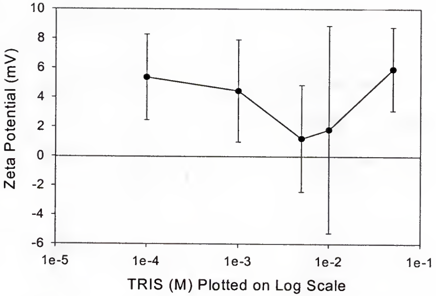

Figure 4.8. The zeta potential of COM particles as a function of Tris-HCl solution within 95% confidence interval.

Detection of Bacteria in AUIS

The Bactericult tubes used in this study, detect aerobic bacteria usually found in pathological urine specimens having a minimum of 25,000 bacteria/ml, were negative after 24 hour incubation at 37°C. Therefore, any bacterial growth in the tubes was below detection limits. The Mueller Hinton agar plates, which are very sensitive to small bacteria colonies, did not have bacteria growth after 24 hour incubation at 37°C. However, after 36 hour incubation period, there were some white and black specks on the agar. Therefore, incubation of AUIS and ultrapure water at 37°C does not form bacteria within 24 hours. In conclusion, the incubation of AUIS and ultrapure water with COM particles overnight does not need a bactericide to prevent bacterial growth in this time frame when cleanliness is maintained during sample preparation.

Aggregation and Dispersion Study

Various methods utilizing turbidity/optical density data have been used by other investigators (101, 182) to quantify aggregation/dispersion behavior of COM. In this analysis, the rate of change in absorbance value from the initial measurement to absorbance at 10 minutes was used as indication of aggregation or dispersion. A smaller rate of absorbance change indicates slow settling of particles, i.e. particles are more dispersed. A higher rate of absorbance change indicates larger particles and faster settling (more aggregated). In other words, the larger size of a particle means more transmittance of light and less absorbance due to a reduction in turbidity. The relationship between absorbance and transmittance is given by (183)

$$A = \log (1/T) \qquad [4.1]$$

where A is absorbance and T is transmittance. In this study, the absorbance data were used to determine an aggregation coefficient (AC) in both statistical designs. The aggregation coefficient was determined as follows:

$$\text{Aggregation Coefficient} = \frac{(A_{T0} - A_{T10})}{10} * 1000 \qquad [4.2]$$

where A_{T0} is Absorbance at time at 0 min, A_{T10} is Absorbance at time at 10 min, and 1000 is used as an arbitrary factor to convert AC into a whole number instead of fractions. The calculated AC values for the screening design are shown in Table 4.2 where the higher the AC value indicates more aggregation.

The aggregation coefficient (AC) was validated by optical microscopy and particle size measurements (Figure 4.9). Figure 4.9a shows particles of COM with a low AC value of 14, which are clearly fairly well dispersed with sauter diameter (defined in Particle Size Analysis section of this chapter) = 0.653 μm, whereas Figure 4.9b has a higher AC value of 48 and clearly has aggregates with a larger sauter diameter = 1.378 μm. Therefore, it is believed that the AC is an acceptable method to evaluate aggregation behavior.

Table 4.2. Aggregation data for Plackett-Burman design. Absorbance Values used to calculate the aggregation coefficient of the Plackett-Burman design.

Run #	Absorbance at T_0	Absorbance at T_{10}	Aggregation Coefficient
1	1.258	0.839	42
2	0.935	0.376	56
3	0.766	0.391	38
4	0.914	0.499	42
5	1.012	0.633	38
6	0.973	0.519	45
7	1.081	0.67	41
8	0.882	0.347	54
9	0.883	0.203	68
10	0.721	0.235	49
11	0.601	0.154	45
12	0.782	0.525	26
13	0.77	0.607	16
14	1.172	0.72	45
15	0.739	0.488	25
16	0.775	0.229	55

Plackett-Burman Design

The aggregation coefficient (Table 4.2) was used as the response in calculating the statistical effect of variables. The effect of variables are calculated as follows:

$$\mathrm{Ei} = \frac{\sum \mathrm{Response}_{(+)} - \sum \mathrm{Response}_{(-)}}{8} \qquad [4.3]$$

The variance is estimated by evaluating the effect of dummy variables and using this equation:

$$\sigma^2 = \mathrm{V}_{\mathrm{eff}} = \frac{\sum \mathrm{E_d}^2}{\mathrm{n}} \qquad [4.4]$$

where Ed = effect of dummy variable and n = number of dummy variables = 7. The statistical significance of the effects is evaluated using the student t-test as calculated using:

$$t = \frac{E_i}{\sqrt{\sigma^2}} \qquad [4.5]$$

where the degrees of freedom = 7, confidence level = 95% and $t_{7,0.05} = 1.895$. Comparing the absolute t-values to 1.895 led to acceptance of variables with a higher t-value and rejecting the variables with lower t-values. In other words, the variables accepted were significant within 95% confidence level. This comparison of the Plackett-Burman design is presented in Table 4.3. The protein concentration t-value is 1.83, which is slightly lower than 1.895. Nevertheless, the protein was considered to be significant as indicated in literature (5, 7). From the Plackett-Burman design, the most significant variables are citrate, oxalate, and protein concentrations.

From the screening design, a model relating the aggregation coefficient to the different variables could be represented by:

$$y = 43 + 5.8X_1 - 4.2X_2 - 5.6X_3, \qquad [4.6]$$

where y represents AC and X_1, X_2, and X_3 represent concentrations of oxalate, protein, and citrate, respectively. All coefficients are statistically significant close to 95% confidence level. The negative sign for the protein and citrate coefficients indicate that both can lead to a decrease in the aggregation coefficient. In other words, both can disperse COM. On the other hand, the positive oxalate value indicates that an increase in oxalate concentration leads to more aggregation. In order to further investigate the interaction among these three significant variables with respect to their effect on

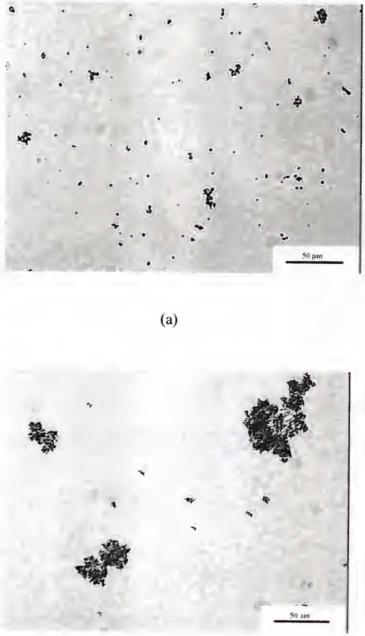

(a)

(b)

Figure 4.9. Dispersed sample versus an aggregated sample via optical microscopy. a) Optical microscopy observation of a more dispersed sample with AC = 14; b) Optical microscopy observation of a more aggregated sample with AC = 48.

Table 4.3. The Plackett-Burman calculated t values for different variables. The decisions to accept or reject the significance of variables on the bases of comparing t-value to critical value at 95% confidence level.

Factors	Effect on Aggregation (t-value)♣	Significant Variable
pH	-0.52	Reject
citrate	-2.43♦	Accept
pyrophosphate	+0.46	Reject
calcium	+1.28	Reject
oxalate	+2.54♦	Accept
protein concentration	-1.83♦♦	Accept
type of solution	-1.50	Reject
order of addition of calcium	-1.66	Reject

♦Statistically significant (95% confidence level)

♦♦Considered significant based on literature and experience

♣(+ ve) sign indicates more aggregation

♣♣(- ve) sign indicates a more stable (dispersed) suspension

aggregation/dispersion of COM, a central composite design focusing on these three variables with five levels was used.

Central Composite Design

The aggregation coefficients for the central composite design are found in Table 4.4. From the analysis of central composite design at 95% confidence level, the data again indicate that protein acts as a dispersant, and oxalate promotes aggregation (Figure 4.10). Citrate by itself does not significantly affect the aggregation coefficient. Oxalate is a potential determining ion; therefore, oxalate will specifically adsorb at the COM surface (58). This leads to a change in surface charge (as observed) resulting in a reduction in electrostatic repulsion. Such a decrease in surface charge, coupled with compression of the double layer due to high ionic strength, will lead to aggregation due to van der Waals attractive forces.

Table 4.4. Aggregation data for central composite design.

Run #	Absorbance at T_0	Absorbance at T_{10}	Aggregation Coefficient
1	0.879	0.571	31
2	0.922	0.756	17
3	0.736	0.53	21
4	0.91	0.77	14
5	0.947	0.468	48
6	1.18	0.942	24
7	0.807	0.399	41
8	0.91	0.521	39
9	0.723	0.535	19
10	0.853	0.501	35
11	0.956	0.556	40
12	1.012	0.695	32
13	0.84	0.362	48
14	0.89	0.634	26
15	1.024	0.784	24
16	0.99	0.61	38
17	1.001	0.634	37
18	1.00	0.65	35
19	0.948	0.66	29

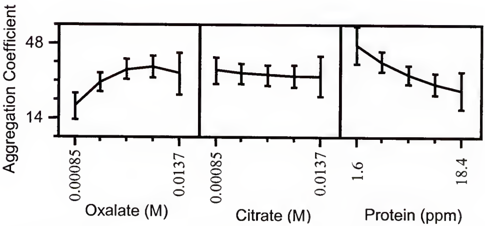

Figure 4.10. Prediction Profiler of oxalate, citrate, and protein as a function of aggregation coefficient. As oxalate concentration increases, aggregation coefficient increases to a certain point. As citrate concentration increases, the aggregation coefficient does not change significantly. As protein concentration increases, aggregation decreases. ($R^2 = 0.8848$)

Protein helps to reduce the aggregating effect of oxalate, as shown in Figure 4.11a. As the protein concentration is increased, aggregation is decreased at all values of oxalate concentrations. Interestingly, interactions between protein and oxalate, along with protein and citrate are observed. These interactions were synergistic or antagonistic, depending on the concentrations of these species. For the oxalate concentration alone, aggregation increases with an increase in oxalate concentration. The protein exhibits the opposite effect, in which aggregation is decreased as protein concentration is increased. The change in citrate concentration alone has little affect on aggregation. However, the citrate and protein concentrations have a strong interaction (Figure 4.11b). Overall, the best dispersion is at high protein and low citrate concentration levels. Yet, this phenomenon is reversed at low protein concentrations such that there is more dispersion at higher citrate levels. This characteristic is also exhibited between the citrate and oxalate concentrations displayed in Figure 4.11c. The best dispersion occurs at low oxalate and high citrate concentrations. In the case of high oxalate concentration, lower citrate is better for dispersion. This may be attributed to site blocking as a result of citrate coating on COM crystals. Lieske, et al. (184) showed that competition exists between urinary anions and anionic sites on surfaces of cultured renal epithelial cells. They thought that the urinary anions could coat the crystals preventing adhesion to the cells, which also have a negatively charged surface. From this discussion, it is clear that this protein (mucin) is affected by other species present in the system. Specifically, the amount of citrate influences the action of the mucin with respect to dispersion capability. This follows similar trends shown by Hess et al. with Tamm-Horsfall mucoprotein (THP) and citrate (101). Although our model protein is

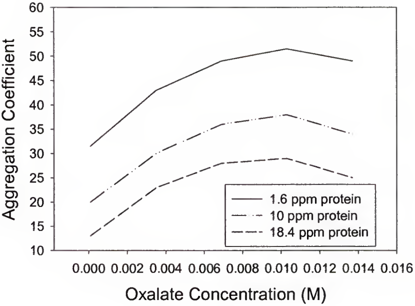

(a)

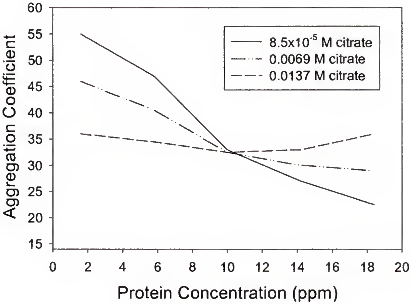

(b)

Figure 4.11. Interaction plots between citrate, protein and oxalate concentrations. a) The interaction of protein and oxalate concentrations; b) The interaction of citrate and protein concentration; c) The interaction of oxalate and citrate concentration. ($R^2 = 0.8848$)

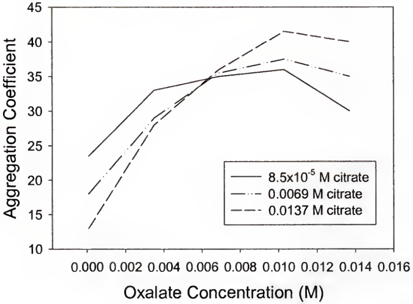

(c)

Figure 4.11—continued

quite different from THP (mainly in terms of molecular weight), it is reassuring that the data do appear to correlate with these other studies.

Surface response for interactions of oxalate and protein at constant citrate concentrations are illustrated in Figure 4.12. The contour plots indicate that at low citrate concentration, protein plays an important role in reducing aggregation at all oxalate levels. However, at higher citrate (0.01 M), protein plays a minor role as seen by the contours, which are approximately parallel to the protein axis. Under such conditions, lower citrate concentration would be desirable for less aggregation. High citrate concentrations contribute to the increase in ionic strength. Such an increase in ionic strength could be a factor in determining the interaction between protein and citrate. This hypothesis is based on the findings in a study by Utsunomiya et al. (185). The authors

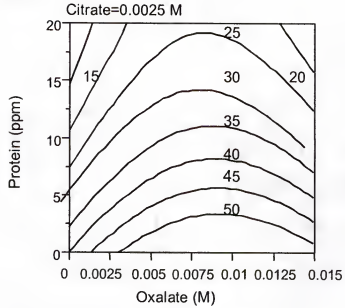

(a)

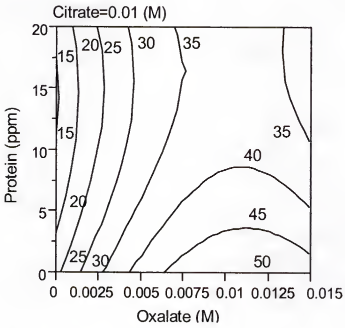

(b)

Figure 4.12. Contour plots illustrating how the aggregation probability changes with respect to oxalate and protein concentration at constant citrate levels a) 0.0025 M and b) 0.01 M.

showed that the inhibitory activity of the macromolecule, heparin, was influenced by ionic strength. Specifically, at lower ionic strength, there was more adsorption of heparin resulting in increase in inhibitory activity. The increase in ionic strength by citrate may influence the inhibitory activity of mucin. The calculated ionic strength for each experimental run by EQUIL (52) varied from 0.301 – 0.366 M (Table 4.5).

Table 4.5. Ionic strength of each experimental runs from central composite design.

Run No.	Oxalate (M)	Citrate (M)	Protein (ppm)	Ionic Strength (M)
1	10^{-4}	10^{-4}	5.0	0.301
2	10^{-4}	10^{-4}	15.0	0.301
3	10^{-4}	10^{-2}	5.0	0.339
4	10^{-4}	10^{-2}	15.0	0.339
5	10^{-2}	10^{-4}	5.0	0.318
6	10^{-2}	10^{-4}	15.0	0.318
7	10^{-2}	10^{-2}	5.0	0.359
8	10^{-2}	10^{-2}	15.0	0.359
9	$8.5\text{x}10^{-5}$	$5.1\text{x}10^{-3}$	10.0	0.318
10	$1.37\text{x}10^{-2}$	$5.1\text{x}10^{-3}$	10.0	0.345
11	$5.1\text{x}10^{-3}$	$8.5\text{x}10^{-5}$	10.0	0.310
12	$5.1\text{x}10^{-3}$	$1.37\text{x}10^{-2}$	10.0	0.366
13	$5.1\text{x}10^{-3}$	$5.1\text{x}10^{-3}$	1.6	0.328
14	$5.1\text{x}10^{-3}$	$5.1\text{x}10^{-3}$	18.4	0.328
15	$5.1\text{x}10^{-3}$	$5.1\text{x}10^{-3}$	10.0	0.328
16	$5.1\text{x}10^{-3}$	$5.1\text{x}10^{-3}$	10.0	0.328
17	$5.1\text{x}10^{-3}$	$5.1\text{x}10^{-3}$	10.0	0.328

Since the central composite design does not evaluate one-variable-at-a-time, the trends calculated from the second order model are as good as the confidence level of the data, based on the repeatability of the central points (0,0,0). So, to verify the data produced from the JMP® program, the effect of varying oxalate concentrations on aggregation of previously grown COM particles was studied. The other two variables, citrate and protein, were kept constant. The aggregation coefficients obtained from this analysis along with the central composite design data for the respective oxalate concentrations are listed in Table 4.6. The aggregation coefficients from the central composite design were extrapolated from the contour plot illustrated in Figure 4.13. It is shown that a similar trend is found where an increase in oxalate concentration results in an increase in aggregation. There is some variation in the aggregation coefficient values. This variation may be due to the order of addition of citrate. In this study, citrate was added to the "5x" AUIS instead of after the addition of oxalate. Therefore, the citrate molecules may have been exposed to the COM particles before oxalate.

Table 4.6. Aggregation coefficients from the verification study of central composite design. The aggregation coefficients extrapolated from the central composite data are also shown.

Oxalate Concentration (M)	AC from Verification Study	AC from Central Composite Data
8.5×10^{-5}	20	28
1×10^{-4}	21	28
5.1×10^{-3}	30	30
1×10^{-2}	40	45
1.37×10^{-2}	49	42

Zeta Potential Analysis

The zeta potential determined for the COM particles in the screening design ranged from +5.3 to -21. The zeta potential determined for the COM particles in artificial urine had average values from +4 to –7.4 mV. This indicates that there are essentially no electrostatic forces exhibited by COM particles in the high ionic strength of artificial urine, which is calculated and shown in a later section. Therefore, it seems that another

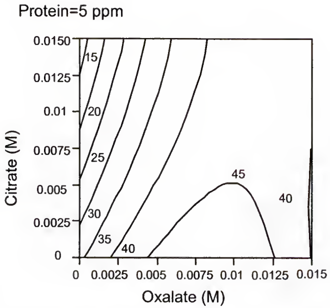

Figure 4.13. Surface response aggregation of citrate versus oxalate at 5 ppm protein.

barrier, such as one arising from steric forces, may be causing the COM particles to be more dispersed. To test this possibility, AFM was used to measure interaction forces present in our system and the results are presented in a later section.

Particle Size Analysis

The results from measuring the particle size of each central composite design sample are illustrated in Figure 4.14. The sauter diameter was the value extracted from the particle size analysis. This number was used because most of the samples had broad particle size distribution. This diameter takes into account the ratio of mean volume diameter to mean surface diameter and illustrates the particle size using one number instead of having to show mean and standard deviation. The sauter diameter also referred to as surface mean and mean volume-surface diameter is given by (186, 187)

$$d_{32} = \frac{\sum_i n_i d_i^3}{\sum_i n_i d_i^2} \qquad [4.7]$$

where d_{32} is the sauter diameter, n_i is the number of particles of equivalent diameter (d_i). The sauter diameter values show a similar trend to the aggregation coefficient. As the aggregation increases, the sauter diameter increases for most of the samples. Note, the COM crystals that comprise the aggregates are not spherical in shape. The particle size analyzer (Coulter LS) used in this study assumes particles are spherical. This could attribute to the differences between the aggregation coefficient values and the sauter diameter. Also, the larger particles may not remain in suspension over time during the analysis. Overall, there is a similar trend between the sauter diameter and the aggregation coefficient.

Force Measurements via Atomic Force Microscopy

In a preliminary study, the AFM was used to measure the interaction forces between a COM particle and a SiN tip. As previously mentioned, the SiN tip was used because the COM particles being used in this study were 10 μm x 20 μm; therefore, there is a greater chance for the tip to be on a particle. From Figures 4.15 and 4.16, it can be seen that in the ultrapure water solution, little to no attraction between COM and SiN tip is observed. This suggests the interparticle forces are primarily controlled by van der Waals forces. This is expected considering the tip we are using has a small radius (~10 nm) and at short range distance, van der Waals attractive forces dominate. Therefore, the tip will not be as sensitive to electrostatic forces. The difference between Figure 4.15 and 4.16 is they are two different COM samples prepared in the same manner. The protein concentrations are 10 ppm and 18 ppm, respectively.

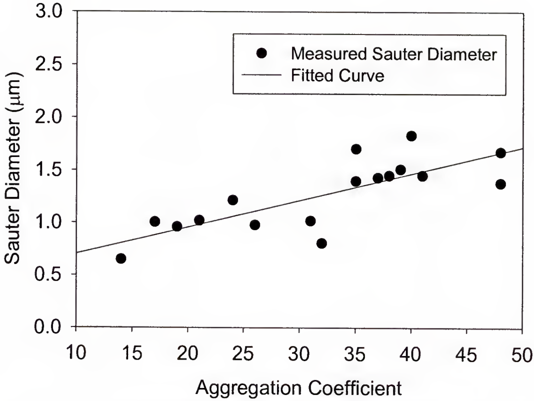

Figure 4.14. Particle size analysis data of central composite design samples. The sauter diameter is illustrated as a function of aggregation coefficient.

In artificial urine solution, however, the high salt concentration of the solution decreases the electrostatic repulsion forces (compression of the double layer) and results in attractive van der Waals forces at short separation distances (~ 4 nm). When 10 ppm protein is added to artificial urine (Figure 4.15), a steric repulsive force appears at separation distances ~ 8 nm. Therefore, steric repulsive forces can be felt at low protein concentration by the AFM, and could explain the dispersion behavior of COM in the presence of protein under the conditions tested in our model system.

During the study of forces, desorption of protein from a COM particle was attempted using AUIS to rinse the particles. Rinsing of the particles was done several times. However, the results show that once protein was adsorbed onto COM surface, it

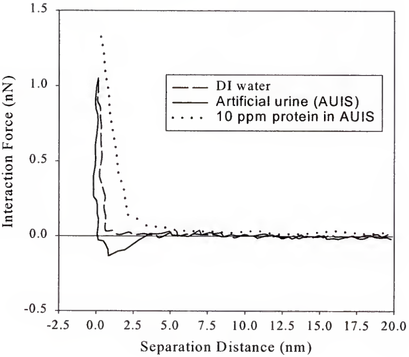

Figure 4.15. Interaction forces measured by atomic force microscopy versus separation distance between calcium oxalate monohydrate particle and silicon nitride tip in various solutions.

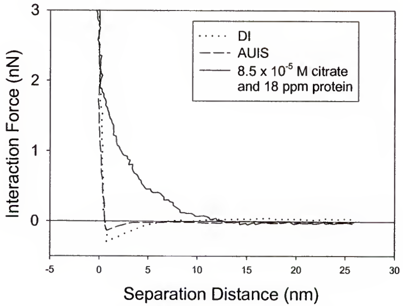

Figure 4.16. AFM force measurements under three solutions using a new COM sample.

was not easily desorbed. In other words, adsorption of protein on COM particles is irreversible. This is confirmed by the data shown in Figure 4.17, which illustrates attractive forces between a COM particle and SiN tip in AUIS (AUIS without protein). Also shown are interaction forces between a COM particle and SiN tip in which the COM particle was exposed to protein in AUIS solution, and then rinsed several times with AUIS. It is clear that there still is a repulsive force between a COM particle and SiN tip in AUIS without protein. This also showed that in order to obtain reasonable data at different protein, citrate, and oxalate concentrations a separate COM sample needs to be used with a new protein solution.

Effect of citrate concentration on interparticle forces was measured in presence of protein and AUIS. The data are presented in Figure 4.18. It can be seen that higher repulsive forces are exhibited by the particles in the presence of low citrate concentration. This may be due to higher protein adsorption (as shown later) leading to higher steric forces that resulted in more dispersion of COM particles under similar chemical conditions as discussed above. It is interesting to see in the same figure a small, but detectable difference in repulsive forces obtained by two different crystallographic faces of COM. Such difference needs to be further confirmed and correlated with atomic structure of these faces.

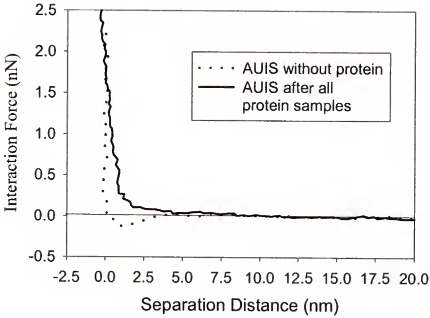

Figure 4.17. Interaction force between COM particle and artificial urine. The interaction force was measured by an AFM between COM particle and SiN tip in artificial urine (AUIS without protein). After exposing COM particle to protein, the interaction force was measured between COM particle and AUIS without protein illustrated by AUIS after all protein samples.

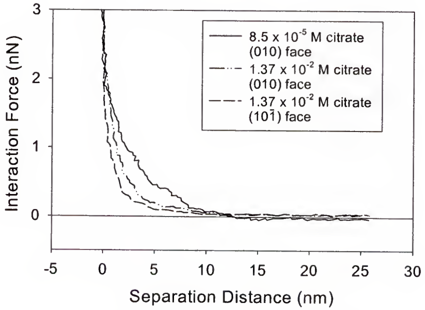

Figure 4.18. Effect of citrate on the interaction forces between COM particles and SiN tip as a function of separation distance. Two different COM crystal faces were measured at 1.37 x 10^{-2} M citrate.

Specific Surface Area Measurements using Brunauer, Emmett, and Teller Method

The specific surface area of COM particles was determined by the BET in order to be used in protein adsorption calculations. Using krypton as the adsorbate, the measured surface area was 4.66 m^2/g. Using nitrogen as the adsorbate, the measured surface areas were 6.55 and 6.67 m^2/g. The average surface area of nitrogen adsorbate is 6.61 m^2/g and this was used in the protein adsorption calculations discussed in the next section. The nitrogen value was chosen because this adsorbate is more commonly found in literature.

Protein Adsorption

Since protein adsorption appears to provide a steric barrier for preventing aggregation, it is desirable to know how other urinary molecules affect the adsorption of the protein. The amount of protein (mucin) adsorption was calculated by

$$\Gamma = \frac{C * V}{m * SA} \qquad [4.8]$$

where Γ is amount of protein adsorption (mg/m^2), C is protein concentration on particle ($\mu g/ml$), V is volume of solution (ml), m is mass of COM particles (g), and SA is specific surface area of COM particles (6.6125 m^2/g). The parking area of protein molecules in each experimental run was calculated by

$$\text{Parking area} = \frac{\left(\dfrac{1x10^{18} * MW}{\Gamma}\right)}{Av} \qquad [4.9]$$

where MW = 400,000 g/mol, Av is Avogadro's number (6.023×10^{23} #/mol) and parking area is $nm^2/\#$ and is shown in Table 4.7.

Table 4.7. Amount of protein adsorption and parking area of central composite design.

Run No.	Oxalate (M)	Citrate (M)	Protein (ppm)	Adsorption (mg/m^2)	Parking Area (nm^2/#)
1	10^{-4}	10^{-4}	5.0	0.477	1391
2	10^{-4}	10^{-4}	15.0	1.64	406
3	10^{-4}	10^{-2}	5.0	0.069	9618
4	10^{-4}	10^{-2}	15.0	0.890	746
5	10^{-2}	10^{-4}	5.0	0.475	1397
6	10^{-2}	10^{-4}	15.0	1.59	418
7	10^{-2}	10^{-2}	5.0	0.199	3346
8	10^{-2}	10^{-2}	15.0	0.816	813
9	$8.5\text{x}10^{-5}$	$5.1\text{x}10^{-3}$	10.0	0.428	1550
10	$1.37\text{x}10^{-2}$	$5.1\text{x}10^{-3}$	10.0	0.782	850
11	$5.1\text{x}10^{-3}$	$8.5\text{x}10^{-5}$	10.0	1.16	572
12	$5.1\text{x}10^{-3}$	$1.37\text{x}10^{-2}$	10.0	0.427	1557
13	$5.1\text{x}10^{-3}$	$5.1\text{x}10^{-3}$	1.6	0.0699	9507
14	$5.1\text{x}10^{-3}$	$5.1\text{x}10^{-3}$	18.4	1.80	368
15	$5.1\text{x}10^{-3}$	$5.1\text{x}10^{-3}$	10.0	0.844	787
16	$5.1\text{x}10^{-3}$	$5.1\text{x}10^{-3}$	10.0	0.824	806
17	$5.1\text{x}10^{-3}$	$5.1\text{x}10^{-3}$	10.0	0.938	708

Figure 4.19 shows that at low citrate concentration, the amount of protein (mucin) adsorption on COM increases with increasing protein concentration up to 2 mg/m^2, while at high citrate concentration, protein adsorption increases only to 1 mg/m^2. Therefore, protein adsorption is diminished by higher citrate levels. Oxalate has little effect on protein adsorption as indicated by the contours, which are approximately parallel to the oxalate axis. Figure 4.20a shows there is an interaction between protein and citrate illustrated by the diagonal contour lines. At high protein and low citrate concentrations, the highest amount of protein adsorption occurs. The amount of protein adsorption is decreased as citrate concentration is increased. Data in Figure 4.20b confirms that oxalate has little effect on protein adsorption and citrate has a significant effect.

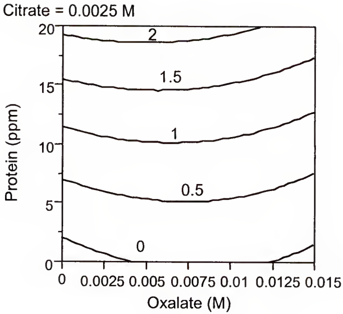

(a)

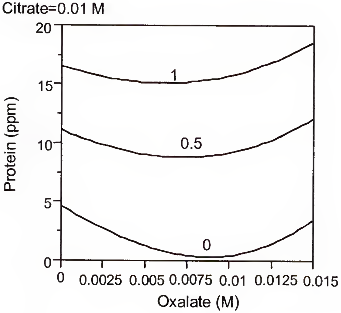

(b)

Figure 4.19. A contour plot illustrating how the amount of protein adsorbed on COM particle changes with respect to oxalate and protein concentrations at constant citrate concentrations of a) 0.0025 M and b) 0.01 M ($R^2 = 0.9693$).

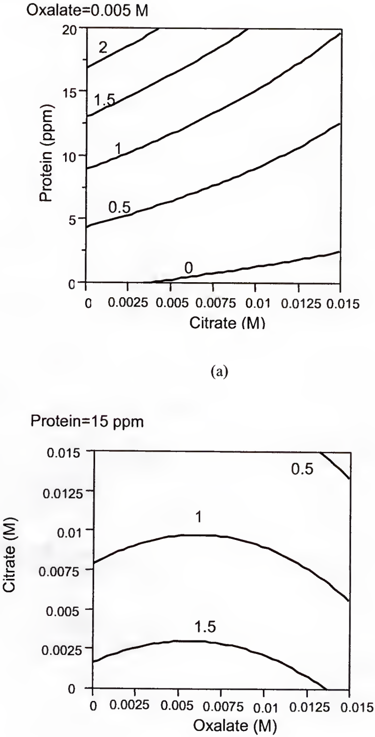

(a)

(b)

Figure 4.20. Surface response for protein adsorption. (a) Citrate concentration versus protein concentration at 0.005 M oxalate. (b) Citrate concentration versus oxalate concentration at 15 ppm of protein.

Protein adsorption may be described by the following equation (188)

$$\Gamma(t) = 2C_b(D_t/\pi) \quad [4.10]$$

where $\Gamma(t)$ is interfacial protein concentration, C_b is the bulk protein concentration and D_t is diffusion coefficient. Thus, in dilute solutions (low protein concentration (low C_b) adsorption is expected to be low.

Polymers may adsorb on surfaces in various conformations depending on bulk (solvent) and surface chemical properties of the substrate, as well as other physical conditions of the system (189). To estimate the adsorbed protein coverage, the radius of gyration (Rg) can be used. The Rg of mucin in these studies ranged from 10–50 nm, which is much smaller than theoretical Rg of 140 nm (190). This suggests that the protein is in the form of brush border conformation. The theoretical amount of mucin needed to fully cover 0.0175 g of COM particles in 50 ml is 0.0285 μg (protein concentration is 0.000571 ppm). When protein adsorbs onto the surface, protein is packed more tightly on the surface than in the bulk solution. The packing of protein could be affected by number of binding sites, electrostatics between protein molecules, protein interactions with the surface and ionic strength. As the ionic strength is increased, the electrostatic repulsion between individual protein molecules decreases. This reduced charge-charge repulsion allows for faster adsorption, saturation, and conformational changes at the interface as explained later (191). In the case that the affinity of protein to surface is not as high, then it is more favorable for more protein to adsorb onto the surface as brush border instead of one macromolecule spreading out over a larger surface. Three possibilities of conformations are illustrated in Figure 4.21. At low protein concentration, the protein may keep its globular structure shown in

Figure 4.21a. At higher protein concentration, more protein may adsorb to the surface with few binding sites and creating more of a brush border structure (Figure 4.21b). If there is a high chemical binding affinity of the protein to the surface, then the macromolecule will spread out over the surface (Figure 4.21c). The latter is less entropically favored; therefore, the former is more probable. Certainly in this study, the high ionic strength of AUIS is in favor of formation of the brush border conformation and high adsorption as shown by the adsorption isotherms given in Figure 4.22. The experimental points from the design are illustrated by a circle and upside-down triangle for citrate concentrations at 1×10^{-4} M and 0.01 M, respectively. The experimental points fit the model well.

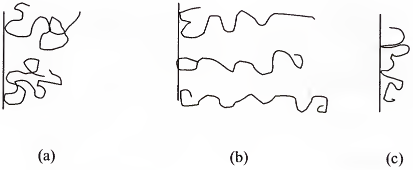

Figure 4.21. Illustration of possible conformations of adsorbed protein to a crystal surface. a) Globular shaped in a favorable solvent; b) Brush border conformation, low chemical affinity; c) Pancake shaped, high chemical affinity.

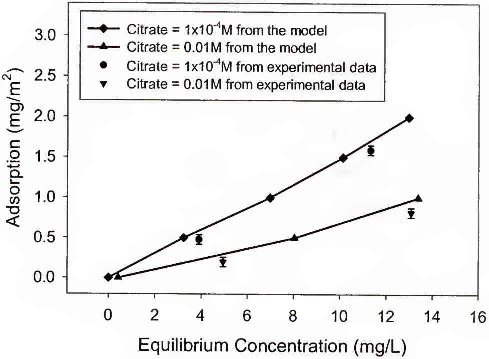

Figure 4.22. Protein Adsorption Isotherms. The amount of protein adsorbed at constant oxalate concentration of 0.01 M as a function of citrate concentration, 1 x 10^{-4} M and 0.01 M ($R^2 = 0.9693$).

The protein adsorption isotherms show that protein adsorption is less at higher citrate concentration. The observed results may be explained based on the following hypothesis (Schematically illustrated in Figure 4.23). It is well known that citrate and acidic protein tend to complex with calcium in solution and also are thought to bind to calcific surfaces (98, 160, 161). At high citrate concentration, citrate occupies the majority of calcium binding sites due to citrate being kinetically favored to diffuse faster to the COM surfaces, relative to the large protein. Therefore, there are less calcium sites available for protein binding, leading to less protein adsorbed on COM. Whereas, at low citrate concentrations, where fewer binding sites are blocked, more protein is able to adsorb onto the COM. In this case, a substantial steric barrier of particle-particle interactions is created by the protein. It must be kept in mind, however, that this study did not examine the effects of competitive adsorption, in which protein could ultimately replace some of the citrate adsorbed to the surfaces if given sufficient time. Macromolecules are generally more tightly bound to surfaces due to the multiple points of attachment. But here, it is assumed that the residence time of the particles in the urinary tract is relatively brief, and that such changes in adsorbed species would occur after aggregation, or some other form of retention of the crystals within the tract (e.g. crystal binding to renal epithelial cells). The size of the steric barrier of adsorbed protein will be much larger compared to bound citrate due to the larger size of protein.

There appears to be an interaction between calcium, oxalate and citrate. Calcium and oxalate and calcium and citrate are known to form soluble complexes in solution. The favorable reactions are given below:

$$Ca^{2+}(aq) + C_2O_4^{2-}(aq) \rightleftarrows [CaC_2O_4^{0}](aq) \qquad [4.11]$$

$$Ca^{2+}(aq) + C_6H_5O_7^{3-}(aq) \rightleftarrows [CaC_6H_5O_7^{-}](aq) \qquad [4.12]$$

The stability constants of Equations [4.11] and [4.12] between 35 and 37°C are 2,740 (59) and 60,000 (60), respectively. It is illustrated that calcium and citrate have a higher affinity for each other than calcium and oxalate. However, the solubility of calcium citrate (0.085 g/100 cc) is higher than calcium oxalate (0.00067 g/100 cc) (192). Therefore, the precipitation of calcium oxalate is more likely to take place resulting in the formation of calcium oxalate crystals. There appears to be competitive binding to calcium between citrate and oxalate, which can affect the degree of aggregation. The competitive effect between oxalate and citrate has been demonstrated in other systems (193).

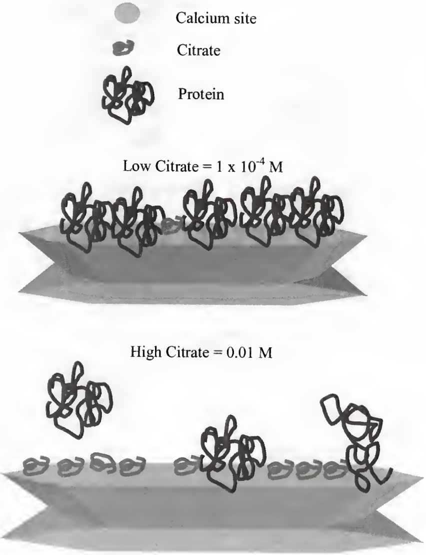

Figure 4.23. Schematic of possible citrate, calcium and protein adsorption. At high citrate concentration, there is less protein adsorption. At low citrate concentration, there is more protein adsorption.

From the aggregation and protein adsorption study, there is clinical implication. The citrate dosage is important. More citrate concentration is not always beneficial, it can be worse in certain cases if the oxalate concentration increases because of calcium complexation with the citrate. The optimum citrate dosage depends on synergistic effects with protein and oxalate. At low protein concentration, higher citrate concentration is favorable. Whereas, at high protein concentration, lower citrate concentration is better for more dispersed COM particles. The trend is similar for oxalate concentrations. At low oxalate concentration, higher citrate concentration is more desirable. In contrast, at high oxalate concentration, lower citrate concentration is more desirable. Thus, there should be an optimum dosage for citrate treatment above which diminishing or even deleterious effects will be experienced in many patients. In addition, biophysical stimuli for the production of urinary proteins would be expected to be important. In general the greater the protein concentration, the better the protective colloid interaction by urinary macromolecules. Thus, both intrinsic and extrinsic stimuli for urinary protein production should be explored in future research to promote dispersion of particles formed in the nephron.

Ions and Small Molecule Adsorption

The concentrations of oxalate, citrate, and calcium were measured by the ion chromatograph. The calcium concentrations are not shown because the detection of the calcium on the ion chromatograph was not sensitive enough due to the larger amount of other cations (potassium, sodium, and ammonium in the artificial urine). Thus, calcium concentration was measured using inductively coupled plasma (ICP) instrument. The initial concentrations for each experimental run are illustrated in Table 4.8 with corresponding aggregation coefficient. The initial calcium concentration was 0.1 mM for each run.

Table 4.8. Central Composite Design with the concentrations of the variables and their corresponding aggregation coefficient.

Run No.	Oxalate (mM)	Citrate (mM)	Protein (ppm)	Aggregation Coefficient
1	0.1	0.1	5.0	31
2	0.1	0.1	15.0	17
3	0.1	10	5.0	21
4	0.1	10	15.0	14
5	10	0.1	5.0	48
6	10	0.1	15.0	24
7	10	10	5.0	41
8	10	10	15.0	39
9	0.085	5.1	10.0	19
10	13.7	5.1	10.0	35
11	5.1	0.085	10.0	40
12	5.1	13.7	10.0	32
13	5.1	5.1	1.6	48
14	5.1	5.1	18.4	26
15	5.1	5.1	10.0	24
16	5.1	5.1	10.0	38
17	5.1	5.1	10.0	37
18	5.1	5.1	10.0	35
19	5.1	5.1	10.0	29

Ion chromatograph analysis

The oxalate and citrate concentrations were measured by the ion chromatograph to determine the amount of species remaining in solution in order to draw some conclusions as to the mechanisms of these urinary species. The amount of species remaining in solution can indicate if the rest of the species are either adsorbed to COM particles or precipitated as a crystal. The results are inconclusive for the oxalate and citrate concentrations and details of the data are shown in Tables A.1 and A.2 in the Appendix.

Inductively coupled plasma analysis (ICP)

The measured calcium amounts by ICP showed the most interesting and reliable results. The layout of Table 4.9 is the first column is the experimental run number from the central composite design. The second column is the initial amount added to the artificial urine. The third column is the measured amount of calcium in the solution of the control. The fourth column is the measured amount of calcium in the solution in the sample (containing COM particles). The fifth column is the measured amount of calcium in the sample minus the measured amount of calcium in the control. A positive number indicates there was more calcium in the sample solution; whereas, a negative number indicates there was less calcium in the sample solution. As mentioned earlier, the response used in the statistical analysis for ICP data was the extracted amount of calcium in solution (initial amount added – final sample amount in solution; Table 4.9). Note, the initial calcium solution was 0.1 mM for all the experimental runs. If the extracted amount has a positive sign, then there was less calcium in solution after the addition of COM particles. If the extracted amount has a negative sign, then there was more calcium in solution. In this case, the extra calcium came from dissolution of COM particles.

Figure 4.24 shows oxalate has an effect on calcium extracted in solution. At low oxalate concentration, the amount of calcium extracted is negative. This shows that there is dissolution of the COM particle, which increases the amount of calcium in the sample solutions. At high oxalate concentration, the amount of calcium extracted is positive. This indicates there is no dissolution of COM particles and the free calcium in solution is possibly complexing with oxalate, precipitating crystals and/or adsorbing onto the COM particle. Oxalate concentration has a great effect on the role of COM dissolution and calcium amount.

Table 4.9. Calcium Concentration measured by ICP

Run No.	Added (mM) Control	Measured (mM) Control	Final (mM) Sample	Difference (Final – Measured)	Extracted (Added – Final)
1	0.1	0.0843	0.2207	0.1364	-0.1207
2	0.1	0.0855	0.1925	0.1070	-0.0925
3	0.1	0.0834	0.5288	0.4454	-0.4288
4	0.1	0.0801	0.4028	0.3227	-0.3028
5	0.1	0.0469	0.0136	-0.0333	0.0864
6	0.1	0.0435	0.0081	-0.0354	0.0919
7	0.1	0.0753	0.0229	-0.0524	0.0771
8	0.1	0.071	0.0145	-0.0565	0.0855
9	0.1	0.0821	0.2335	0.1514	-0.1335
10	0.1	0.0604	0.0195	-0.0409	0.0805
11	0.1	0.0626	0.0147	-0.0479	0.0853
12	0.1	0.0313	0.0564	0.0251	0.0436
13	0.1	0.0707	0.0355	-0.0352	0.0645
14	0.1	0.0737	0.0172	-0.0565	0.0828
15	0.1	0.0301	0.0160	-0.0141	0.084
16	0.1	0.0569	0.0224	-0.0345	0.0776
17	0.1	0.0653	0.0173	-0.048	0.0827

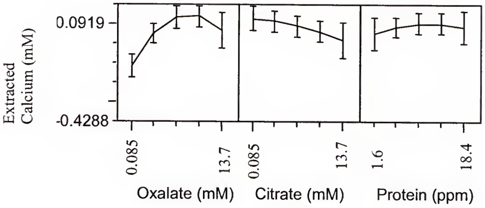

Figure 4.24. Prediction Profile of extracted calcium as a function of oxalate, citrate and protein concentration ($R^2 = 0.9399$).

There is some correlation between calcium concentration and citrate concentration. When there is a high citrate concentration, the extracted calcium is negative indicating possible dissolution of COM. Also, there may be more soluble calcium citrate complexes formed. The inverse is true at low citrate concentration; there is less free calcium in solution. Thus, calcium is adsorbing onto particles and/or precipitating crystals. Protein does not have a significant effect on extracted calcium concentration. There is an interaction between citrate and oxalate initial concentrations as exhibited by the diagonal lines in Figure 4.25.

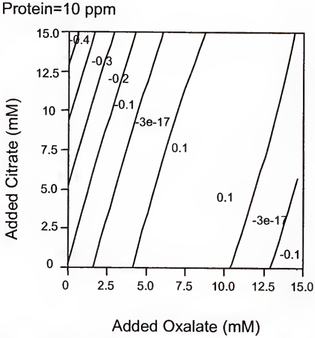

Figure 4.25. Surface response of extracted calcium as a function of oxalate and citrate concentrations. The protein concentration is constant at 10 ppm ($R^2 = 0.09399$).

At low citrate and oxalate concentrations, the amount of extracted calcium is high (Figure 4.26a). At high oxalate concentration, there is less calcium in solution. This may

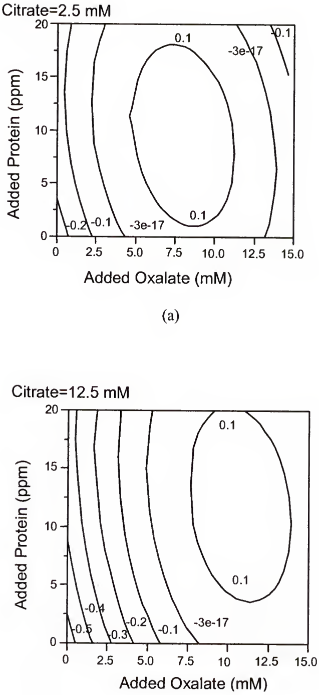

(a)

(b)

Figure 4.26. Surface response of extracted calcium as a function of oxalate and protein concentration at constant citrate concentration a) 2.5 mM; b) 12.5 mM.

be due to calcium adsorbing onto COM particle and/ or precipitation of COM particles. Protein does not play a major role in amount of calcium in solution. At high citrate concentration (Figure 4.26b), there is more calcium in solution compared to low citrate concentration (Figure 4.26a). Therefore, citrate contributes to an increase in extracted calcium. Citrate may be promoting dissolution and/or forming more soluble complexes with calcium.

In summary, at high citrate concentration, there is higher amount of calcium in solution. At low oxalate concentration, there is a higher amount of calcium. The inverse is also true, at high oxalate concentration; there is less calcium in solution. It appears that the concentration of citrate and oxalate influences the extracted calcium amount by causing dissolution of COM particles.

Theoretical Interaction Energy Curves

As previously discussed, the calculated zeta potential values in the central composite design were low (+4 to –7.4 mV). To predict the interaction energy of the samples in the central composite design, the zeta potential value was utilized along with the concentration of ions in solution to determine the energy versus distance profiles for a sphere/sphere geometry (145). For a linear approximation of Poisson-Boltzmann Distribution, one can write:

$$\zeta = \psi_s e^{(-\kappa H)} \qquad [4.13]$$

where ζ is the zeta potential, ψ_s is potential at surface, κ is Debye-Hückel parameter, and H is the separation distance from the Stern to shear planes. In the following calculations, H is taken to be 0.4 nm (194). Equation 4.13 was rewritten and the surface potential was calculated from the measured zeta potential as given by

$$\psi_s = \frac{\zeta}{e^{(-\kappa H)}} \qquad [4.14]$$

The electrostatic potential was calculated using the Hogg-Healy-Fuerstenau equation for dissimilar double layers with constant potential assumption expanded for moderate potentials by Oshima, Healy, and White (195). For systems containing both monovalent and divalent counterions, the Debye-Hückel parameter, κ, was modified according to

$$\kappa = \left(\frac{2e^2 \sum n_i Z_i^2}{\varepsilon_r \varepsilon_0 kT} \right)^{\frac{1}{2}} \qquad [4.15]$$

following Pashley et al. (196) where e is the charge on an electron, n_i is the ionic concentration of counterion specie i, Z_i the corresponding valency, ε_r the relative dielectric constant of water, ε_0 the permittivity of a vacuum, k the Boltzmann constant, and T is absolute temperature. Considering the relatively high electrolyte concentrations this formula more closely follows the exact calculation than the linear approximation. The constant potential boundary condition was used in the calculations because it has a lower boundary (electrostatic energy curve will be lower) compared to constant charge. Therefore, if under the given conditions, the particles are prevented from coagulation using constant potential, then coagulation will definitely be prevented with constant charge. In addition, at the high salt concentrations (0.301–0.366M), constant potential and constant charge are about the same.

The retarded van der Waals was taken into account for these calculations because the separation distance of the secondary minimum, where initial coagulation first becomes evident, was approximately greater than 5 nm (155). In this methodology the retarded Hamaker constant, A_{ret}, is

$$A_{ret} = A\left[1 - 5.32\frac{H}{\lambda}\ln\left(1 + \frac{1}{5.32H/\lambda}\right)\right] \qquad [4.16]$$

where A is Hamaker's constant, H is the separation distance, and l is the London wavelength corresponding to frequency of oscillation of the instantaneous dipoles, approximately 100 nm. It is illustrated (Figure 4.27), that taking into account only DLVO theory, the attraction between particulates is significant. In fact, van der Waals attraction is observed to completely dominate any electrostatic repulsive potential present. Note that this particular set of interaction energy profiles was generated for the highest zeta potential measured (-7.4 mV) and, even with the correction for ionic strength, it is not great enough to produce a significant barrier to agglomeration. Hence, it may be concluded that if a barrier to agglomeration does exist in this system, it must be of non-DLVO origin. Given that such a barrier must prevent the particles from approaching closer than approximately 20 nm, where van der Waals attraction starts to become large, it is likely that a steric repulsion is needed.

Treating protein (mucin) as a polymeric molecule, the de Gennes theory predicts steric repulsion energy as a function of separation distance, given a layer thickness (L = 2Rg) and end-to-end distance (s = 2 Rg) (148).

The layer thickness and end-to-end distance of mucin was determined from measured values from AFM and from literature (Rg = 140 nm) (190). Commonly seen from AFM measurements, using the AFM tip, was a repulsive force at ~ 8 nm separation distance. This could correspond to twice the layer thickness or one layer thickness

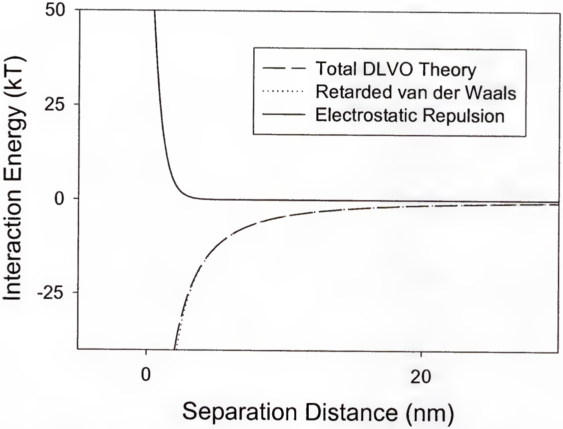

Figure 4.27. Theoretical DLVO trend for a sample in the central composite design. Curves were fit using the electrostatic energy theory of Oshima et al. (195) with constant potential boundary condition, a Hamaker constant of 13.7 x 10^{-21} J, retarded van der Waals, and zeta potential = -7.4 mV (Stern potential = -14.56 mV). The van der Waals attraction dominates and predicts aggregation of two COM particles under DLVO theory. The primary minimum is large under DLVO theory. The electrostatic repulsion is small under these conditions, probably because the ionic strength in the solution is high (0.35 M) and potential is low.

depending on whether or not protein adsorbs to the AFM tip. Hypothetical layer thicknesses and end-to-end distances used for de Gennes theory were 4 nm, 8 nm, and 200 nm based on AFM and literature. The DLVO theory fails to predict interaction energy between COM particles in the presence of polymer. Figure 4.28 shows the DLVO energy with the steric energy resulting from a polymer layer of 4 nm thickness. Even for this very small layer thickness the depth of the secondary minimum is relatively small and may prevent agglomeration. This layer thickness however, is probably underestimated due to the relatively small radius of the AFM tip. For polymer layer thickness greater than this value, an even higher barrier to agglomeration is expected.

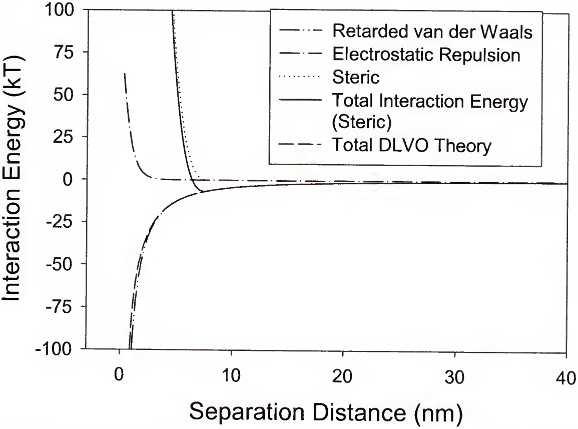

Figure 4.28. Comparison of DLVO theory and steric on interaction energy. Curves were fit using the DLVO theory by Oshima et al. (195) and de Gennes theory with constant potential boundary condition, a Hamaker constant of 13.7 x 10^{-21} J, retarded van der Waals, polymer layer thickness of 4 nm (from the AFM profile assuming protein adsorbed on both surfaces), and zeta potential of -7.4 mV (surface potential of -14.56 mV). The steric energy dominates at 8 nm creating a strong repulsive energy. A secondary minimum of -6.5 kT is exhibited where aggregation of COM particles is possible. The DLVO theory fails to predict the interaction energy between two COM particles in the presence of polymer.

The addition of de Gennes theory models the environment of the experiments more realistically than just DLVO theory. The highest layer thickness used was less than the 2Rg from literature, but it is illustrated that the steric repulsion energy is felt at such large separation distances at just 200 nm. Therefore, steric energy would follow a similar trend for 280 nm. The interaction energy curves for all three levels of protein thickness are illustrated in Figures 4.29. It is shown that the larger the polymer thickness (L) means the steric repulsion is felt at a larger separation distance. Low polymer layer thickness < 8 nm may result in a secondary minimum potential well. However, at larger polymer thickness (such as 200 nm) there is no secondary minimum and a net only repulsion is felt by the two interacting particles.

In summary, the aggregation and dispersion characteristics of COM crystals was studied under various urinary environments including effect of citrate, oxalate, and protein concentrations. The experimental data revealed the use of statistical design was important in terms of clarification of main and interaction effects in this complex system. Mechanisms responsible for aggregation and dispersion have elucidated based on experimental data. A summary of the important conclusions together with recommendations for future work is presented in the next chapter.

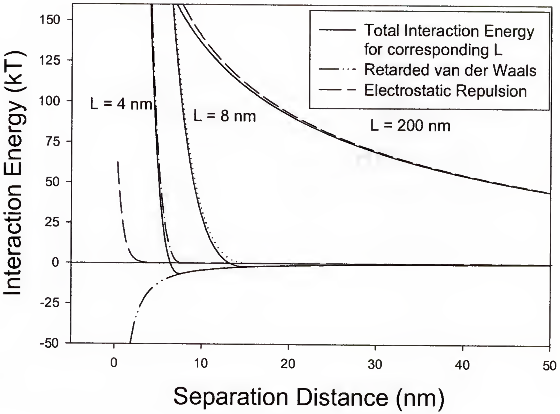

Figure 4.29. Comparison of polymer layer thickness on steric energy. Curves were calculated using the electrostatic interaction energy theory by Oshima et al. (195) with a zeta potential of -7.4 mV (surface potential of –14.56 mV), a constant potential boundary condition, a Hamaker constant of 13.7 x 10^{-21} J, retarded van der Waals attraction, and de Gennes theory with a varying polymer layer thickness of 4 nm, 8 nm, and 200 nm. The steric energy dominates at 8 nm creating a strong repulsive energy. A secondary minimum is exhibited for polymer layer thickness of 4 and 8 nm indicating possible aggregation. The polymer layer thickness of 200 nm exhibits a steric barrier at large separation distances (> 100 nm); therefore, a secondary minimum is not exhibited. The corresponding interaction energy is next to the corresponding steric energy of the same L. The van der Waals attraction and electrostatic repulsion are the same for each polymer thickness.

CHAPTER 5
CONCLUSIONS AND FUTURE WORK

Conclusions

In this study, experimental statistical design was used to determine the effect of factors on aggregation/ dispersion of calcium oxalate monohydrate (COM) in different artificial urinary environments. Several techniques were used to support and understand this data.

For synthesis of COM crystals, the rate of mixing during crystallization was found to control the crystal particle size distribution and the breadth of the distribution of COM particles. Rapid mixing produces smaller particles with more narrow distributions. In contrast, slow mixing conditions produce larger particles with broader distributions. While the comparison of COM crystals prepared by slow mixing and rapid mixing techniques shows little differences among the crystal shapes produced, there are differences in induction times.

In the aggregation and dispersion study, an empirical coefficient was used to evaluate aggregation behavior of COM particles. The coefficient has been validated by optical microscopy and particle size measurements. Statistical experimental designs (both screening and optimization designs) were used to evaluate the role of different and important parameters related to the conditions in the urinary environment. From the screening design, it was concluded that protein, citrate, and oxalate concentrations were the most significant variables close to 95% confidence level. From the analysis of central composite design, the data indicate that our model protein mucin acts as a dispersant. This is attributed to steric hindrance resulting from the adsorbed mucoprotein. Oxalate, however, promotes aggregation. This is attributed to oxalate changing the surface charge of COM coupled with compression in the double layer due to high ionic strength. These conditions will lead to aggregation of COM due to van der Waals attractive forces. The change in citrate concentration alone has little effect on aggregation.

Synergistic and antagonistic interactions between protein and oxalate along with protein and citrate are found to depend on the concentrations of these species. Citrate and protein concentrations have a strong interaction. Overall, the best dispersion is at high protein and low citrate concentration levels. Yet, this phenomenon is reversed at low protein concentrations where there is more dispersion at higher citrate concentration levels. This characteristic is also exhibited between the citrate and oxalate concentrations. This may be attributed to site blocking as a result of citrate coating on COM crystals. Mucin is affected by other species present in the system. Specifically, the amount of citrate influences the action of the mucin with respect to dispersion capability.

At low citrate concentration (0.025 M), protein plays an important role in reducing aggregation at all oxalate levels. However, at higher citrate concentration (0.01 M), protein plays a minor role. Under such conditions, lower citrate concentration would be desirable for less aggregation. High citrate concentration contributes to an increase in ionic strength, which may influence the inhibitory activity of mucin.

From the low zeta potential values (+4 to –7 mV) for the COM particles in artificial urine, there are essentially no electrostatic forces exhibited by COM particles in the high ionic strength of artificial urine. The theoretical calculations using DLVO theory only shows primary minimum well at all zeta potential values. A secondary minimum was shown to exist at low protein thickness (8 nm). This supports the idea that another barrier, steric forces, is causing the COM particles to be more dispersed.

From the AFM force measurements in artificial urine solution, the high salt concentration of the solution decreases the electrostatic repulsion forces (compression of the double layer) and results in attractive van der Waals forces at short separation distances (~ 4 nm). When 10 ppm protein is added to artificial urine, a steric repulsive force appears at separation distances ~ 8 nm. Therefore, steric repulsive forces can be felt at low protein concentration by the AFM, and is considered a likely reason for dispersion of COM in the presence of protein under the conditions tested in our model system.

During the AFM study, it was shown that once protein was adsorbed onto COM surface, it was not reversible. Also, in the presence of protein there is a greater repulsion force at low citrate concentration compared to high citrate concentration. This confirms the aggregation data, which shows there is more dispersion at high protein concentration and lower citrate concentrations.

Adsorption data for protein on COM in the presence of citrate and oxalate are used to explain the results of the aggregation/ dispersion characteristics of COM particles under similar chemical conditions. For example, the amount of protein adsorption on COM particles is lower at high citrate levels. On the other hand, oxalate has little effect on protein adsorption.

To estimate the adsorbed protein coverage on COM particles, the Rg is used. In general, Rg in samples ranging from 10–50 nm is much smaller than theoretical Rg of

140 nm (190). When protein adsorbs onto a surface, protein is packing more tightly on the surface than in the bulk solution. The packing of protein could be affected by number of binding sites, electrostatics between protein molecules, protein interactions with the surface and ionic strength. From zeta potential measurements, it was shown that an increase in ionic strength reduced zeta potential of mucin. Conformational changes of protein are most likely due to high ionic strength environment.

There are interactions among urinary species, thus affecting their influence on dispersion/ aggregation behavior of COM crystals. For instance, at high citrate concentration, there is more dissolution of calcium from COM crystals. This is confirmed by the fact that citrate is used as a sequestering reagent for calcium. The reverse trend is exhibited in the presence of oxalate. At high oxalate concentration, there is a lower amount of calcium. This could be due to calcium oxalate precipitation. At low oxalate concentration, there is a higher amount of calcium due to dissolution of COM particles and formation of soluble calcium oxalate complexes.

Thus, the experimental data for protein adsorption and interparticle force measurements as well as aggregation results may be explained based on the following hypothesis. It is well known that citrate and acidic protein tend to complex with calcium in solution and thought to bind to calcific surfaces. At high citrate concentration, citrate occupies the majority of calcium binding sites due to citrate being kinetically favored to diffuse faster to the COM surfaces, relative to the large protein. Therefore, there are fewer calcium sites available for protein binding, leading to less protein adsorbed on COM, whereas, at low citrate concentrations, where fewer binding sites are blocked, more protein is able to adsorb onto the COM. In this case, a substantial steric barrier of particle-particle interactions is created by the protein as confirmed by atomic force microscopy force measurements. The size of the steric barrier of adsorbed protein will be much larger compared to bound citrate due to the larger size of protein. It is assumed that the residence time of the particles in the urinary tract is relatively brief, and that such changes in adsorbed species would occur after aggregation, or some other form of retention of the crystals within the tract (e.g. crystal binding to renal epithelial cells).

From the aggregation and protein adsorption studies, a clinical implication is that citrate dosage is important. The beneficial citrate concentration is dependent on oxalate and protein concentrations. At high oxalate and high protein concentrations, lower citrate concentration is desirable. In contrast, at low oxalate and low protein concentrations, higher citrate concentration is the most beneficial for dispersion of COM crystals, which may prevent stone formation.

In summary, solution, surface, and interface chemistries interact in a complex manner in the physiological environment to either inhibit or promote aggregation. The data indicate the interactions between species specifically calcium, oxalate, citrate, and protein play an important role in dispersion/ aggregation of kidney stone constituents.

Future Work

There are several suggestions for future work:

- Confirm aggregation study with urinary protein, Tamm-Horsfall mucoprotein (similar physicochemical properties to mucin used in this study)
- Test other urinary acidic glycoproteins i.e. osteopontin for aggregation characteristics
- Evaluate aggregation with high calcium concentrations and suppress oxalate concentration

- Order of addition of constituents to COM crystals in the following manner: calcium, protein, calcium, and citrate. To observe if calcium helps bind protein to COM particles and helps bind citrate to protein via calcium.

- Test effects of competitive adsorption between citrate and protein (e.g. if given sufficient amount of time, would protein replace bound citrate)

- Determine accurate amount of citrate and oxalate remaining in solution or bound to COM surface

- Perform crystallization studies using experimental design and study the effect of variables on growth and aggregation of crystals (high concentrations of oxalate and calcium can be used at the same time)

- Synthesize atomically smooth CaOx particles for AFM (eliminate noise from surface roughness)

- Measure particle-particle interactions in AUIS using the AFM

- Measure interaction forces between CaOx particle and protein coated silica sphere in AUIS

APPENDIX
ION CHROMATOGRAPH DATA

The layout of each table is the first column is the experimental run number from the central composite design. The second column is the initial amount added to the artificial urine. The third column is the measured amount of free specie in the solution of the control. The fourth column is the measured amount of free specie in the solution in the sample (containing COM particles). The fifth column is the measured amount of species in the sample minus the measured amount of species in the control. A positive number indicates there was more species (oxalate or citrate) in the sample solution; whereas, a negative number indicates there was less species (oxalate or citrate) in the sample solution. The thought behind measuring a control and sample was to determine the amount of soluble complexes because the ion chromatograph only measures free amount of a species. The samples were diluted with 1 mM HCl to try to break up any soluble complexes with citrate and oxalate.

Table A.1. Oxalate Concentration measured by Ion Chromatograph

Run No.	Added (mM) Control	Measured (mM) Control	Final (mM) Sample	Difference (Final – Measured)
1	0.1	0.195	0.32	0.125
2	0.1	0.175	0.25	0.075
3	0.1	0.185	0.695	0.51
4	0.1	0.175	0.67	0.495
5	10	8.06	9.355	1.295
6	10	9.815	10.43	0.615
7	10	10.295	11.195	0.9
8	10	10.33	8.33	-2.0
9	0.085	0.175	0.495	0.32
10	13.7	14.29	14.08	-0.21
11	5.1	6.055	5.83	-0.225
12	5.1	5.72	5.335	-0.385
13	5.1	5.87	5.83	-0.04
14	5.1	5.605	5.56	-0.045
15	5.1	5.91	5.46	-0.45
16	5.1	4.59	4.72	0.13
17	5.1	5.66	5.035	-0.625

Table A.2. Citrate Concentration measured by Ion Chromatograph

Run No.	Added (mM) Control	Measured (mM) Control	Final (mM) Sample	Difference (Final – Measured)
1	0.1	0.11	0.1	-0.01
2	0.1	0.115	0.105	-0.01
3	10	8.29	9.115	0.825
4	10	8.745	9.39	0.915
5	0.1	0.125	0.12	-0.005
6	0.1	0.12	0.115	-0.005
7	10	9.115	9.985	0.87
8	10	9.24	9.125	-0.115
9	5.1	6.875	5.075	-1.8
10	5.1	4.84	4.675	-0.165
11	0.085	0.05	0.03	-0.02
12	13.7	14.155	12.835	-1.32
13	5.1	5.51	5.455	-0.055
14	5.1	5.035	5.075	0.04
15	5.1	5.005	4.76	-0.245
16	5.1	4.91	4.575	-0.335
17	5.1	5.16	4.655	-0.505

LIST OF REFERENCES

1. Khan, S. R., Atmani, F., Glenton, P., Hou, Z. C., Talham, D. R., Khurshid, M., *Calcif. Tissue Int.* **59**, 357 (1996).

2. Khan, S. R., *Scanning Microscopy* **9**, 89 (1995).

3. Kok, D. J., Papapoulos, S. E., Bijovoet, O. L. M., *Lancet* **1**, 1056 (1986).

4. Kok, D. J., Papapoulos, S. E., Buvoet, O. L. M., *Kidney Int.* **37**, 51 (1990).

5. Hess, B., Nakagawa, Y., Coe, F. L., *Am. J. Physiol.* **257**, F99 (1989).

6. Benkovic, J., Furedi-Milhofer, H., Hlady, V., Cvoriscec, D., Stavljenic-Rukavina, A., *Eur. J. Clin. Chem. Clin. Biochem.* **33**, 705 (1995).

7. Hess, B., Jordi, S., Zipperle, L., Ettinger, E., Giovanoli, R., *Nephrol. Dial. Transplant.* **15**, 366 (2000).

8. Mason, R. L., Gunst, R. F., Hess, J. L., *Statistical Design and Analysis of Experiments with Applications to Engineering and Science* (John Wiley & Sons, New York, 1989).

9. Ambulatory care visits to physician offices, hospital outpatient departments, and emergency departments: United States, 1996. *NCHS, CDC, HHS* (February 1998).

10. National Hospital Discharge Survey: Annual summary, 1996. *NCHS, CDC, HHS* (1999).

11. Clark, J. Y., Thompson, I. M., Optenberg, S. A., *Journal of Urology* **154**, 2020 (1995).

12. Coe, F. L., Parks, J. H., Asplin, J. R., *N Engl J Med* **327**, 1141 (1992).

13. Sutherland, J. W., Parks, J. H., Coe, F. L., *Miner. Electrolyte Metab.* **11**, 267 (1985).

14. Vander, A. J., *Renal Physiology* (McGraw-Hill, Inc., New York, 4th ed., 1991).

15. Guyton, A. C., Hall, J. E., *Textbook of Medical Physiology* (W.B. Saunders Company, Philadelphia, 9th ed., 1996).

16. Goldfarb, S., *Kidney Int.* **34**, 544 (1988).

17. Parivar, F., Low, R. K., Stoller, M. L., *J. Urol.* **155**, 432 (1996).

18. Duarte, C. G., Knox, F. G., in *Textbook of Renal Pathophysiology* . (Harper and Row, New York, 1978) p. 148.

19. Lemann Jr., J., Worcester, E. M., Gray, R. W., *Am. J. Kidney Diseases* **17**, 386 (1991).

20. Koide, T., Bowyer, R. C., Brockis, J. G., *Br. J. Urol.* **57**, 505 (1985).

21. Conte, A., Genestar, C., Grases, F., *Urol. Int.* **45**, 25 (1990).

22. Zarembski, A., Hodgkinson, A., *Clin. Chim. Acta* **25**, 1 (1969).

23. Hagler, L., Herman, R. H., *Amer. J. Clin. Nutr.* **26**, 758 (1973).

24. Williams, H. E., in *Urolithiasis Research* H. Fleisch, W. G. Robertson, L. H. Smith, W. Vahlensieck, Eds. (Plenum Press Co., New York, 1976) p. 181.

25. Menon, M., Mahle, C. J., *J. Urol.* **127**, 148 (1982).

26. Laminski, N. A., Meyers, A. M., Kruger, M., Sonnekus, M. I., Margolius, L. P., *Brit. J. Urol.* **68**, 454 (1991).

27. Goldfarb, D. S., Coe, F. L., *Am. Fam. Physician* **60**, 2269 (1999).

28. Hatch, M., *Urol. Res.* **21**, 55 (1993).

29. Simpson, D. P., *Am. J. Physiol.* **244**, F223 (1983).

30. Berg, C., Ph.D. thesis, Linkoping University (1990).

31. Jenkins, A. D., Dousa, T. P., Smith, L. H., *Am. J. Physiol.* **249**, F590 (1985).

32. Pak, C. Y. C., *Miner. Electr. Meta.* **20**, 371 (1994).

33. Pak, C. Y. C., Fuller, C., Sakhaee, K., Preminger, G., Britton, F., *J. Urol.* **134**, 11 (1985).

34. Parks, J. H., Coe, F. L., *Kidney Int.* **30**, 85 (1986).

35. Nicar, M. J., Hill, K., Pak, C. Y. C., *J. Bone Miner. Res.* **2**, 215 (1987).

36. Kok, D. J., Ph.D. thesis, University of Leiden (1991).

37. Marangella, M., Bianco, O., Martini, C., Petrarwla, M., Vitale, C., Linari, F., *Brit. J. Urol.* **63**, 348 (1989).

38. Trinchieri, A., Mandressi, A., Luongo, P., Longo, G., Pisani, E., *Brit. J. Urol.* **67**, 230 (1991).

39. Fuselier, H. A., Ward, D. M., Lindberg, J. S., Allen, J. M., Husserl, F. E., Marcucci, P. A., Cole, F. E., Turnipseed, J., Alam, J., Kok, D. J., *Urology* **45**, 942 (1995).

40. Finlayson, B., *Urol. Clin. North Am.* **1**, 181 (1974).

41. Coe, F. L., Favus, M. J., in *The Kidney* B. M. Brenner, J. F.L. Rector, Eds. (WB Saunders, Philadelphia, 1986) p. 1403.

42. Hess, B., Kok, D. J., in *Kidney Stones: Medical and Surgical Management* F. L. Coe, M. J. Favus, C. Y. C. Pak, J. H. Parks, G. M. Preminger, Eds. (Lippincott-Raven Publishers, Philadelphia, 1996) p. 3.

43. Burns, J. R., Finlayson, B., *Invest. Urol.* **18**, 174 (1980).

44. Leal, J. J., Finlayson, B., *Invest. Urol.* **14**, 278 (1977).

45. Skrtic, D., Furedi-Milhofer, H., Markovic, M., *J. Crystal Growth* **80**, 113 (1987).

46. Furedi-Milhofer, H., Babic-Ivancic, V., Brecevic, L., Filipovic-Vincekovic, N., Kralj, D., Komunjer, L., Markovic, M., Skrtic, D., *Colloids and Surfaces* **48**, 219 (1990).

47. Brown, C. M., Ackermann, D. K., Purich, D. L., Finlayson, B., *J. Crystal Growth* **108**, 455 (1991).

48. Adair, J. H., Linhart, R. V., Habeger, C. F., Khan, S. R., in *Calcium Oxalate in Biological Systems* S. R. Khan, Ed. (CRC Press, Boca Raton, FL, 1995) p. 37.

49. Habeger, C. F., Linhart, R. V., Adair, J. H., in *Science, Technology and Applications of Colloidal Suspensions, Ceramic Transactions* J. H. Adair, J. A. Casey, C. A. Randall, S. Venigalla, Eds. (American Ceramic Society, Westerville, OH, 1995), vol. 54, p. 111.

50. Mandel, N., *J. Am. Soc. of Nephrol.* **5**, S37 (1994).

51. Lieske, J. C., Leonard, R., Swift, H., Toback, F. G., *Am. J. Physiol.* **270**, F192 (1996).

52. Werness, P. G., Brown, C. M., Smith, L. H., Finlayson, B., *J. Urol.* **134**, 1242 (1985).

53. Khan, S. R., Hackett, R. L., *Calcif. Tissue Int.* **41**, 157 (1987).

54. Nancollas, G. H., Smesko, S. A., Campbell, A. A., Richardson, C. F., Johnsson, M., Indiccico, R. A., Binette, J. P., Binette, M., *American J. Kidney Disease* **17**, 392 (1991).

55. Deganello, S., *Scanning Electron Microsc.* **4**, 1721 (1986).

56. Gardner, G. L., *J. Cryst. Growth* **30**, 158 (1975).

57. Cifuentes, D. L., in *Stones: Clinical Management of Urolithiasis* R. A. Roth, B. Finlayson, Eds. (Williams & Wilkins, Baltimore, 1983) p. 23.

58. Curreri, P., Y. Onoda, J., Finlayson, B., *J. Colloid Interface Sci.* **69**, 170 (1979).

59. Finlayson, B., Roth, R. A., DuBois, L. G., in *Urinary Calculi* L. Cifuentes, A. Delatte, A. Rapado, A. Hodgkinson, Eds. (Karger, Basel, 1973).

60. Finlayson, B., in *Calcium Metabolism in Renal Failure and Nephrolithiasis* D. S. David, Ed. (John Wiley & Sons, New York, 1977) p. 337.

61. Boyce, W. H., Garvey, F. K., *J. Urol.* **76**, 213 (1956).

62. Khan, S. R., Hackett, R. L., *J. Urol.* **150**, 239 (1993).

63. Khan, S. R., in *Calcification in Biological Systems* E. Bonnuci, Ed. (CRC Press, Boca Raton, 1992) p. 345.

64. Malek, R. S., Boyce, W. H., *J. Urol.* **117**, 336 (1977).

65. Morner, K. A. H., *Skand. Arch. Physiol.* **6**, 332 (1895).

66. Tamm, I., Horsfall, F. L., *Proc. Soc. Exp. Biol. Med.* **74**, 108 (1950).

67. Hunt, J. S., McGiven, A. R., Groufsky, A., Lynn, K. L., Taylor, M. C., *Biochem. J.* **227**, 957 (1985).

68. Kumar, S., Muchmore, A., *Kidney Int.* **37**, 1395 (1990).

69. Hoyer, J. R., Seiler, M. W., *Kidney Int.* **16**, 279 (1979).

70. Rindler, M. J., Naik, S. S., Li, N., Hoops, T. C., Peraldi, M. N., *J. Biol. Chem.* **265**, 20784 (1990).

71. Ronco, P., Brunisholz, M., Geniteau-Legendre, M., Chatelet, F., Verroust, P., Richet, G., *Adv. Nephrol. Necker Hosp.* **16**, 231 (1987).

72. Sikri, K. L., Foster, C. L., MacHugh, N., Marshall, R. D., *J. Anat.* **132**, 597 (1981).

73. Hunt, J. S., Peach, R. J., Brunisholz, M. C., Lynn, K. L., McGiven, A. R., *J. Immunol. Meth.* **91**, 35 (1986).

74. Avis, P. J. G., *Clin. Sci. Mol. Med.* **52**, 183 (1977).

75. Curtain, C. C., *Aust. J. Exp. Biol.* **31**, 615 (1953).

76. Friedman, T., Johnson, P., *Biochim. Biophys. Acta* **121**, 292 (1966).

77. Fletcher, A. P., McLaughlin, J. E., Ratcliffe, W. A., Woods, P. A., *Biochim. Biophys. Acta* **214**, 299 (1970).

78. Stevenson, F. K., Kent, P. W., *Biochem. J.* **116**, 791 (1970).

79. Fletcher, A. P., Neuberger, A., Ratcliffe, W. A., *Biochem. J.* **120**, 417 (1970).

80. Williams, J., Marshall, R., van Halbeek, H., Vliegenthart, J. F. G., *Carbohydr. Res.* **134**, 141 (1984).

81. Stevenson, F. K., Cleave, A. J., Kent, P. W., *Biochim. Biophys. Acta* **236**, 59 (1971).

82. Curtain, C. C., *Austr. J. Exp. Biol.* **31**, 255 (1953).

83. Cleave, A. J., Kent, P. W., Peacocke, A. R., *Biochim. Biophys. Acta* **285**, 208 (1972).

84. McQueen, E. G., Engel, G. B., *J. Clin. Pathol.* **19**, 392 (1966).

85. Pesce, A. J., Kant, K. S., Clyne, D. H., Pollak, V. E., *Clin. Chem.* **23**, 1146 (1977).

86. Sanders, P. W., Booker, B. B., Bishop, J. B., Cheung, H. C., *J. Clin. Invest.* **85**, 570 (1990).

87. Orskov, I., Ferencz, A., Orskov, F., *Lancet* **1**, 887 (1980).

88. Kuriyama, S. M., Silverblatt, F. J., *Infect. Immun.* **51**, 193 (1986).

89. Sherbloom, A., Decker, J., Muchmore, A., *J. Biol. Chem.* **263**, 5418 (1988).
90. Sherbloom, A., Sathyamoorthy, M., Decker, J. M., Muchmore, A. V., *J. Immunol.* **143**, 939 (1989).
91. Moonen, P., Gaffner, R., Wingfield, P., *FEBS Lett* **226**, 314 (1988).

92. Hallson, P. C., Rose, G. A., *Lancet* **1**, 1000 (1979).

93. Rose, G. A., Sulaiman, S., *J. Urol.* **127**, 177 (1982).

94. Gjaldbaek, J. C., Robertson, W. G., *Clin. Chim. Acta* **108**, 75 (1980).

95. Scurr, D. S., Robertson, W. G., *J. Urol.* **136**, 505 (1986).

96. Sophasan, S., Chatasingh, S., Thanaphaichitr, P., Dhanamitta, S., *J. Urol.* **124**, 522 (1980).

97. Hess, B., *Urol. Res.* **20**, 83 (1992).

98. Fleisch, H., *Kidney Int.* **13**, 361 (1978).

99. Finlayson, B., *Kidney Int.* **13**, 344 (1978).

100. Robertson, W. G., Scurr, D. S., Bridge, M., *J. Crystal Growth* **18**, 484 (1981).

101. Hess, B., Zipperele, L., Jaeger, P., *Am J Physiol* **265**, F784 (1993).

102. Erwin, D. T., Kok, D. J., Alam, J., Vaughn, J., Coker, K., Carriere, B. T., Lindberg, J., Husserl, F. E., Fuselier, H. J., Cole, F. E., *J. Am Soc. Nephrol.* **4**, 706 (1993).

103. Kreis, T., Vale, R., Eds., *Guidebook to the Extracellular Matrix, Anchor, and Adhesion Proteins* (Oxford University Press, Oxford, 1999).

104. Mantle, M., Allen, A., in *Gastrointestinal Secretion* J. S. Davison, Ed. (Butterworths and Co., Ltd., London, 1989) p. 202.

105. Nisizawa, K., Pigman, W., *Arch. Oral. Biol.* **1**, 161 (1959).

106. Gottschalk, A., *Nature London* **186**, 949 (1960).

107. Tettamanti, G., Pigman, W., *Arch. Biochem. Biophys.* **124**, 41 (1968).

108. Tguiki, S., Hashimoto, Y., Pigman, W., *J. Biol. Chem.* **236**, 2172 (1961).

109. Weiping, J., Woitach, J. T., Keil, R. L., Bhavanandan, V. P., *Biochem. J.* **331**, 193 (1998).

110. Strous, G. J., Dekker, J., *Critical Review in Biochemistry and Molecular Biology* **27**, 57 (1992).

111. Budvari, S., Ed., *The Merck Index* (Merck and Co., Inc., Whitehouse Station, NJ, 1996).

112. Gum, J. R., Hicks, J. W., Toribara, N. W., Siddiki, B., Kim, Y. S., *J. Biol. Chem.* **269**, 2440 (1994).

113. Pigman, W., Moschera, J., Weis, M., Tettamanti, G., *Eur. J. Biochem.* **32**, 148 (1973).

114. Bhargava, A. K., Woitach, J. T., Davidson, E. A., Bhavanandan, V. P., *Proc. Natl. Acad. Sci.* **87**, 6798 (1990).

115. Paerregaard, A., Espersen, F., Jensen, O. M., Skurnik, M., *Infect. Immun.* **59**, 253 (1991).

116. Mantle, M., Basaraba, L., Peacock, S. C., Gall, D. G., *Infect. Immun.* **57**, 3292 (1989).

117. Dulawa, J., Jann, K., Thomsen, M., Rambusek, M., Ritz, E., *Eur. J. Clin. Invest.* **18**, 87 (1988).

118. Weiner, S., Addadi, L., *Trends Biochem. Sci.* **16**, 252 (1991).

119. Nielsen, A. E., *Kinetics of Precipitation* (MacMillan Co., New York, 1964).

120. Robinson, R. A., Stokes, R. H., *Electroyte Solutions* (Butterworths, London, 1959).

121. Brown, C. M., Purich, D. L., in *Disorders of Bone and Mineral Metabolism* F. L. Coe, M. J. Favus, Eds. (Raven Press, New York, 1992) p. 613.

122. Nyvlt, J., Sohnel, O., Matuchova, M., Broul, M., in *Chemical Engineering Monographs 19* . (Elsevier Science Publishers, Ambsterdam, 1985).

123. Walton, A. G., *The Formation and Properties of Precipitates* (Robert E. Krieger Publishing Co., Huntington, NY, ed., 1979).

124. Kingery, W. D., Bowen, H. K., Uhlmann, D. R., *Introduction to Ceramics* (John Wiley & Sons, New York, 2nd ed., 1976).

125. Sohnel, O., Garside, J., *Precipitation: Basic Principles and Industrial Applications* (Butterworth-Heineman Ltd, Oxford, 1992).

126. Tavare, N. S., in *Industrial Crystallization Process Simulation Analysis and Design* . (Plenum Press, New York, 1995) p. 353.

127. Villermaux, J., David, R., *Chem. Eng. Commun.* **21**, 105 (1983).

128. Garside, J., Gaska, J., Mullin, J. W., *J. Crystal Growth* **13**, 510 (1972).

129. Ives, K. J., ASCE, M., Bhole, A. G., *J. Environmental Engineering Division EE1, 9540* , 17 (1973).

130. Robertson, W. G., *Clin. Chim. Acta* **26**, 105 (1969).

131. Adair, J. H., Roese, A. J., McCoy, L. G., in *Advances in Ceramics Processing for Improved Productivity* K. M. Nair, Ed. (E.I. du Pont de Nemours & Co., Niagara Falls, New York, 1984), vol. 11, p. 142.

132. Grases, F., Masarova, L., Sohnel, O., Costa-Bauza, A., *Brit.J. Urol.* **70**, 240 (1992).

133. Meyer, J. L., in *Urolithiasis: A Medical and Surgical Reference* M. I. Resnick, C. Y. C. Pak, Eds. (W.B. Saunders Company, Philadelphia, 1990) p. 11.

134. Kok, D. J., Khan, S. R., *Kidney Int.* **46**, 847 (1994).

135. Finlayson, B., Reid, F., *Invest. Urol.* **15**, 442 (1978).

136. Khan, S. R., *Urol. Res.* **23**, 71 (1995).

137. Kok, D. J., Papapoulos, S. E., *Bone Min.* **20**, 1 (1993).

138. Kok, D. J., *World J. Urol.* **15**, 219 (1997).

139. Finlayson, B., Khan, S. R., Hackett, R. L., *Scan. Elec. Microsc.* **3**, 1419 (1984).

140. Rumpf, H., Schubert, H., in *Ceramic Processing Before Firing* J. G.Y. Onoda, L. L. Hench, Eds. (John Wiley & Sons, New York, 1978) p. 357.

141. Worcester, E. M., Nakagawa, Y., Wabner, C. L., Kumar, S., Coe, F. L., *Am. J. Physiol.* **255**, F1197 (1988).

142. Hunter, R. J., *Foundations of Colloid Science* (Oxford University Press Inc., New York, 1986), vol. I.

143. Hunter, R. J., *Zeta Potential in Colloid Science: Principles and Applications* (Academic Press, New York, 1981).

144. Hunter, R. J., *Introduction to Modern Colloid Science* (Oxford Science Publications, Oxford, ed., 1993).

145. Israelachvili, J., *Intermolecular and Surface Forces* (Academic Press, San Diego, 2nd ed., 1992).

146. Alexander, S. J., *J. Physique* **38**, 983 (1977).

147. de Gennes, P. G., *C.R. Acad. Sci.* **300**, 839 (1985).

148. de Gennes, P. G., *Adv. Colloid Interface Sci.* **27**, 189 (1987).

149. Derjaguin, B. V., *Kolloid Zeitschrift* **69**, 155 (1934).

150. Hamaker, H. C., *Physica* **4**, 1058 (1937).

151. Lifshitz, E. M., *Sov. Phys. JETP* **2**, 73 (1956).

152. Tabor, D., Winterton, R. H. S., *Proc. R. Soc. London A* **312**, 435 (1969).

153. Pashley, R. M., *J. Colloid and Interface Sci.* **62**, 344 (1977).

154. Mahanty, J., Ninham, B. W., *Dispersion Forces* (Academic Press, New York, 1976).

155. Gregory, J., *J. Colloid and Interface Sci.* **83**, 138 (1981).

156. Verwey, Overbeek, *Theory of Stability of Lyophobic Colloids* (Elsevier, New York, 1948).

157. Derjaguin, B. V., Landau, L., *Acta Physicochim. URSS* **14**, 633 (1941).

158. Daudon, M., Hennequin, C., Bader, C., Jungers, P., Lacour, B., Druecke, T., *Advances in Nephrology* **24**, 167 (1995).

159. Russell, R. G. G., Bisaz, S., Fleisch, H., *Clin. Sci. Mol. Med.* **51**, 435 (1976).

160. Hennequin, C., Lalanne, V., Daudon, M., Lacour, B., Druecke, T., *Urol. Res.* **21**, 101 (1993).

161. Grases, F., Costa-Bauza, A., *Br. J. Urol.* **66**, 240 (1990).

162. Grases, F., Gil, J. J., Conte, A., *Urol. Res.* **17**, 163 (1989).

163. Antinozzi, P., Brown, C. M., Khan, S. R., al., e., Inhibitory action of citrate on calcium oxalate monohydrate crystal nucleation and growth, Proceedings of the VIIth International Symposium on Urolithiasis, Cairns, Australia (1992).

164. Coe, F. L., Parks, J. H., Lindheimer, M. D., in *Disorders of Bone and Mineral Metabolism* F. L. Coe, M. J. Favus, Eds. (Raven Press, New York, 1992) p. 757.

165. Zerwekh, J. E., Hwang, T. I. S., Poindexter, J., Hill, K., Wendell, G., Pak, C. Y., *Kidney Int.* **33**, 1005 (1988).

166. Andrade, J. D., Hladly, V., *Biopolymers/ Non-Exclusion HPLC* Adv. Polymer Sci. Series (Springer-Verlag, New York, ed., 1986), vol. 79.

167. Anderson, V. L., McLean, R. A., *Design on Experiments: A Realistic Approach* (Marcel Dekker, Inc., New York, 1974).

168. Box, G. E. P., Hunter, W. G., Hunter, J. S., *Statistics for Experiments* (John Wiley & Sons, Inc., New York, 1978).

169. Cochran, W. G., Cox, D. R., *Experimental Designs* (John Wiley & Sons, New York, 3rd ed., 1962).

170. Fox, R. W., McDonald, A. T., *Introduction to Fluid Mechanics* (John Wiley & Sons, Inc., New York, 4th ed., 1992).

171. Burns, J. R., Finlayson, B., *Invest. Urol.* **18**, 167 (1980).

172. Ducker, W. A., Senden, T. J., *Langmuir* **8**, 1831 (1992).

173. Ip, L., Chan, D., *AFM Analysis Software.* (Parkville, Australia, 1994).

174. Albeck, S., Aizenberg, J., Addadi, L., Weiner, S., *J. Am. Chem. Soc.* **115**, 11691 (1993).

175. Atmani, F., Opalko, F. J., Khan, S. R., *Urol. Res.* **24**, 45 (1996).

176. Atmani, F., Glenton, P. A., Khan, S. R., *Urol. Res.* **26**, 201 (1998).

177. Khan, S. R., in *Calcium Oxalate in Biological Systems* S. R. Khan, Ed. (CRC Press, Boca Raton, FL, 1995) p. 343.

178. Ryall, R. L., Marshall, V. R., *Clinica Chimica Acta* **83**, 99 (1978).

179. Ryall, R. L., Ryall, R. G., Doyle, I. R., Marshall, V. R., *J. Crystal Growth* **133**, 87 (1993).

180. Nancollas, G. H., in *Ceramic Powder Science II, Ceramic Transactions* G. L. Messing, J. E.R. Fuller, H. Hauser, Eds. (American Ceramic Society, Inc., Westerville, OH, 1988), vol. 1, p. 8.

181. Singh, R. P., Gaur, S. S., Sheehan, M. E., Nancollas, G. H., *J. Crystal Growth* **87**, 318 (1988).

182. Tiselius, H. G., Fornander, A. M., Nilsson, M. A., *Urol. Res.* **21**, 363 (1993).

183. Dean, J. A., *Lange's Handbook of Chemistry* (McGraw-Hill, Inc., New York, 14th ed., 1992).

184. Lieske, J. C., Deganello, S., *J. Am. Soc. Nephrol.* **10**, S422 (1999).

185. Utsunomiya, M., Koide, T., Yoshioka, T., Yamaguchi, S., Okuyama, A., *Br. J. Urol.* **71**, 516 (1994).

186. Kollmer, A., Schmid, A., Rohr, P. R. v., Sonnleitner, B., *Bioprocess Eng.* **20**, 441 (1999).

187. Kousaka, Y., Endo, Y., in *Powder Technology Handbook* K. Gotoh, H. Masuda, K. Higashitani, Eds. (Marcel Dekker, Inc., New York, 1997) p. 3.

188. Ward, A. F. H., Tordai, L., *J. Chem. Phys.* **14**, 453 (1946).

189. Somansundaran, P., Ramachandran, R., Innovative approaches to elucidate floc structures and polymer conformations at interfaces, B. M. Moudgil, B. J. Scheiner, Eds., Engineering Foundation Conference, Palm Coast, FL (Engineering Foundation, 1988).

190. Baszkin, A., Deyme, M., Perez, E., Proust, J. E., Reversible-Irreversible protein adsorption and polymer surface characterization, J. L. Brash, T. A. Horbett, Eds., American Chemical Society, Anaheim, CA (American Chemical Society, 1987).

191. Beverung, C. J., Radke, C. J., Blanch, H. W., *Biophys. Chem.* **81**, 59 (1999).

192. Lide, D. R., Frederikse, H. P. R., *CRC Handbook of Chemistry and Physics* (CRC Press, Inc., Boca Raton, FL, 75th ed., 1994).

193. Wijnja, H., Schulthess, C. P., *Soil Sci. Soc. Am. J.* **64**, 898 (2000).

194. Attard, P., Antelmi, D., Larson, I., *Langmuir* **16**, 1542 (2000).

195. Oshima, H., Healy, T. W., White, L. R., *J. Colloid and Interface Sci.* **89**, 484 (1982).

196. Pashley, R. M., Israelachvili, J. N., *J. Colloid and Interface Sci.* **97**, 446 (1983).

BIOGRAPHICAL SKETCH

Kimberly Gail Christmas was born on May 26, 1972, in Daytona Beach, Florida. She attended Seabreeze High School and participated in activities ranging from track and field to National Honor Society. She left her home state of Florida to attend Clemson University in Clemson, South Carolina. There, she became interested in engineering and obtained her B.S. in Ceramic Engineering in December 1994. During her co-op at Coors Electronic Package Company in Chattanooga, Tennessee, she decided to pursue a graduate degree in materials engineering.

She began pursuing her Doctor of Philosophy degree in materials science and engineering at the University of Florida in 1995. Dr. James Adair and Dr. Hassan El-Shall were her advisors during her study of colloids and interfacial chemistry. Currently, she is a member of Keramos Honor Fraternity, American Ceramic Society, Society for Biomaterials, and Materials Research Society, and Tau Beta Pi Honor Society.

Once she leaves the University of Florida in July 2001, she will begin work as a Senior Process Engineer at Intel in Portland, Oregon.

I certify that I have read this study and that in my opinion it conforms to acceptable standards of scholarly presentation and is fully adequate, in scope and quality, as a dissertation for the degree of Doctor of Philosophy.

elShall

Hassan El-Shall, Chairman
Associate Professor of Materials Science
and Engineering

I certify that I have read this study and that in my opinion it conforms to acceptable standards of scholarly presentation and is fully adequate, in scope and quality, as a dissertation for the degree of Doctor of Philosophy.

Laurie Gower

Laurie B. Gower, Cochairman
Assistant Professor of Materials Science
and Engineering

I certify that I have read this study and that in my opinion it conforms to acceptable standards of scholarly presentation and is fully adequate, in scope and quality, as a dissertation for the degree of Doctor of Philosophy.

Chris Batich

Christopher D. Batich.
Professor of Materials Science and
Engineering

I certify that I have read this study and that in my opinion it conforms to acceptable standards of scholarly presentation and is fully adequate, in scope and quality, as a dissertation for the degree of Doctor of Philosophy.

John J. Mecholsky, Jr.
Professor of Materials Science and
Engineering

I certify that I have read this study and that in my opinion it conforms to acceptable standards of scholarly presentation and is fully adequate, in scope and quality, as a dissertation for the degree of Doctor of Philosophy.

Saeed R. Khan
Professor of Pathology, Immunology and Laboratory Medicine

I certify that I have read this study and that in my opinion it conforms to acceptable standards of scholarly presentation and is fully adequate, in scope and quality, as a dissertation for the degree of Doctor of Philosophy.

James H. Adair
Associate Professor of Materials Science and Engineering, The Pennsylvania State University

This dissertation was submitted to the Graduate Faculty of the College of Engineering and to the Graduate School and was accepted as partial fulfillment of the requirements for the degree of Doctor of Philosophy.

August 2001

Pramod Khargonekar
Dean, College of Engineering

Winfred M. Phillips
Dean, Graduate School